Bjerrums Foredrag Nr. 25

Corneliu Athanasiu

From Theory to Practical Solutions in Geotechnical Engineering.

Utgitt av

LAURITS BJERRUMS MINNEFOND

Norsk Geoteknisk Forening

Oslo 2016

Laurits Bjerrums Minneforedrag

Nr. 1	6. februar 1975 ”Formation and Geotechnical Characteristics of Glacial-Lake Varved Soils” by T.Cameron Kenney
Nr. 2	14. mars 1977 ”Deformation computations in Geotechnical Engineering”” av Kaare Høeg
Nr. 3	27. februar 1978 ”Deformation Behaviour of Soils in Terms of Soil Moduli” av Oddvin Tokheim
Nr. 4	19. mars 1979 ”A Geotechnical Engineer’s 7th Sense” av Elmo DiBiagio
Nr. 5	5. mai 1980 ”Where Has All The Judgement Gone?” by Ralph B. Peck
Nr. 6	15. mars 1982 ”Is Limit State Design a Judgement Killer?” by Knud Mortensen
Nr. 7	7. mars 1983 ”En vegs geotekniske liv” av Geir Refsdal (ikke publisert)
Nr. 8	4. mars 1985 ”Deformation phenomena in jointed rock” by Nick Barton (ikke publisert)
Nr. 9	21 april 1986 ”Small is beautiful – the stiffness of soils at small strains” by John B. Burland
Nr. 10	16. mars 1987 ”Udrenert skjærstyrke som funksjon av effektive spenninger” av Gunnar Aas (ikke publisert)
Nr. 11	11. april 1998 ”Grundförstarkning av gamla hus med stålrörspålar” av Håkan Stille (ikke publisert)
Nr. 12	17. april 1989 ”Norsk geoteknikk 1950-75 Tilbakeblikk med refleksjoner” Av Håkon Hartmark, Gudrun Bjerrum, Ove Eide, Jan Friis, Bjørn Kjærnsli, og Nilmar Janbu
Nr. 13	29. april 1991 ”A case history of mysterious settlements in a building” by James M. Duncan
Nr. 14	3. mars 1993 ”Snow avalanche experience through 20 years” av Karstein Lied
Nr. 15	15. mars 1995 ”Laurits Bjerrums fornemmelse for utstyr” av Arild Aa. Andresen
Nr. 16	23. september 1998 ”Fundamentering av plattformer, observasjoner og refleksjoner” av Carl J. Frimann Clausen
Nr. 17	5. april 2000 ”Eurocode 7 og geoteknikerens hverdag” av Niels Krebs Ovesen (ikke publisert)
Nr. 18	24. april 2002 ”Forurensning av grunnen – et spørsmål om naturens bæreevne” av Gijs D. Breedveld
Nr. 19	21. november 2003 “Laurits Bjerrum – more than an engineer” av Kaare Flaate
Nr. 20	25. november 2005 “The magic of sands” av David Muir Wood
Nr. 21	23. november 2007 “Bearing capacity under cyclic loading - offshore, along the coast, and on land” av Knut H. Andersen
Nr. 22	27. november 2009 "Geomorphology as an integrating tool for failure and post-failure analysis of submarine mass movements" av Jacques Locat
Nr. 23	26. november 2010 "Strength and deformation properties of Norwegian clays from laboratory tests on high quality block samples" av Kjell Karlsrud
Nr. 24	28. november 2014 "Meeting today's Ground Improvement Challenges"" av James K. Mitchell
Nr. 25	25. November 2016 "From Theory to Practical Solutions in Geotechnical Engineering" av Corneliu Athanasiu

Bjerrums Foredrag Nr. 25

Corneliu Athanasiu

From Theory to Practical Solutions in Geotechnical Engineering.

Utgitt av

LAURITS BJERRUMS MINNEFOND

Norsk Geoteknisk Forening

Oslo 2016

From Theory to Practical Solutions in Geotechnical Engineering
The 25th Bjerrum Lecture presented in Oslo 25th November 2016

Corneliu Athanasiu
Multiconsult ASA

ABSTRACT

INTRODUCTION

First of all, I would like to thank the Committee of Bjerrum Memorial Foundation for choosing me to deliver the 25th Bjerrum Lecture. It is an honor and a privilege to which I will try to answer with the best of my abilities, being, at the same time, aware of my limitations and shortcomings.

One of the reasons that they picked me up is probably the fact that I met Laurits and I had the opportunity to work under his guidance and fully appreciate his tremendous personality, his professional skills and his passion for work and life. I can, therefore come to day in front of you to give, among many others, my testimony of all his capacities that made him the leading figure of the geotechnical community.

Working with him, I have learned that, in Geotechnical Engineering, it is always better to be approximately right than precisely wrong, or too late.

This expression was variously attributed to Milton Keynes and Warren Buffet, as quoted by Hamma and Curran (2009). Hamma and Curran (2009) pointed out that in Science and Engineering, accuracy is the degree to which a measurement or calculated quantity matches its "true" value (Fig.1.1). The calculated values shown in Fig.1.1 are both right because they are within the allowable range (Upper limit-Lower Limit), but they have different degrees of accuracy.

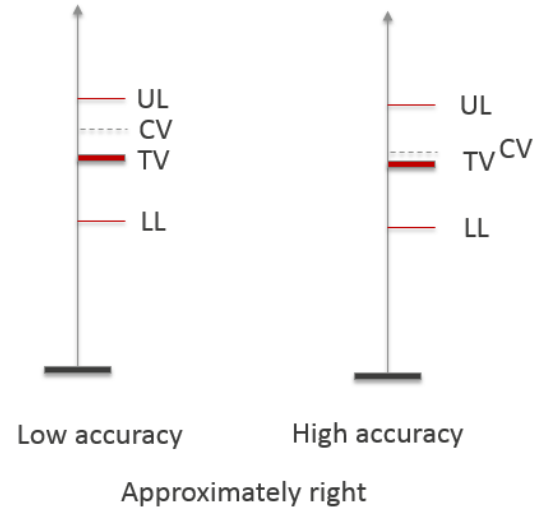

Fig.1.1. Approximatively right: TV-True Value; UL-Upper limit; LL-Lower Limit; CV-Calculated Value.

Precision is a closely related, but different concept. Precision is the degree to which repeated measurements or calculations produce same or similar results. It is possible, for example, for a calculation to produce inaccurate but precise answers (Fig.1.2). This would occur if the answers are consistently close to each other, but are in reality far from being correct (outside the allowable range), because, for instance, the required sophisticated soil parameters were inadequate.

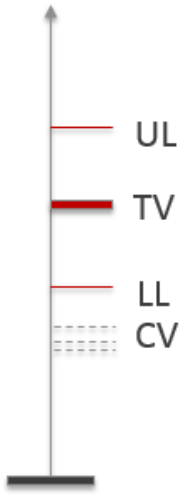

Precisely wrong

Fig.1.2. Precisely wrong: TV-True Value; UL-Upper limit; LL-Lower Limit; CV-Calculated Values.

Another aspect in Geotechnical Engineering is that in early phases of design, one has to decide the foundation solution within a limited time interval where sophisticated analyses requiring selection of soil parameters and many trial runs cannot be performed. In this respect, again, we need simple but reliable models to be used several times with different foundation geometry and soil parameters, before a solution is established and can be analyzed in detail. Simple models should ideally be also more effective, user friendly and should enable the developer to make changes and to validate them in order to answer different demands during the design. The relation between theoretical/sophisticated methods and simple models is summarized in Table 1.1.

Table 1.1 is an oversimplification of the real amount of methods and models used within Geotechnical Engineering to answer the questions and find the solutions. These solutions must be robust, economical, within the required accuracy and the work must be performed within the allocated time interval.

In this lecture, I will try to illustrate, with some examples, how can we use the theoretical methods and develop simple methods of different degrees of simplifications and accuracy in order to obtain the right answer at the right time, both, in Land and Offshore Geotechnical Engineering.

Table 1.1. The relation between theoretical/sophisticated methods and simple models

	Theoretical/sophisticated numerical methods	**Simple methods/models**
Description/Examples	-Use of Theory of Elasticity and Plasticity to determine stresses and strains in soil due to applied loads/Use of finite element analysis; -2D-3D theory of water flow and consolidation of excess pore water pressures/Finite element coupled consolidation analysis; -2D-3D dynamic analysis of structures with large number of DOF in time/frequency domain/2D-3DFinite element dynamic analyses;	-Simplified stress distribution under rectangular, uniformly loaded area; -Calculation of settlements by 1D, summation of elemental layer settlements; -Uncoupled finite difference solution of consolidation theory; …
Advantages	-Rigorous solutions; -Enable understanding of failure mechanisms, detailed soil/structure interaction; -Can be used to confirm/validate the results from simple models;	-Require small number of soil parameters readily obtained from correlations or laboratory tests -Simple input data; -Can be run many times to perform parametric studies and to evaluate the effect of different factors on the performance of foundations; -Can be easily changed/adjusted to respond to new demands from the design;
Disadvantages	-Require time to construct the model and to select the soil parameters; -It is more difficult than with simple methods to capture the influence of one soil parameter on the performance of the structure, due to complexity of the soil models; -Require longer period of time than simple methods to run a problem; -Require more work than the simple models to change input data;	-Less rigorous than theoretical methods; -The output is less comprehensive than that of the theoretical methods; -Some aspects of soil behaviour may be overseen because of the simplicity of the methods
Requirements	-Require theoretical background to understand and prepare the input, particularly the soil parameters, to construct the model in finite element method and to understand the results;	-Every change/adjustment to the model requires the verification and validation of the model; -Require a geotechnical data bank that enable selection of soil parameters from correlations with identification indices.

FOUNDATION BEARING CAPACITY AND CONTACT STRESSES

The first example is of the distribution of contact stresses between soil and foundation. Often the geotechnician is facing the problem of recommending to the structural engineer a value for the soil reaction coefficient, k, to be used as soil spring stiffness at the bottom of the

foundation in structural analyses. The value of k is defined by Winkler (1867) as:

$$k = \frac{p}{s} \qquad (2.1)$$

In which p is the contact stress in a point at the interface soil-foundation and s is the soil settlement at the same point. While the structural engineer expects a constant value of k, the geotechnical engineer knows that the k value:

- depends on the load intensity (degree of mobilization of bearing capacity of the foundation) as the behavior of the soil is non-linear and stress dependent;

Consequently, in order to solve the problem, one solution is to use an iterative procedure were both the structural and geotechnical engineer co-operate, as described by Houser and Karlsrud (2014). However, for preliminary conceptual studies, we need simple models. The method of solution of such a simple model is described as follows.

Assess the relative stiffness soil-foundation, Kr:

$$K_r = 12 \cdot \pi \cdot \frac{(1-\upsilon_c^2)}{(1-\upsilon_s^2)} \cdot \frac{E_s}{E_c} \cdot \left(\frac{L}{2t}\right)^2 \cdot \left(\frac{B}{2t}\right) \qquad (2.2)$$

- refers only to the point for which it is defined and cannot model that the soil settlement at **a** point is due to contact stresses at **all** the points of the surface;
- varies from the corner to the center of foundation and the variation depends on the foundation-soil relative stiffness (Fig.2.1);

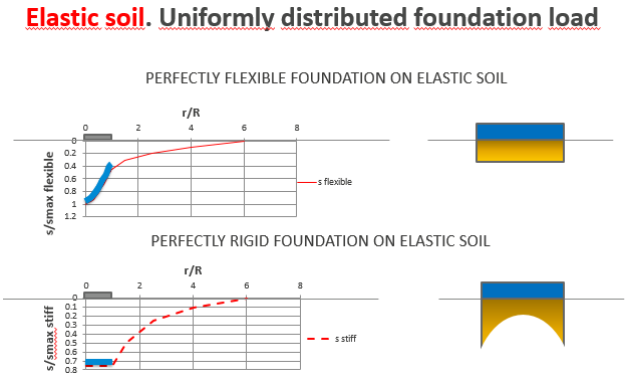

Fig.2.1.a. Elastic soil.

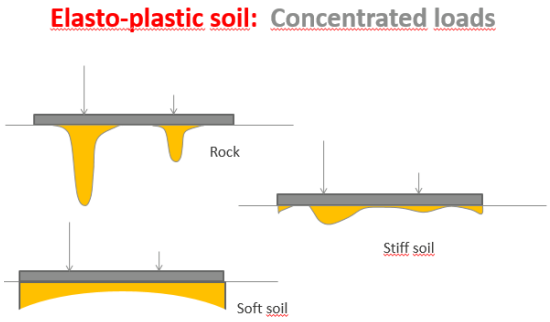

Fig.2.1.b. Elasto-plastic soil

$$K_{r,\,limit} = \frac{8}{\sqrt{L/B}} \qquad (2.3)$$

where: E_f = Young's modulus for foundation material; E_s = Young's modulus for soil; ν_c = Poisson's ratio for foundation material; ν_s = Poisson's ratio for soil; t = thickness of foundation plate; B = Width of foundation; L = Length of foundation.

The foundation plate is relatively stiff if:

$$K_r < K_{r,\,limit} \qquad (2.4)$$

Select the method used to calculate contact stresses and settlements; if the foundation is stiff relative to the soil, use "**stiff model**" (SPLATE, DEAP, STFMAT); if the foundation is flexible relative to the soil, use "**flexible model**" (FPLATES);

Contact stresses between stiff foundation and soil

When the relative foundation-soil stiffness is high enough that the foundation will remain a plane after the loads are applied, i.e. it will only translate vertically and rotate about the two axes, the foundation can be considered stiff (rigid). A simple model that can be used to calculate the contact stresses at the interface rigid foundation-soil is described as follows:

Measurements of contact stresses between rigid foundations and soil show that the stress distribution has large values at the corners and edges and lower values under the middle of foundation for small foundation loads. However, as the load increases, the stress distribution changes gradually towards larger values in the middle and lower values at the edges and corners. An example of such measurements is shown in Fig.2.2, Leussink and Schweickert (1963), where contact stresses along two diagonals of a rigid plate on sand are measured at different degrees of mobilization of bearing capacity.

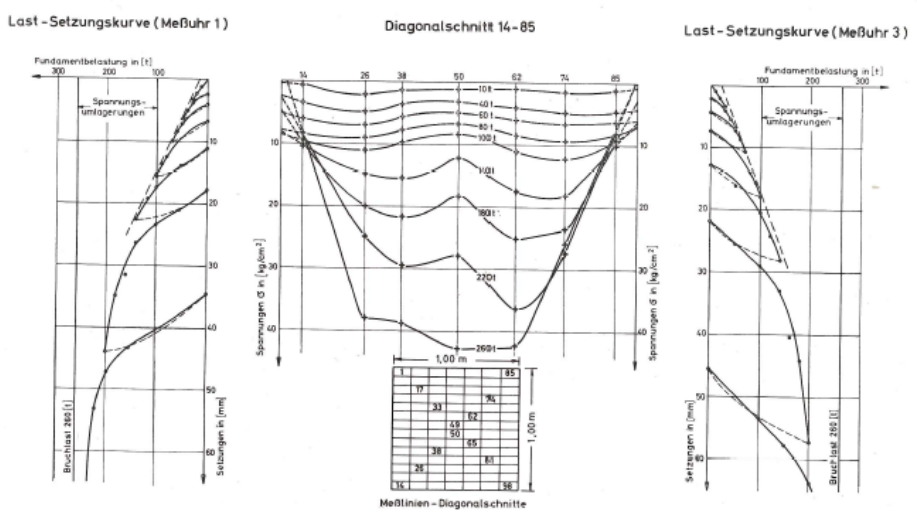

Fig.2.2a. Contact stresses under 1mx1m stiff foundation loaded centrically on the surface of sand (t=0 m)

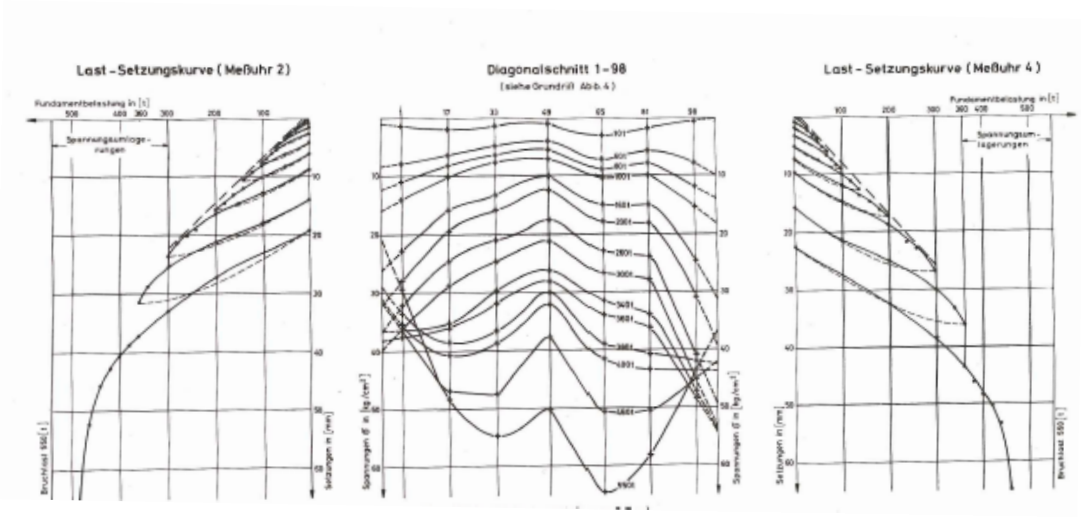

Fig.2.2b. Contact stresses under 1mx1m stiff foundation loaded centrically. Depth, t=0.7 m.

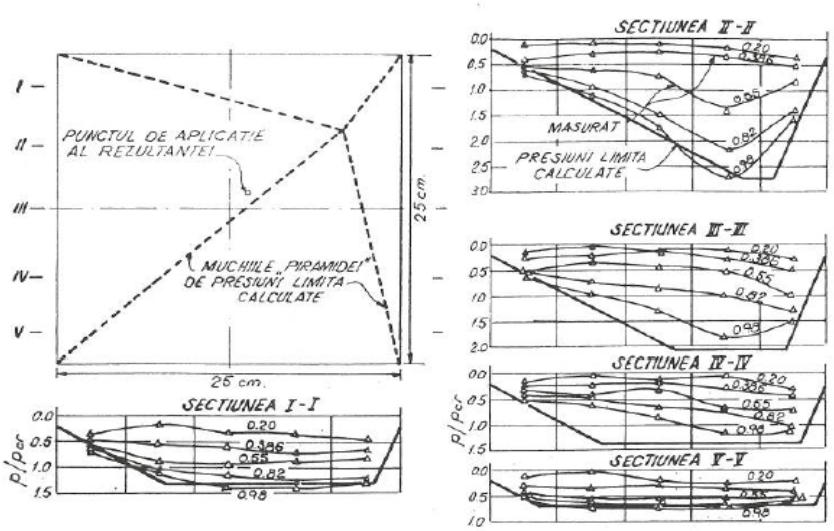

Fig.2.3. Stress distribution between sand and a rigid, eccentrically loaded foundation at different degrees of bearing capacity mobilization, Athanasiu (1978).

Wiebel (1971) presents similar measurements from small-scale tests on circular foundations on sand. Peterson and Schmidt (1974) present the measurements of contact stresses between sand and raft foundation of Hamburg underground line under different construction stages (different applied loads).

Small scale tests were also performed both under centric and eccentric loads on a rigid foundation on sand, Athanasiu (1978), Fig.2.3.

All measurements indicate a clear tendency of stress redistribution from an "elastic" distribution with larger stresses at the edges to an elasto-plastic distribution with larger stresses in the middle of the foundation. Interpretation of measurements resulted in a discrete element method for analysis of contact stresses between soil and stiff mat foundation, Athanasiu (1978). The method was incorporated into a FORTRAN program, **STFMAT**, re-written to answer different demands, particularly for off-shore projects, as **SPLATE**, Athanasiu (2004). When the bearing capacity is fully mobilized, the stress distribution under foundation consists of a limit stress, p_l at the edge of foundation and a pyramid with its apex, p_v, at the centre of foundation. The total volume of limiting stress is equal to bearing capacity, p_{ult}, times area of the foundation, Fig.2.4.

The principle of stress redistribution is described as follows:

- For each discrete element of foundation-soil contact surface, a critical normal stress, p_{cr}, is calculated as the ordinate of the pyramid diagram, at the centre of the element.
- If the elastic normal stress calculated in an iteration exceeds the critical stress, the normal stress is set equal to critical stress. The "yielded" element is no longer active;
- Calculate the additional load vector by adding up the "excess" stresses;
- Perform a new elastic analysis were only the "non-yielded" elements are active;
- Repeat the iterations until the "excess" load to be redistributed become negligible

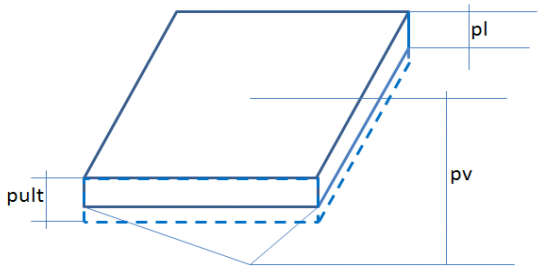

Fig.2.4. *Assumed limit stress distribution, Athanasiu (1978).*

The method of solution is described in **Appendix 1**. The original program, **STFMAT**, can use a variant of the method of solution, based on stress-dependent, non-linear, tangent soil reaction coefficient to solve contact stresses between foundation and loess, collapsible soil by wetting. A variant of the program **SPLATE**, **DEAP**, is also developed to incorporate undrained, effective stress bearing capacity analysis for irregular foundations (see Section 2.4).

Example 1. Contact stresses between rigid foundations and soil

Projects with large number of isolated foundations (as illustrated in Fig. 2.5), that include installations sensible to differential settlements, require not only determination of contact stresses and displacements, but also an evaluation of differential settlements between any different adjacent footings.

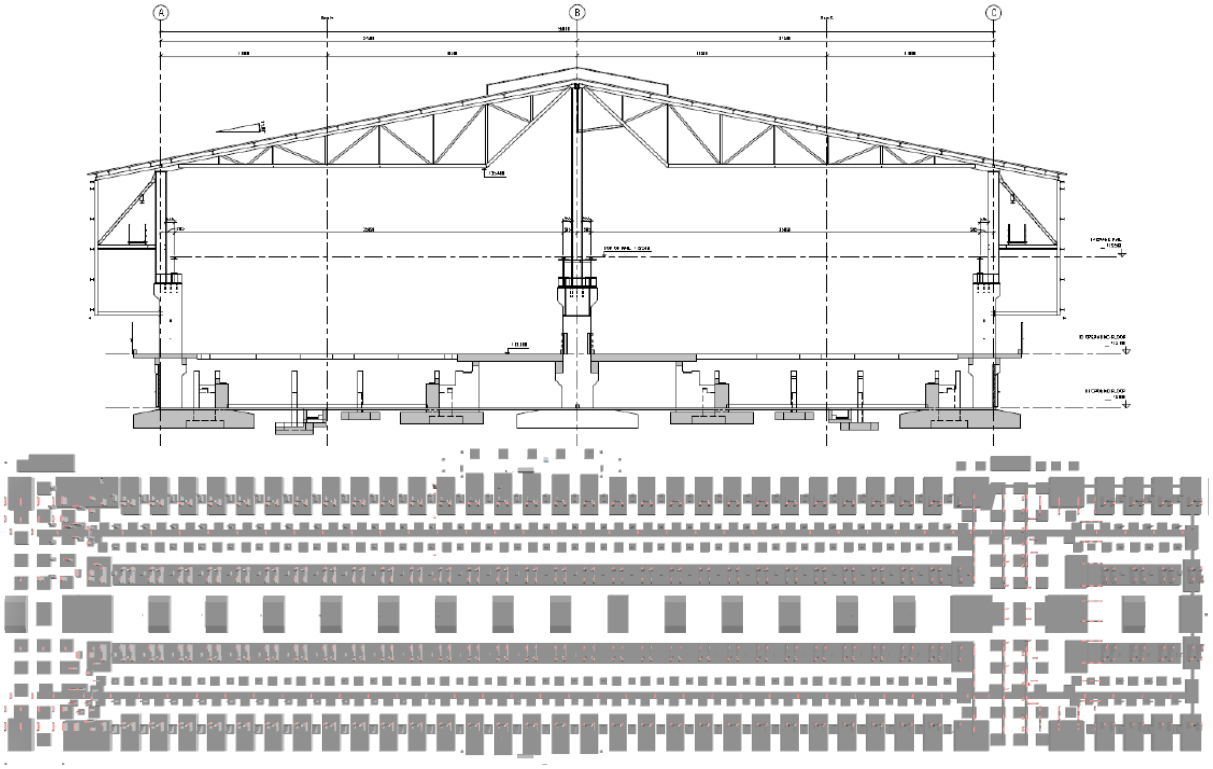

Fig. 2.5. Foundation plan and cross section of a large industrial plant.

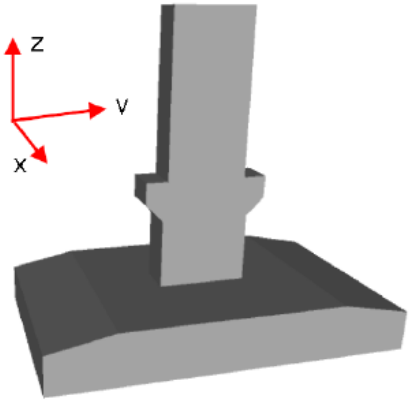

Fig.2.6. Isolated footing on rock fill (left).

It follows that a large number of analyses are required for determination of displacements and rotations of each isolated footing under different load combinations. The method used with SPLATE program suits this type of projects due to its simplicity of input parameters. In the following, an example of isolated footing resting on rock fill of a few meters thickness down to bedrock is presented.

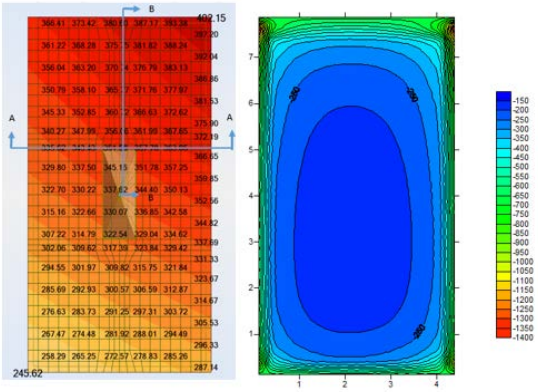

Fig.2.7. Contact stresses determined using the programs ROBOT (left) and SPLATE (right) (right).

The 8 m x 3.8 m foundation, with 1.5 m thickness, (Fig.2.6) rests on 2.5 m thick rock fill with elastic parameters, Young modulus, E=50000 kPa and Poisson's ratio, ν=0.25. As SPLATE assumes elastic half space, a correction factor for depth to bedrock, f_H=1.78 is applied to the Young modulus. In order to compare the contact stresses based on a constant value of soil reaction coefficient, k, and the elasto-plastic solution, two parallel analyses, one with the program ROBOT (constant k) and one with the program SPLATE, were run with the same loads and foundation geometry. The contact stresses from the two analyses are presented in Fig. 2.7.

The comparison of the contact stresses calculated with the two methods in Fig.2.8, shows a stress concentration towards the edge of the foundation and a reduction of stresses at the centre, when the simplified, yet more realistic elasto-plastic model of **SPLATE** is used. It is clear that a constant reaction coefficient, k, will lead to un-conservative design bending moment at cross section A-A and consequently to un-conservative amount of reinforcement steel bars.

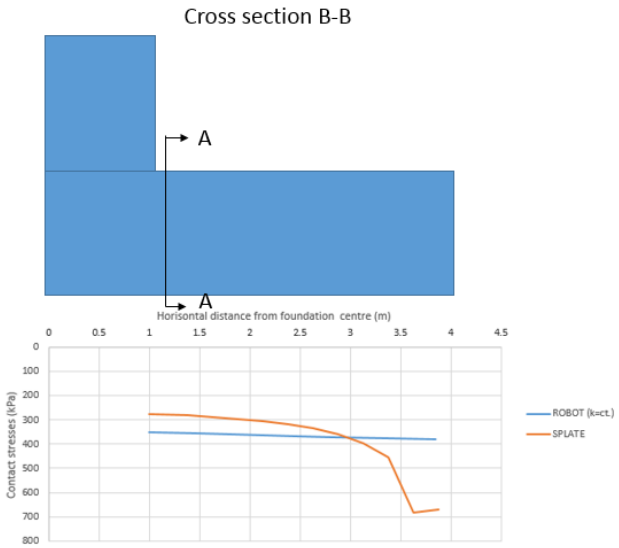

Fig.2.8. Comparison of contact stresses calculated with SPLATE and with constant soil reaction coefficient using the program ROBOT.

Example 2. Contact stresses between rigid foundations and loessial, collapsible soil. Effect of inundation.

Approximately 17% of the Romanian territory is covered by loessial, collapsible soil (Fig.2.9). It is an wind-blown (æolian)

deposit having the fine sand and silt as the main components of the grain size distribution. In arid areas, in time, the salts crystalize and the particles become cemented to each other, leaving a rigid and relatively strong structure with high porosity (n=45-55%). As the salts are soluble, the loess is very sensitive to wetting, showing a great amount of sudden, additional volume changes under constant load that, in dry conditions, is carried without significant compression.

The additional settlements by wetting cause damages to the structures founded on loess. It was therefore decided that a large scale test research program be initiated in 1975, in the town of Galatz, next to the Danube swing from South-North to West-East, some hundred Km from Donau Delta and the Black Sea.

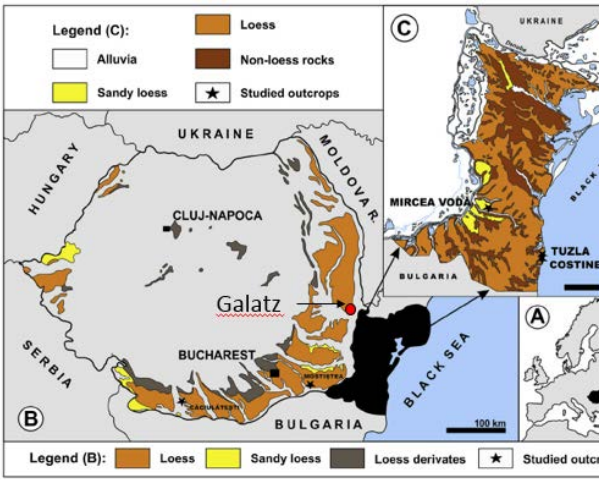

Fig.2.9. Extension of loess covered areas on Romanian territory.

A five story, reinforced concrete, apartment building (Fig.2.10) was subjected to water inundation under different sections of the Northern strap footing part. After the inundation, the building was rehabilitated (corrected to horizontal) by controlled sub-excavation of the soil under the bottom of the foundations in the Southern part. The settlements, contact pressures, changes in water content in the loess under the bottom of the foundations, as well as the strains in the superstructure were measured during the different phases of inundation and sub-excavation.

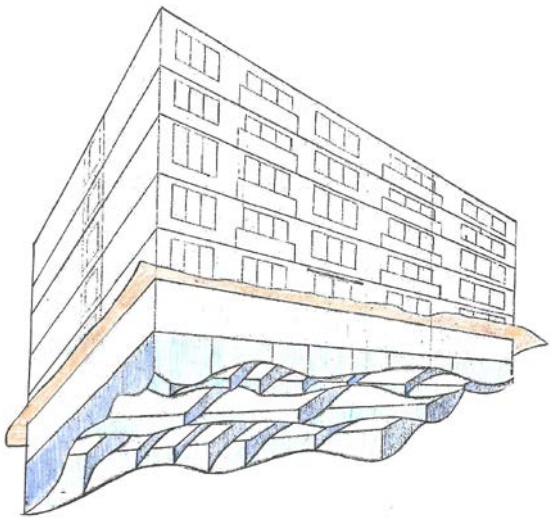

Fig.2.10. Experimental apartment building. Architect view with contact stress distribution.

A simplified method was developed, (Stanculescu et al. 1977 and Athanasiu 1978) in order to enable the comparison between calculated and observed contact pressures at the measurement points and to extend the prediction of contact stresses over the entire foundation area in view of evaluation the global bending moments, torsional moments and shear forces acting on the building.

The method is based on variable, tangent soil reaction modulus. The modulus incorporates the influence of confining (consolidation) pressure, of the degree of mobilization of shear strength and of "elastic" tendency of pressure distribution over the area of a rigid strap foundation:

$$K_{v,t} = K_i \cdot (1 - \frac{p}{p_{ult}})^m \cdot f_e \qquad (2.5)$$

in which:
K_i is the initial soil reaction modulus, p is the contact stress at the considered point of the foundation area in the previous loading step, p_{ult} is the ultimate contact stress at the same point defined as described in Section

2.1, m is the exponent determined from laboratory tests and f_e is the factor accounting for the "elastic" tendency of pressure distribution. It is calculated as the ratio between contact pressure of the foundation resting on elastic half-space, under the applied loads, and the corresponding linear pressure distribution.

The determination of variable, tangent soil reaction modulus from laboratory and field plate loading tests is presented in **Appendix 2**.

The simplified method using variable tangent Winkler modulus was used to predict contact stresses between foundations and soil during different phases of the experimental project. Broadly, the experiment can be divided into three main stages: stage I- the construction of the building; stage II- inundation of the half part of foundation area and stage III- under-excavation of the opposite half. Calculated and measured contact pressures are presented in Fig.2.11 for five different locations within the foundation area.

The distribution of contact stresses along the foundation areas for stage I of experiment is shown in Fig.2.12.

The accuracy to which the calculated pressures predict the measured ones is considered acceptable. The global bending moments acting on the building, determined from the resultants of measured pressures and from the calculated ones (Fig. 2.13) differ by about 20%.

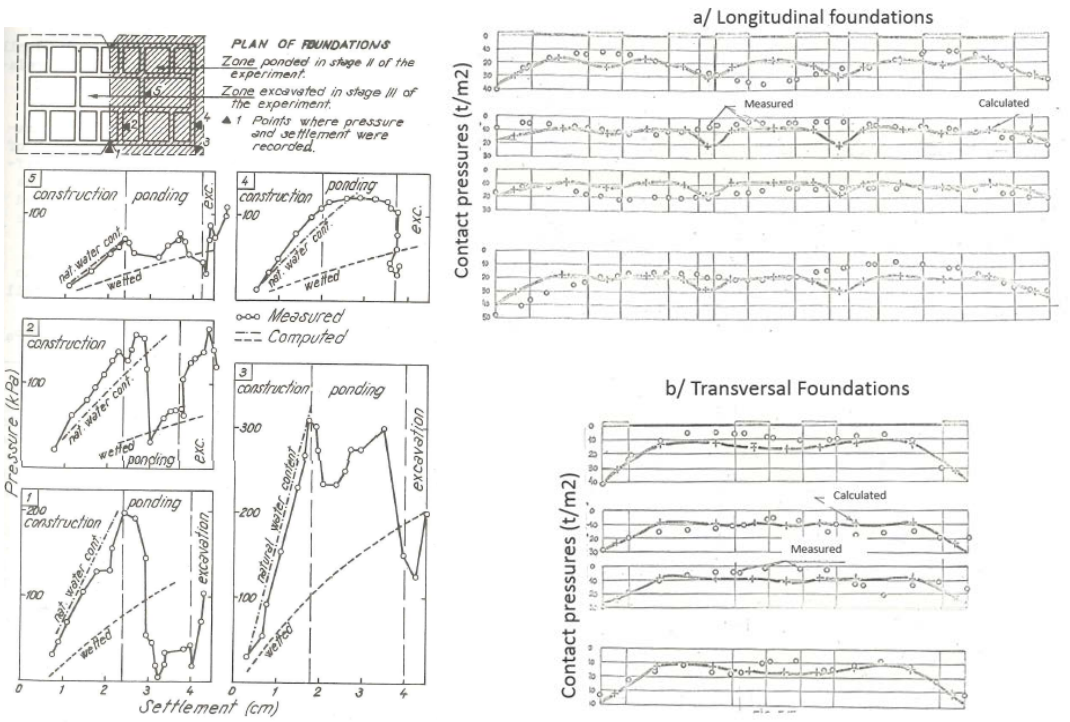

Fig.2.11. Pressure-settlement relations measured during "in situ" test of the five story building (left). Fig.2.12. Calculated and measured contact pressures (stage I). a- Longitudinal foundations; b- Transversal foundations. (right).

The method of variable, tangent Winkler modulus, incorporated into a computer program, **STFMAT-06**, was therefore used to determine the bending moments acting on the building in different stages of the experiment, Fig.2.14.

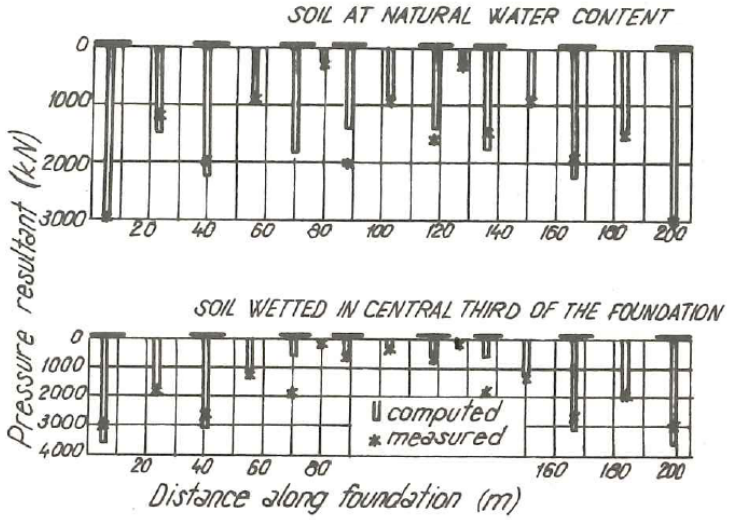

Fig.2.13. Contact pressure resultants over transversal foundations.

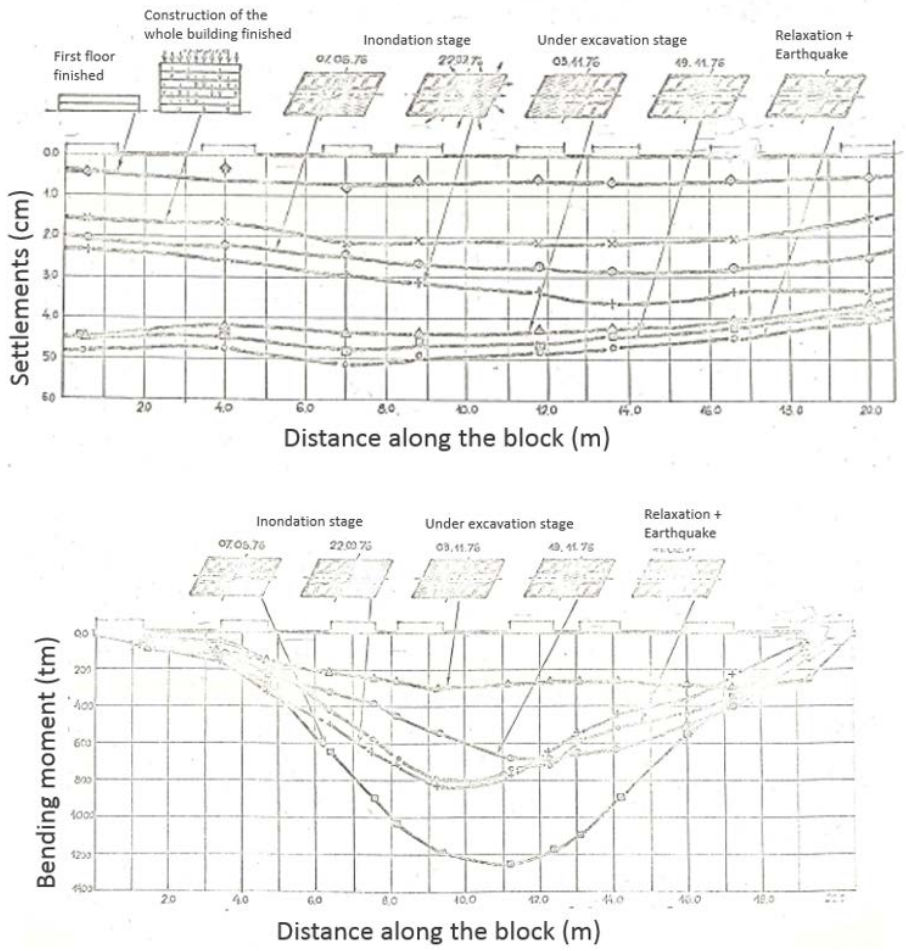

Fig.2.14. Settlements and global bending moments during different stages of the experiment

The large amount of experimental information could, thus be used with the help of the simplified model of variable, tangent Winkler modulus to quantify the degree of damage, (as defined by Burland et al., 1977), produced by different stages

of the experiment to the structure of the studied apartment block.

As seen from Fig.2.15, the relative deflection of the block (Δ/L) was already in the dangerous zone at the final stage of construction but has also increased under the final stages of inundation and under excavation. In spite of the predictions from Fig.2.15, there were no fissures or cracks observed in the structure and this is attributed to a carefully chosen critical strain, ε_{cr}, = 0.03 %, for the reinforced concrete of the block. The main lessons from the experimental project were:

- The wetting of an extremity of the foundation area on loess will redistribute the contact pressures and will generally reduce the bending moment at central part of block;
- Wetting at the center of the foundation area is much more dangerous for the bending moment;
- The ratio between length of building, L and its height, H, should either be larger than 4-5, or less than 1. The later solution will probably not increase the bending moment but will induce large rigid rotations of the block, which will be dangerous for the general stability of the building.
- The simplified method of variable, tangent Winkler modulus, based on laboratory triaxial tests on dry and wet samples can be used to predict the contact stresses between foundation and soil that will enable a realistic soil-foundation structure interaction analyses for the structural design.

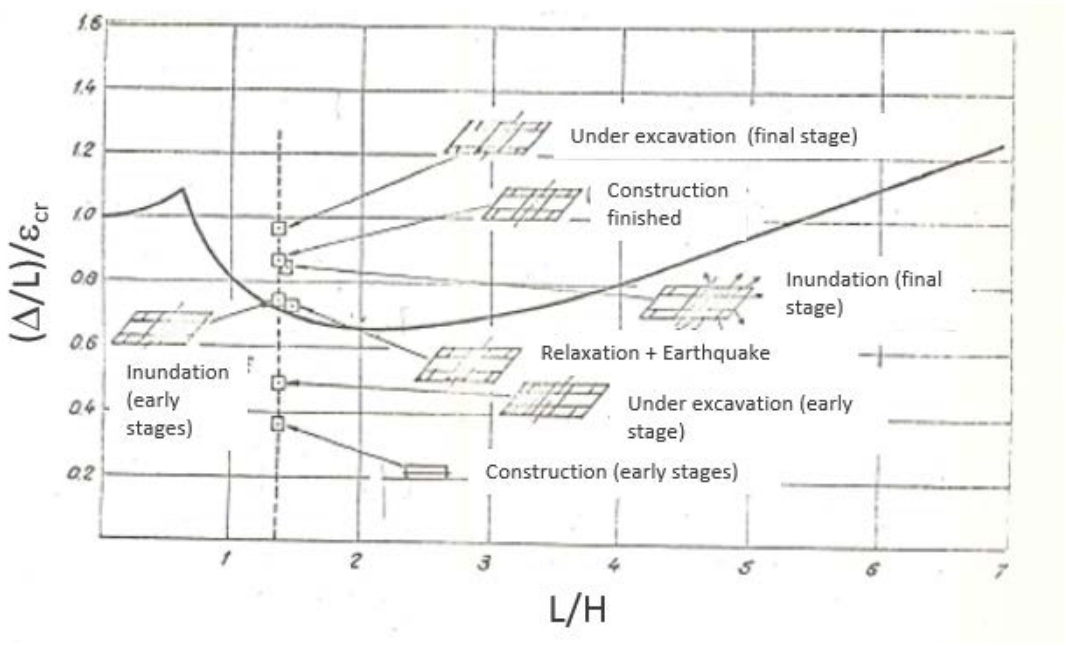

Fig.2.15. Differential settlements compared to "allowable degree of damage" (Burland et al., 1977).

Example 3. Contact stresses and stability of gravity platforms with irregular rigid foundations

Sometimes we are facing the problem of stability analysis of discontinuous or irregular foundations like tripod platforms, circular ring protective barriers (as illustrated in Fig. 2.16), jackets in unpiled conditions, etc. The on bottom stability of either full ring foundation or half ring during installation phases requires a full 3-D non-linear finite element analysis. In

view of large number of load cases and geometries in conceptual phases, a simplified model, based on elastic solutions and on redistribution of contact stresses, adapted for circular ring, was incorporated into a discrete element program, **DEAP**, Athanasiu, Alm and Bye (1989). The principle of contact stress redistribution is the same as used for stiff foundations (Section 2.1). It is graphically presented in Fig.2.17 together with assumed, radial failure mode for discrete elements of the ring foundation. The failure mode for each discrete element is essentially the same as for a footing having the same width as the element and a given direction to failure (radial). The critical normal and shear stresses for each discrete element are calculated using undrained bearing capacity formulation in effective stresses, as described in **Appendix 3**.

To illustrate the use of simplified method for ring foundations, the normal forces and the displaced shape of the half ring foundation under the forward wave forces are presented in Fig.2.18.

Fig.2.16.Ekofisk protective barrier. Example of circular ring foundation (semicircular ring during installation phase).

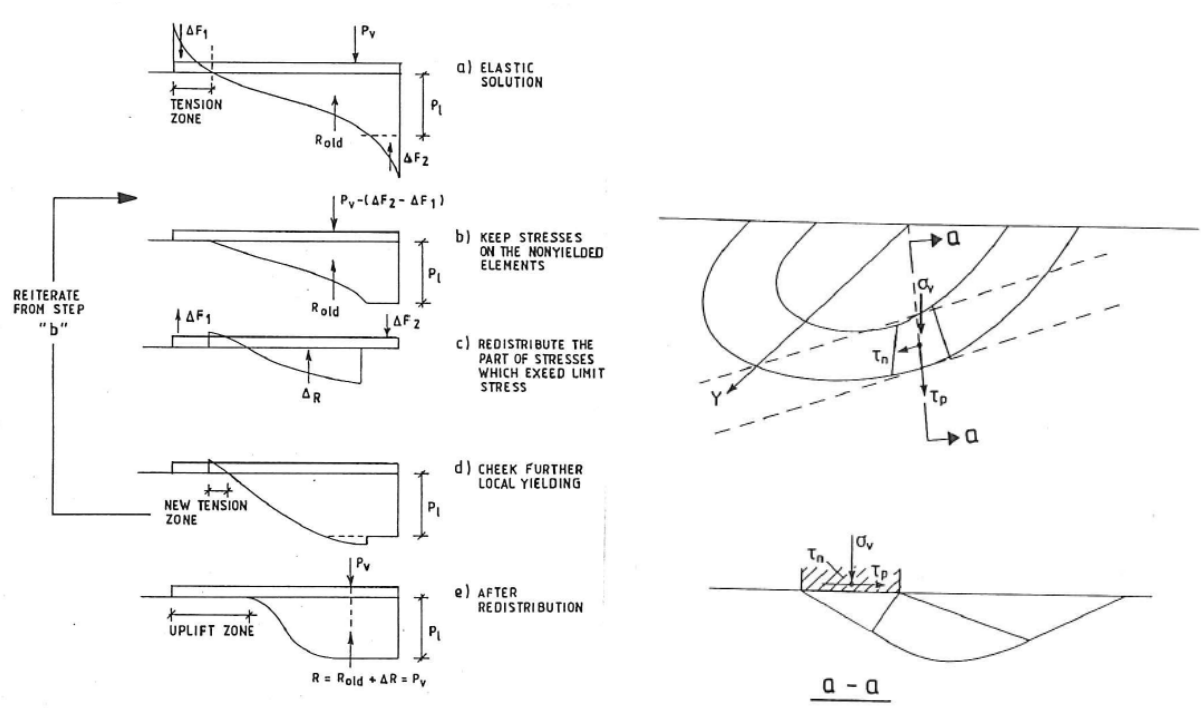

Fig.2.17. a/ Redistribution of contact stresses (left) and b/ Failure mode of a ring foundation.

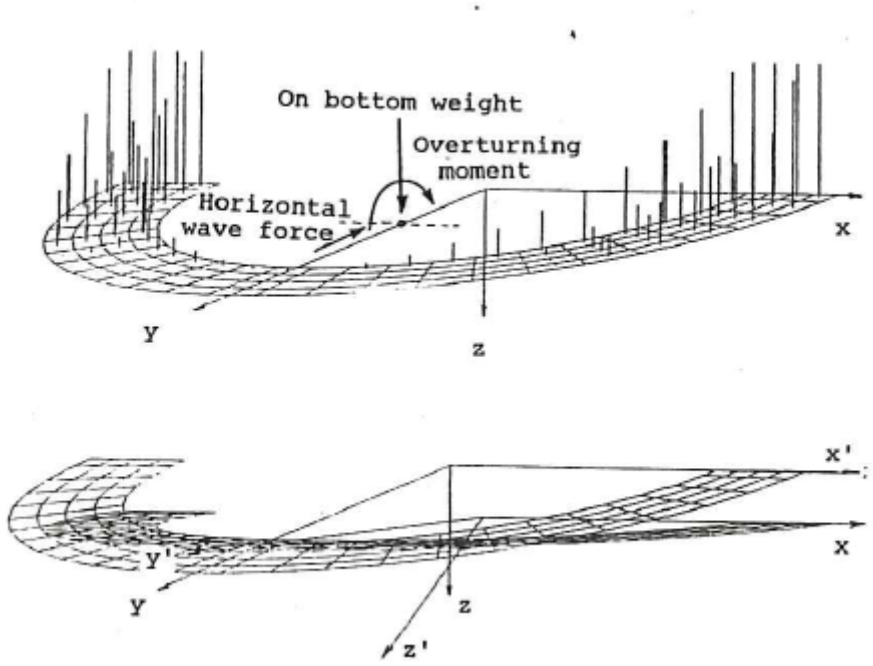

Fig.2.18. 3-D view of the displaced half of the ring foundation under the forward wave forces.

Fig.2.19.a illustrates the results of displacements, normal and shear forces for the half ring foundation under skew force and torsion moment.

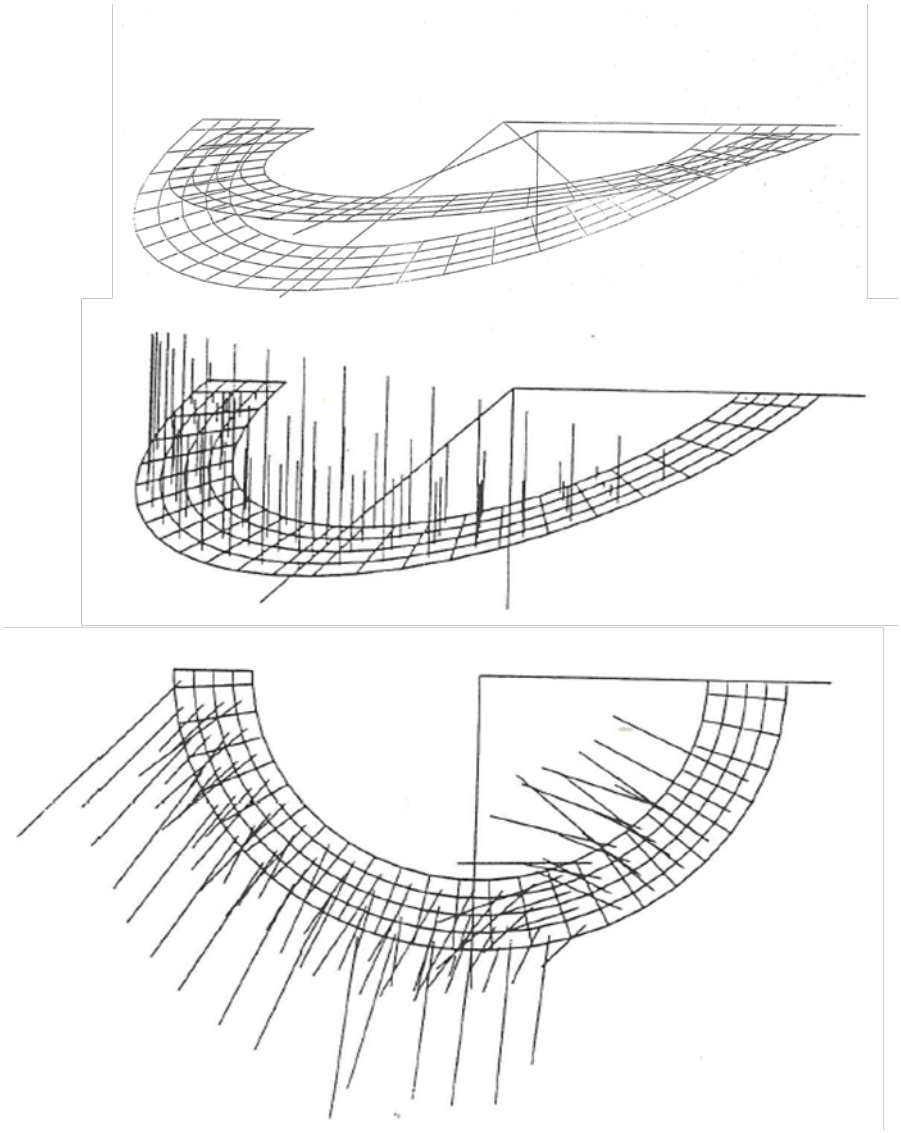

Fig.2.19.a. 3-D view of the displaced half of the ring foundation, normal and shear stresses under the skew wave force and torsion moment.

Parametric studies can be conducted to optimize the on bottom weight of the platform in order to minimize the uplift area under extreme horizontal wave loads and moments. Fig.2.19.b illustrates such a study where the uplift area are determined for two on bottom weights W2>W1 and different applied lateral loads.

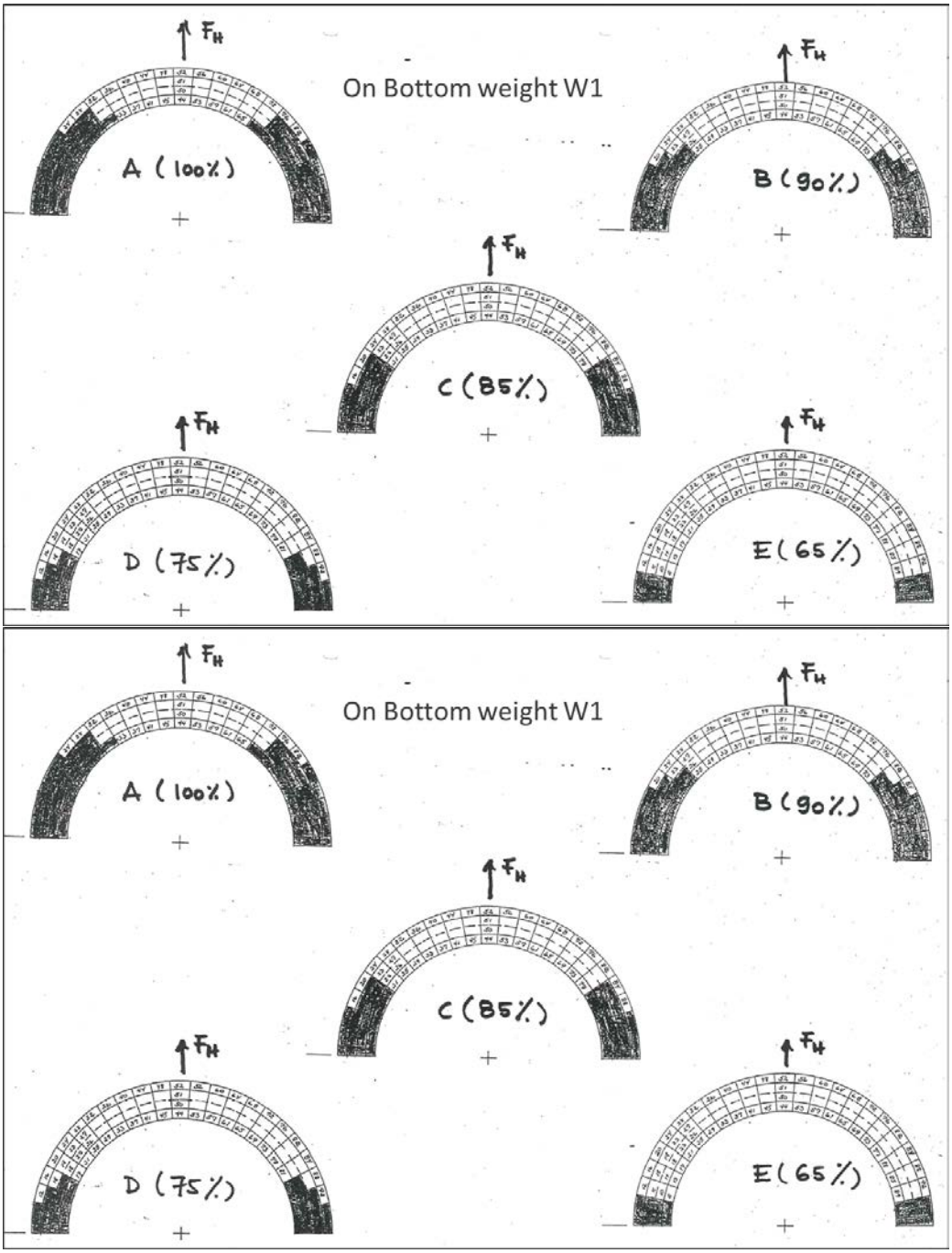

Fig.2.19.b. Parametric study of the influence of on bottom weight on the uplift area (W2>W1).

Contact stresses between flexible foundation and soil

When the relative stiffness of foundation-soil is such that the foundation slab will undergo deflections, in addition to vertical translation and rotations about the two axes, the foundation can be treated as

flexible. A simplified method to calculate the contact stresses is described as follows:

- The flexible plate is modelled by plate elements and the soil is modelled as variable, non-linear secant Winkler spring stiffness at the nodes of the plate elements
- The first iteration starts with an uniform distribution of contact stresses
- The deflection of the plate under the applied loads, the soil reactions and settlements under the contact stresses are calculated (Fig.2.20).
- New spring stiffness are calculated at nodes as the ratio between the contact stresses and settlements in the previous iteration.
- The calculation of plate deflections and soil settlements continues until convergence in contact stresses and deflections is obtained.

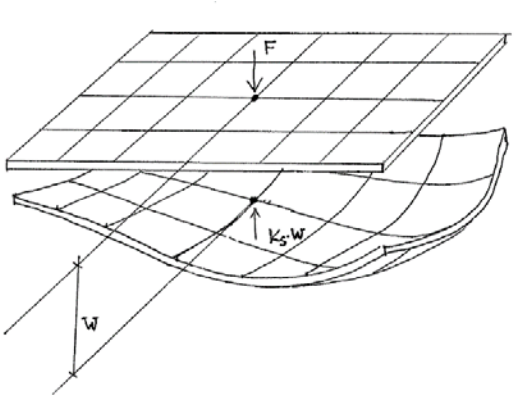

Fig.2.20. Simplified method for contact stresses under flexible plates.

The simplified method is presented in Appendix 4 and is incorporated into a computer program **FPLATES.** A post-processing, Visual Basic program, **FPLATES-VB**, is also developed in order to assist the user to inspect and present the input and output data. The supporting spring reactions (contact stresses at nodal points) are modelled by using one of the following four soil models: a/elastic layered continuum, b/Winkler springs, c/non-linear supporting spring, d/1-D soil compression (settlement) model. The soil model most commonly used is the 1-D compression (settlement) model.

Different depths to bedrock can be specified within the area of the plate (Fig.2.21).
As it results from the description of the model, there is no limitation in the contact stresses of flexible foundations. While contact stresses of stiff foundations can exceed the limit stresses, particularly at the edge and corners, this is not the case for flexible foundations (at list when mobilization degree of bearing capacity is in the range of 0-0.7), where the most important effect is the tendency of the ground to settle under the contact stresses.

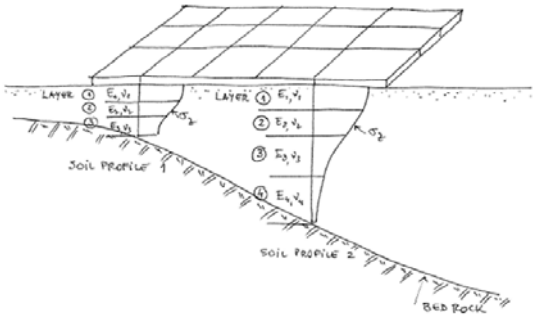

Fig.2.21. Specifying variable depth to bedrock.

As it results from the description of the model, there is no limitation in the contact stresses of flexible foundations. While contact stresses of stiff foundations can exceed the limit stresses, particularly at the edge and corners, this is not the case for flexible foundations (at list when mobilization degree of bearing capacity is in the range of 0-0.7), where the most important effect is the tendency of the ground to settle under the contact stresses.

Example 4. Contact stresses and settlements of flexible foundations.

Example 4a. An example of flexible plate is analyzed with the program FPLATES. The foundations consist of beam grid over a thin concrete plate 12 m x 40.8 m, resting

on a soil profile of a ca. 2 m thick sand layer over NC clay. A layer of expanded glass with low unit weight and high stiffness replaces the upper 85 cm of sand layer. The geometry of the plate, soil profile and contact pressure diagrams are shown in Figs. 2.22.-2.24.

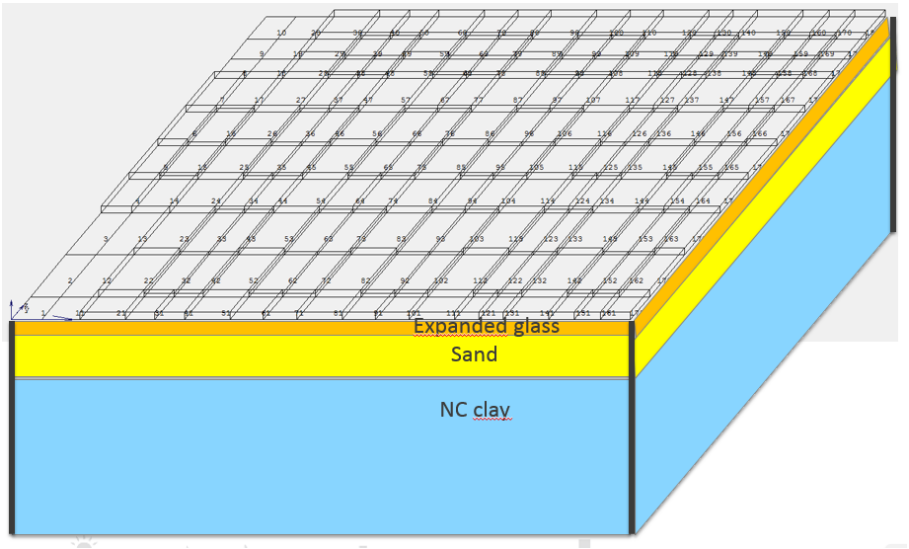

Fig.2.22. Flexible plate

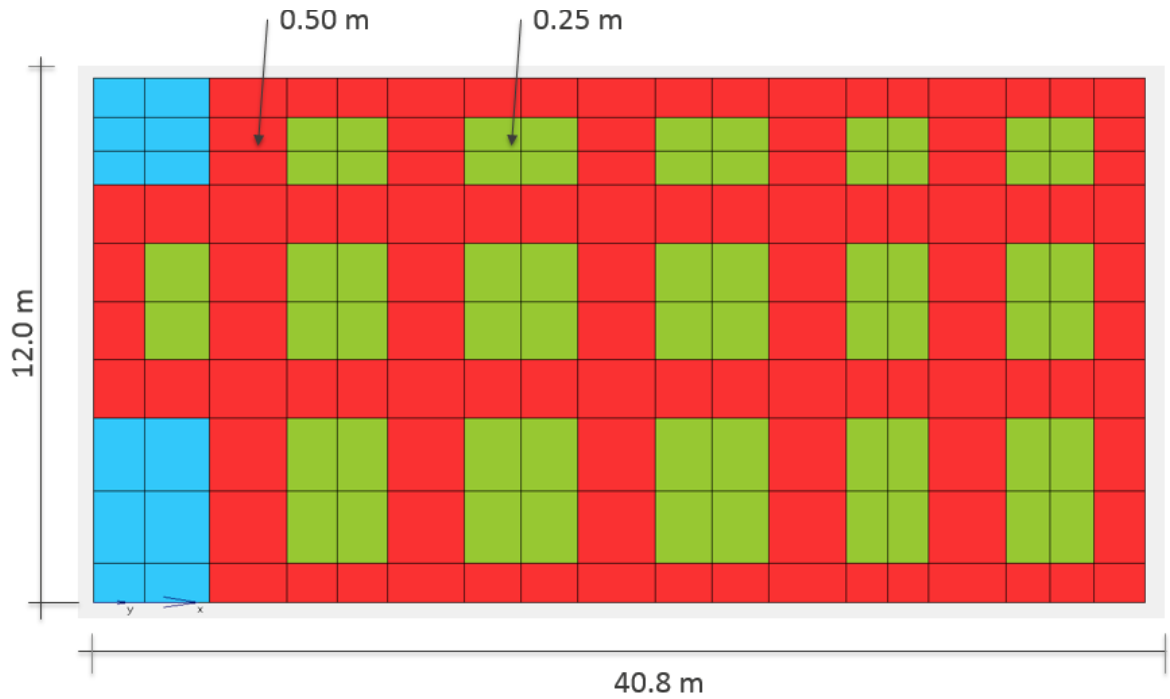

Fig.2.23. Plan of foundation grid and slab

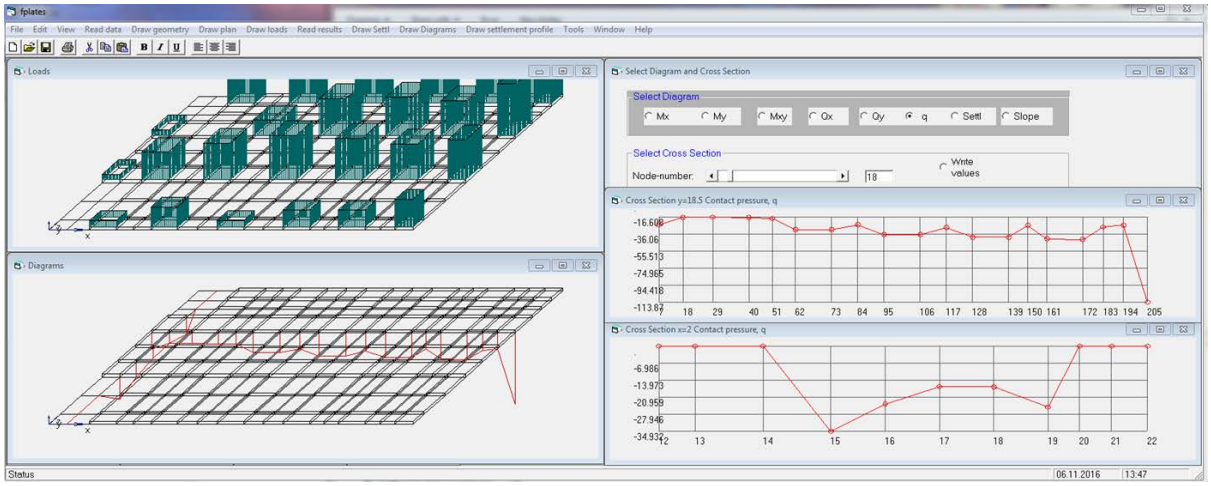

Fig. 2.24. Loads and contact pressures.

Example 4b. The settlements of a 35m x 85 m flexible foundation for a GBS platform, with four rigid shafts are calculated using the program FPLATES (Fig.2.25). The settlement calculations include the area outside the foundation where a scour protection rock fill is placed (Fig.2.26 a). Concerns were also expressed about the differential settlements between the edge of the platform and the outside seabed floor where pipes are installed (Fig.2.26b).

The settlement profiles from the edge of the platform and outside of the platform are shown in Fig.2.27. The profiles enable structural pipe engineers evaluate the additional bending moments induced in the pipes by the differential settlements.

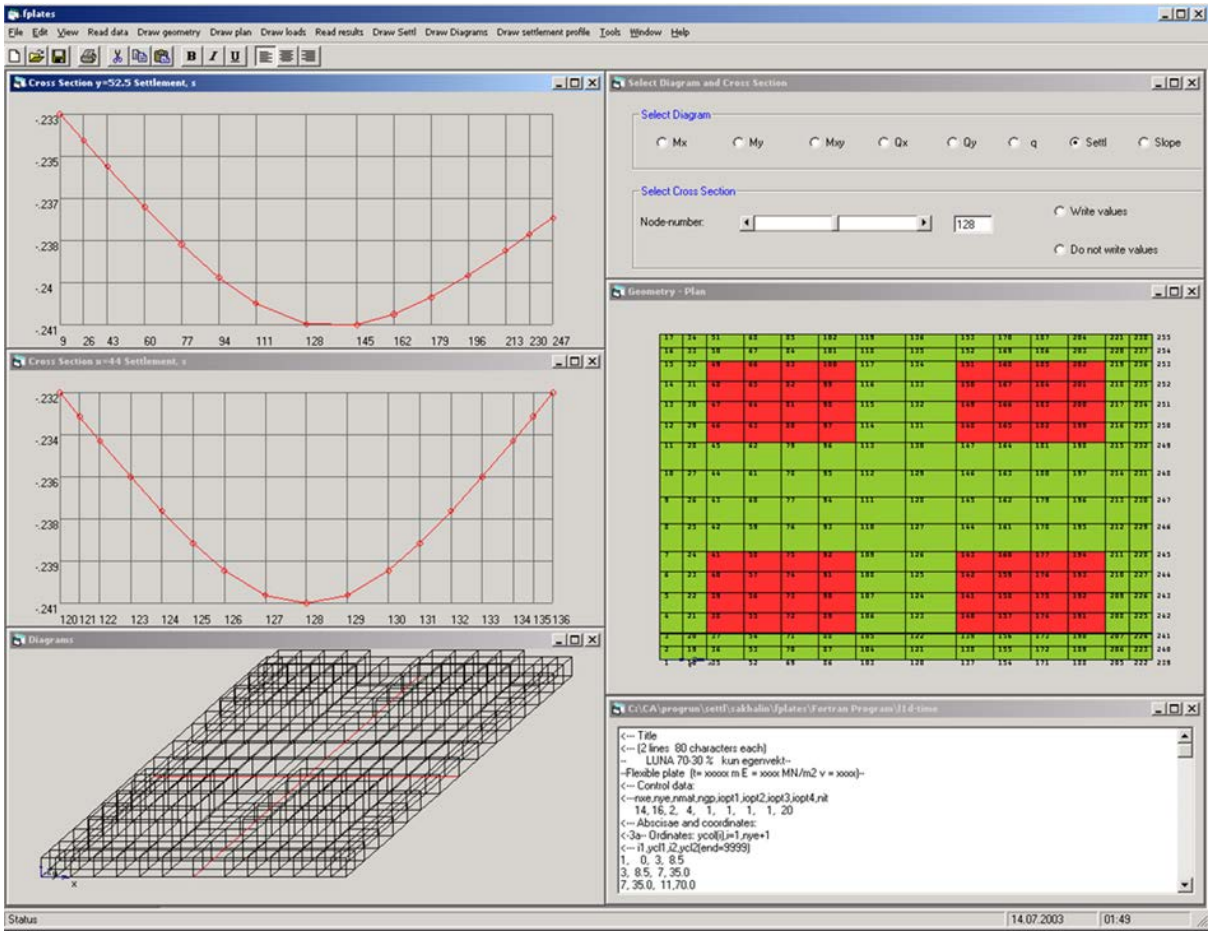

*Fig.2.25. Results from **FPLATES** analysis.*

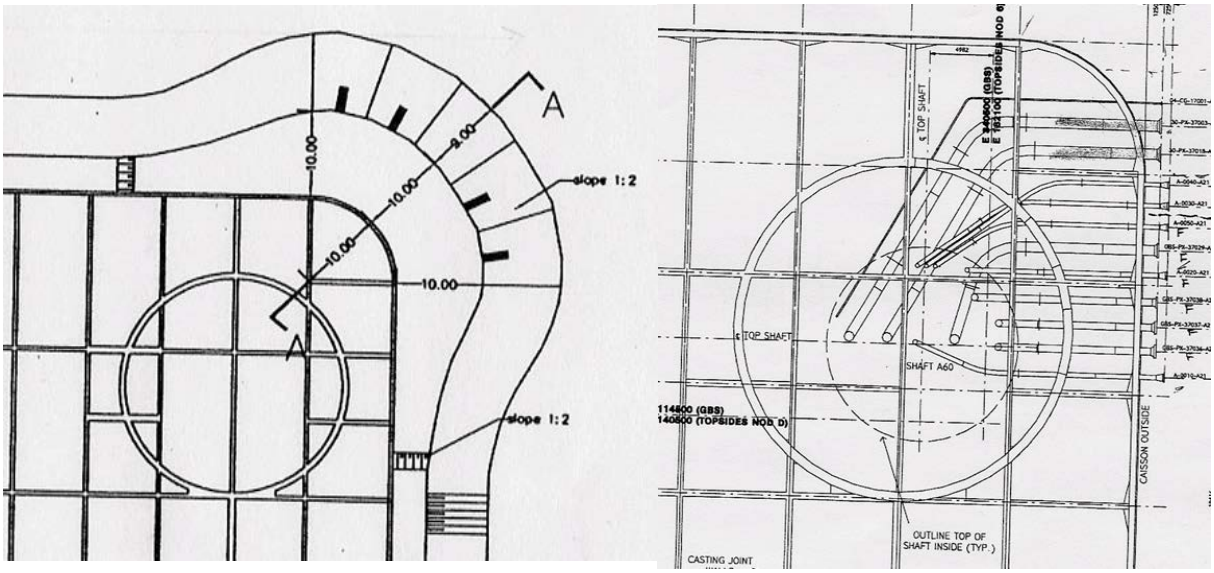

Fig.2.26. a/Detail of scour protection rock fill (left) and b/pipes entering the edge of the platform slab (right).

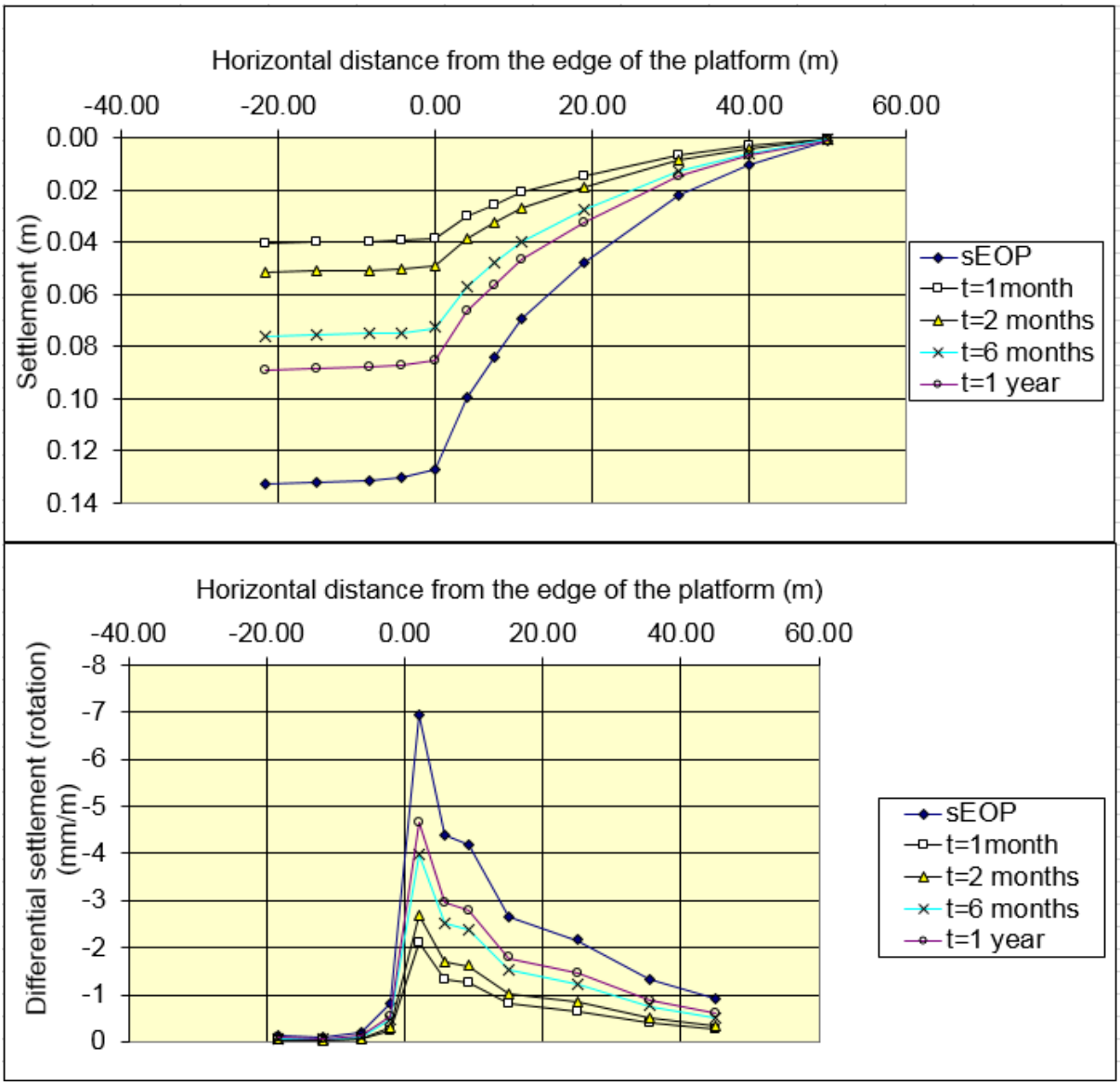

Fig.2.27. a/ Profiles of settlements (upper part) and b/ profiles of differential settlements (lower part).

ROCK FILL SETTLEMENTS

Simplified method for calculation of creep and elastic settlements of the rock fills.

Rock fills are widely used to ensure a proper foundation ground for large industrial plants, airports and other structures were very strict tolerances are required for the magnitude of settlements and differential settlements. With these v very strict requirements (allowable settlements within few centimeters,

allowable differential settlements within few millimeters per meter) for the whole lifetime of the structures, the estimation of elastic and particularly of creep settlements of the rock fills becomes a crucial issue in the foundation design.

It is well recognized and illustrated by settlement measurements of rock fills that the grain structure of such fills does not react instantaneously to changes in stresses

although there is no time lag caused by the dissipation of excess pore pressures.

The study of creep settlements in rock fills shows (as illustrated in Fig.3.1) that there is an initial phase where settlements increase with log time along a "S-shaped" curve (diffusion phase) and a subsequent phase where settlements increase linearly with log time (linear phase), see for instance Marshal, (Marsal, 1973).

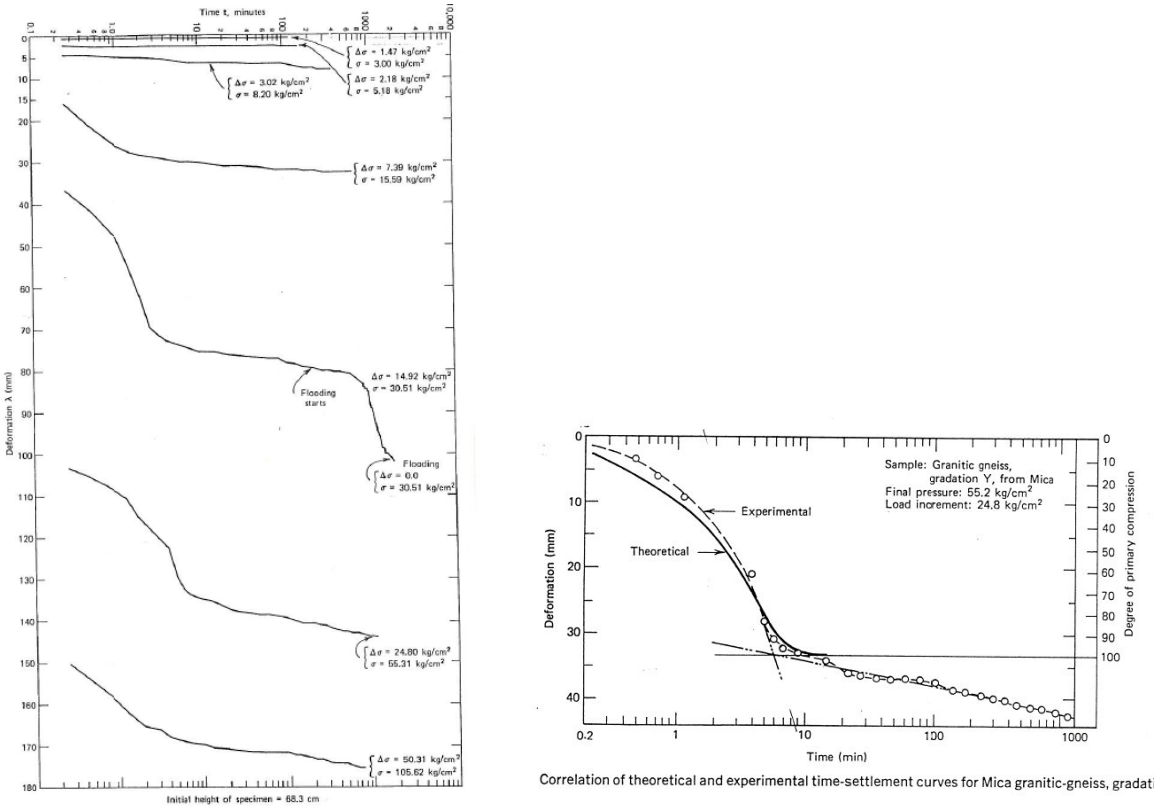

Fig.3.1. Typical oedometer compression-time curve for Mica granitic-gneiss (after Marsal, 1973)

The “S-shape” curve observed in settlement-time curves of rock fills is attributed to the presence of high contact stresses between corners of neighbouring particles (red points in Fig.3.2). At some of the contact points, where the contact stresses exceed the strength of the material, failure occurs and as a result, due to contact flattening and rearrangement of particles, some deformation takes place (blue points in Fig. 3.2). The unbalanced contact force at the contact carrying originally high stresses is redistributed to the neighbouring contacts, in-creasing their stresses which, in turn, may become larger than the material strength and cause new deformation increments. The process continues towards a more uniform distribution of contact stresses between particles. The number of unbalanced contacts will, however, decrease as the redistribution process goes on and the deformation increments will be smaller and smaller (linear phase in log time plot, Fig.3.2).

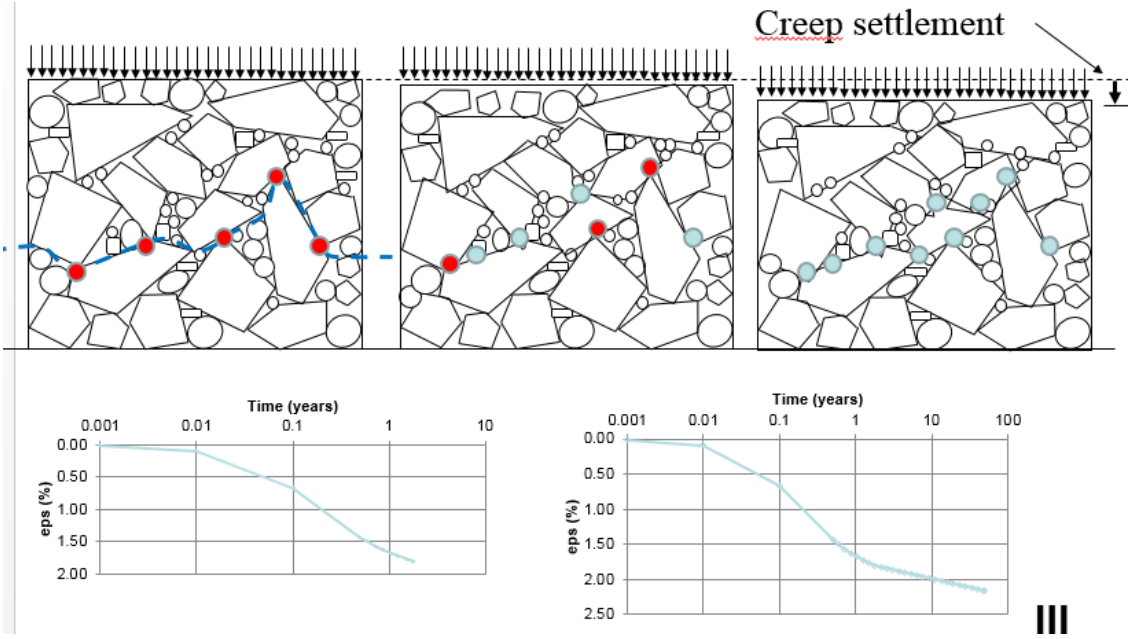

Fig.3.2. Phases of creep in rock fill

The settlement magnitude and rate depend on the size, shape and constituent material of the particles as well as on the applied stresses (both mean and deviatoric stresses).

Marsal (Marsal, 1965) analyzed the process by stochastic methods and found the process is governed by Fokker-Plank diffusion equation. A simplified finite element method to describe the creep settlements of rock fills was developed as described in Appendix 5.

In connection to foundation detail design at three large On-shore Plants on rock fills in Norway, including Kollsnes Onshore plant, Hammerfest LNG Terminal and Ormen Lange LNG, the calculation of elastic and creep settlements of large number of foundations constructed on or in the rock fill, subjected to different loads and interacting with each other required 3-D settlement analyses. A simplified method was derived using theoretical assumptions described in Appendix 5. The method calculates the settlements by summing up the vertical creep strains in the rock fill along vertical lines. The stresses distribution along vertical lines from foundation loads are calculated using the Theory of Elasticity and are supper-posed to the stresses form own weight of the fill. The simplified 3-D procedure is described as follows.

The linear creep settlement of a point in or on the rock fill can be estimated as:

$$s_{cc} = \beta \cdot s_f \cdot A_\sigma \cdot \log_{10}(\frac{t}{t_o}) \qquad (3.1)$$

where: scc– creep settlement during linear phase (linear increase of settlement with log time); β - creep parameter for rock-fill material; sf – slope factor:

$$s_f = 1 + \frac{\tan\alpha}{1+\tan^2\alpha} \cdot (1 - K_o) \qquad (3.1a)$$

α -the slope of bed-rock; ko – earth pressure coefficient at rest; A σ - area of the effective vertical stress under the level of observation and down to the bed-rock; t- the time elapsed from the completion of the rock-fill up to observation level; to- reference time;

The diffusion creep settlement is calculated as:

$$s_{cd} = \frac{2\beta_o}{c} s_f \cdot A_\sigma \tan^{-1}\left[e^{c \log\left(\frac{t}{t_m}\right)} \right] \quad (3.2)$$

The ratio between diffusion settlement and the settlement along the creep line for the same time, is defined as the "degree of diffusion process", R and can be calculated as follows:

$$R = \frac{s_{cd}}{s_{cc}} = \frac{2 \cdot \tan^{-1}\left[e^{c \cdot \log_{10}\left(\frac{t}{t_m}\right)} \right]}{c \cdot r_t \cdot \log_{10} \cdot \left(\frac{t}{t_o}\right)} \quad (3.2a)$$

where: c and rt – constants (rt is the ratio between the creep parameter, β, and maximum slope of diffusion curve (at inflection point), βo; tm – the time corresponding to inflection point on diffusion settlement curve; The method is incorporated into a computer program, ROCKFILL, to calculate primary (elastic) and creep settlements of foundations on rock fills.

The parameters in equations 3.1 to 3.2a are determined by back-calculating measured creep settlements of rock fill dams and embankments as illustrated in Figs 3.3 to 3.5.

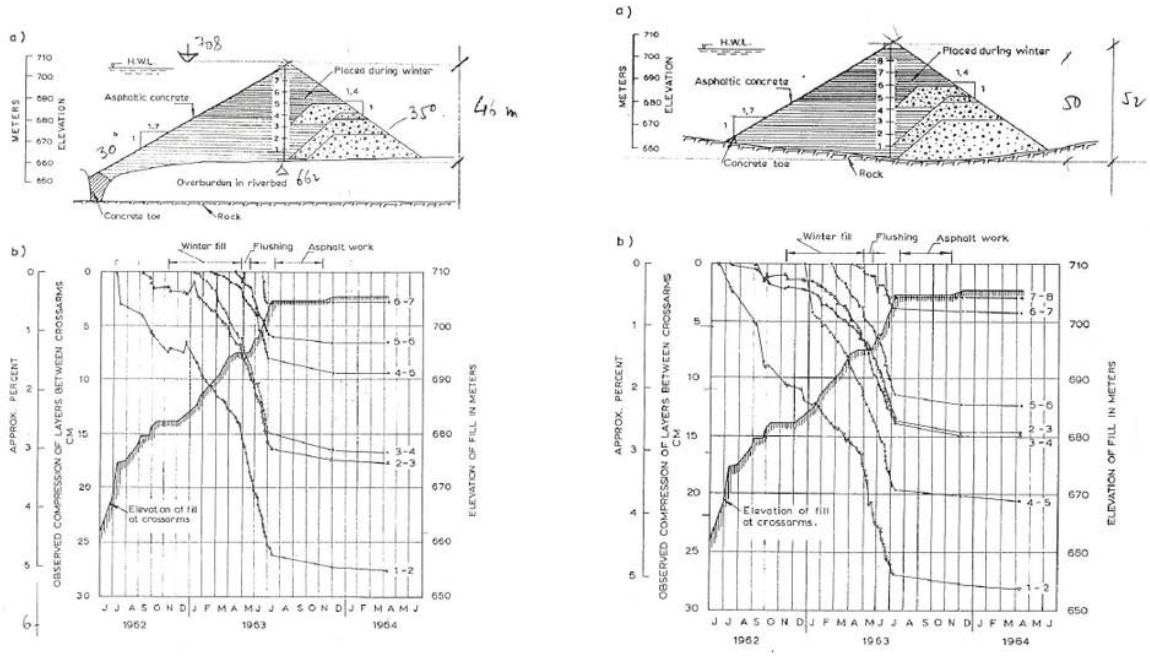

Fig.3.3. Observed settlements at two rock fill dams in Norway.

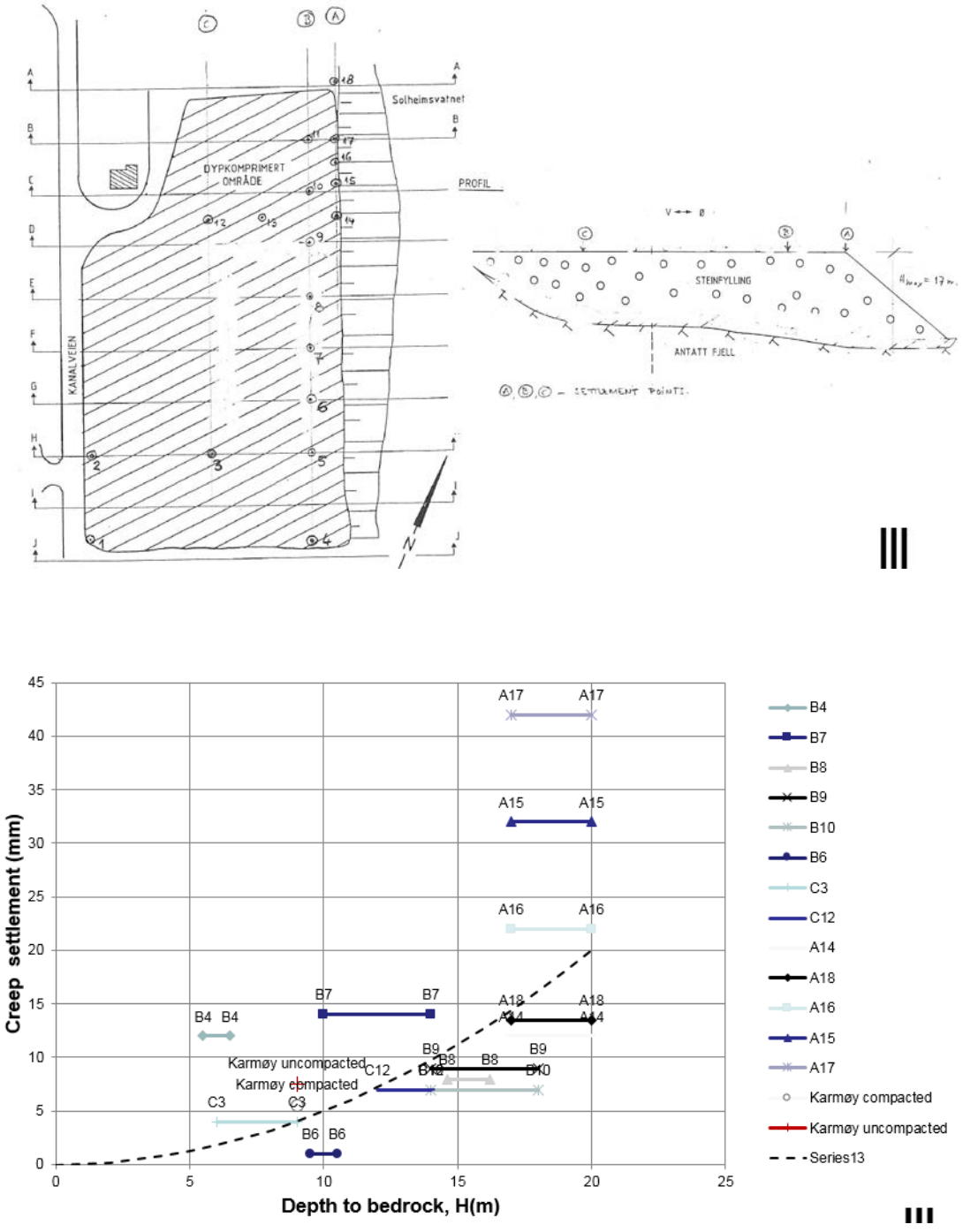

Fig.3.4. Measured creep settlements at Bergen Post Terminal rock fill.

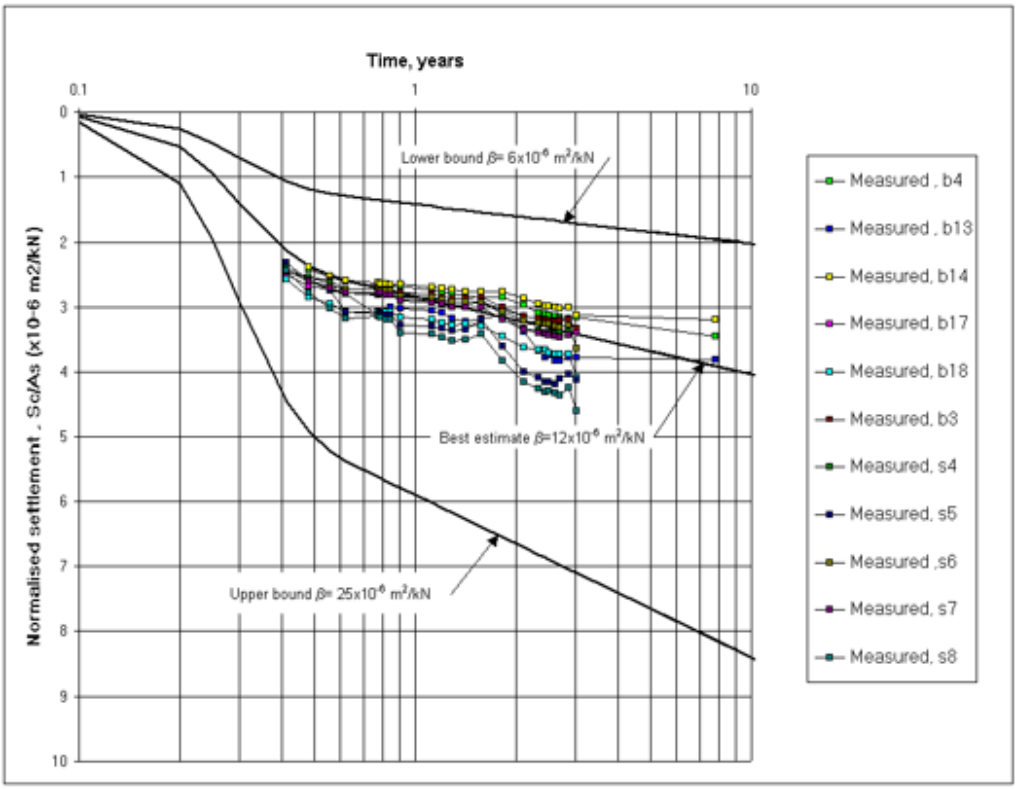

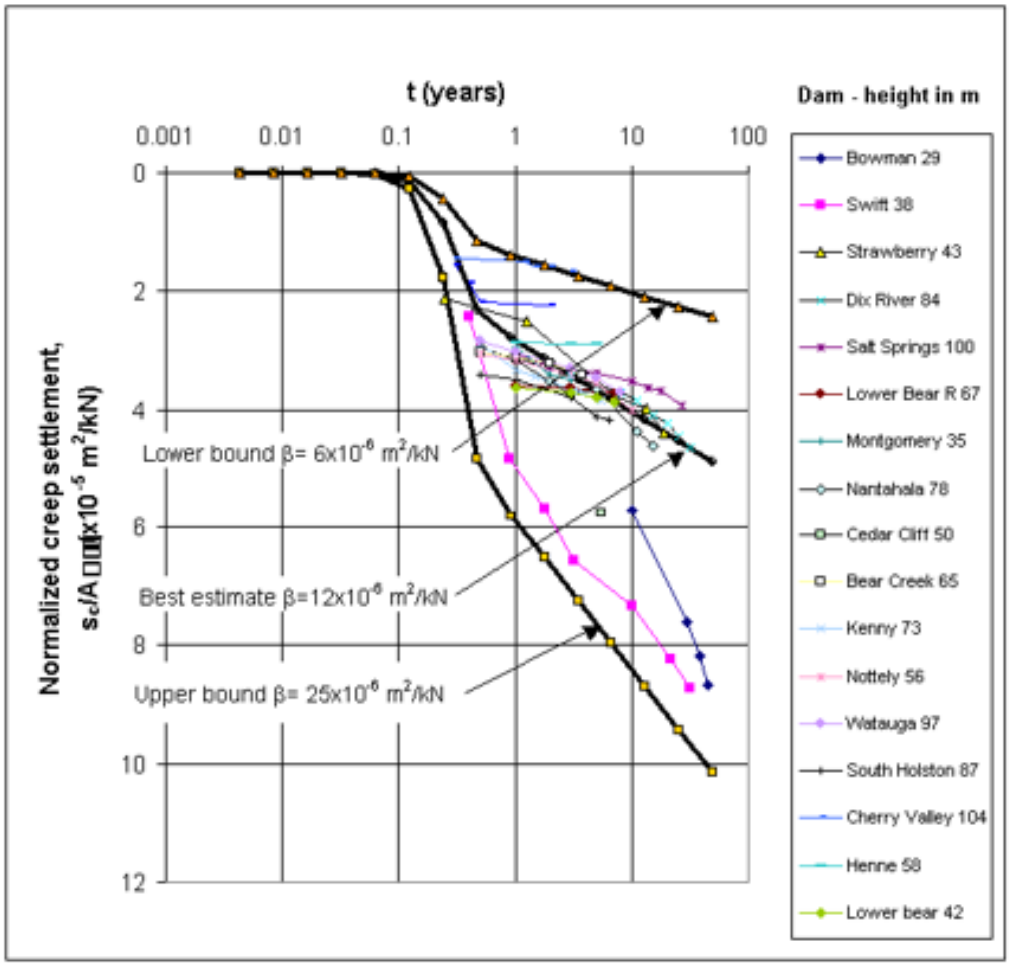

Fig.3.5. Rock fill creep parameters from measurements.

Example 5. Settlements of rock fills

Fig.3.6 shows different phases of site preparation work at Ormen Lange On-shore Plant. It results in variable depth to bed rock and consequently variations in settlements of the rock fill. When there is about 1500 foundations for which the settlements must be calculated and the differential settlements evaluated and when the installations (pipes) are very sensitive to differential settlements it is obvious that the design must perform a large amount of calculations.

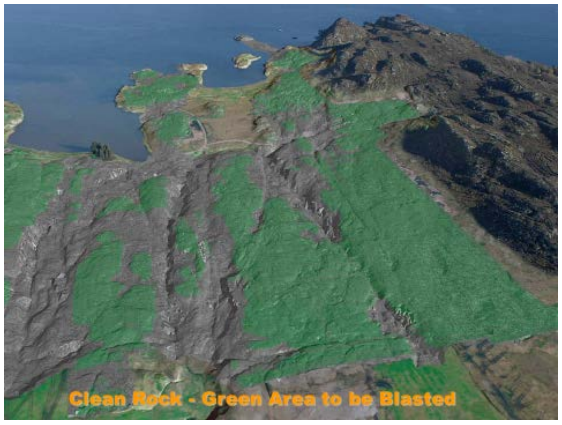

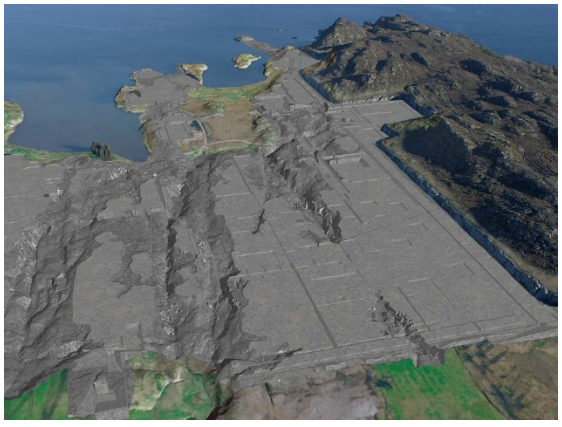

Fig.3.6. Ormen Lange On-shore Plant. Phases of Site Preparation Work.

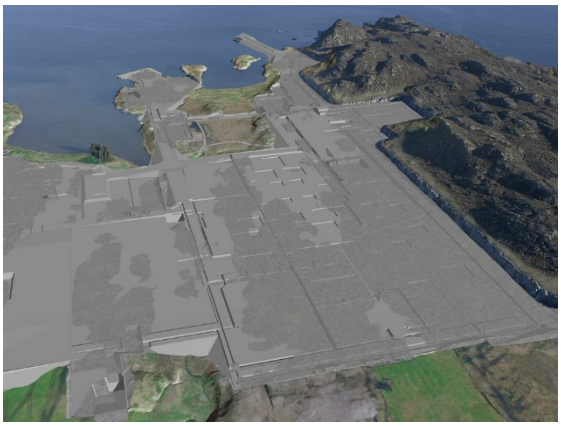

Fig.3.6. (cont.) Ormen Lange On-shore Plant. Phases of Site Preparation Work.

The Visual Basic program **ROCKFILL** was used to incorporate the simplified method for creep settlements as described in Section 3.1. It enable not only the calculation but also the presentation of the output so the user may verify the assumptions and may evaluate the results while running the program. The first task is to realistically represent the variation of the rock fill thickness and the position of the foundations. Fig.3.7a illustrates the output of depth to bedrock and foundation positions for one area of the On-shore Plant.

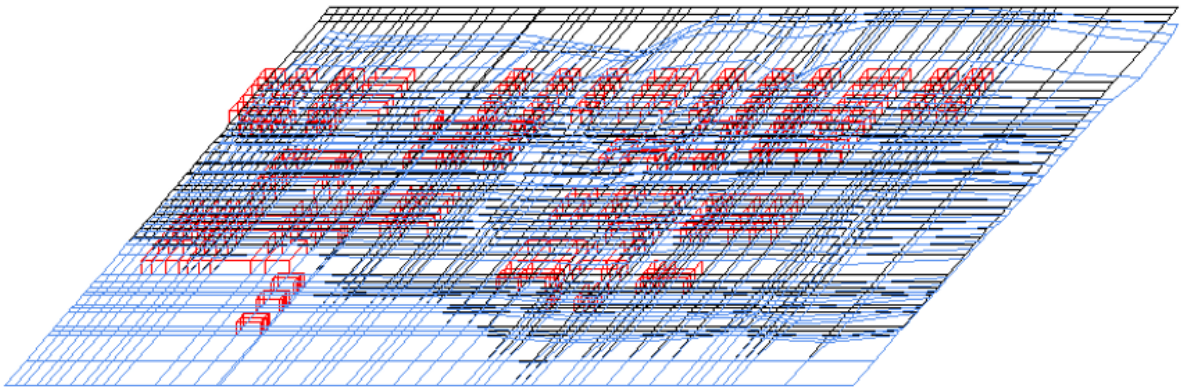

Fig.3.7.a. Depth to bed rock and foundation position.

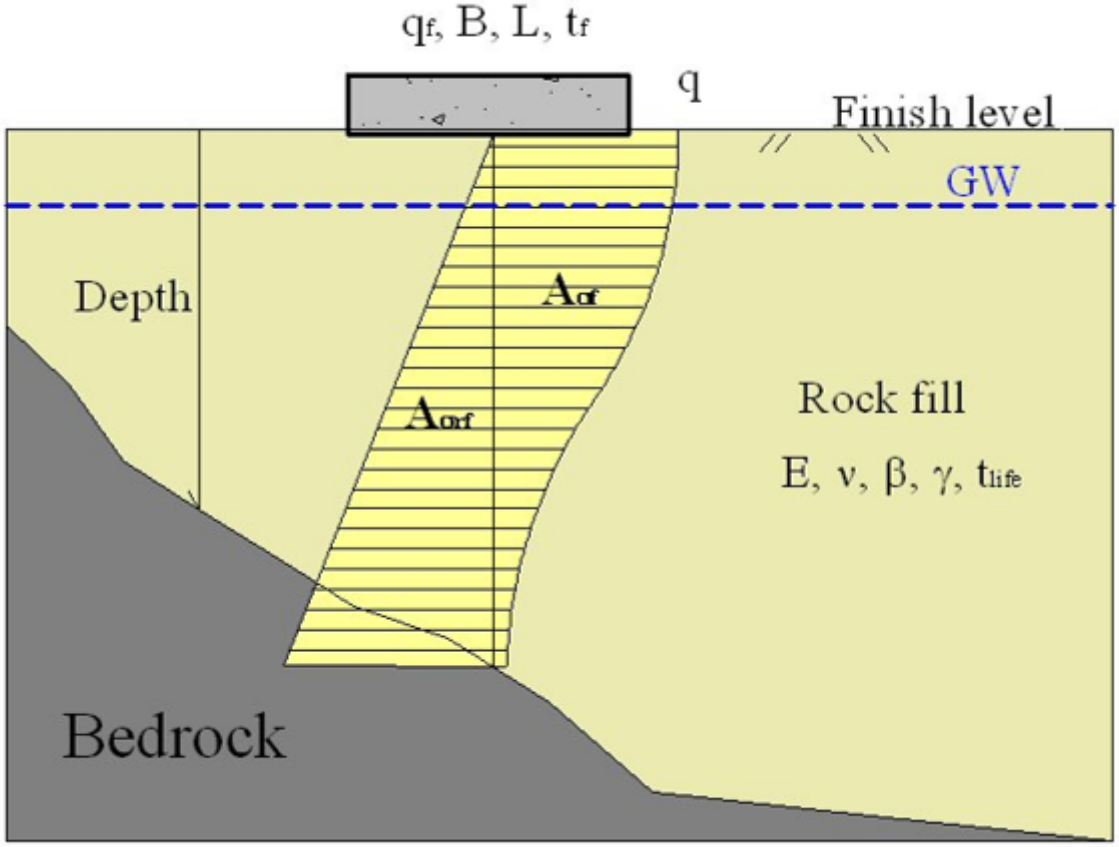

Fig.3.7.b. Input parameters for calculation of elastic and creep settlements.

Fig.3.7.b. illustrates the input parameters required for calculation of elastic and creep settlements of the foundation: for the foundation: the time of installation, t_f, from the time the site preparation is finished, the equipment load, qf, the foundation size and depth; for the rock fill: the elastic and creep parameters, the life time of the fill, the inclination of the bedrock.

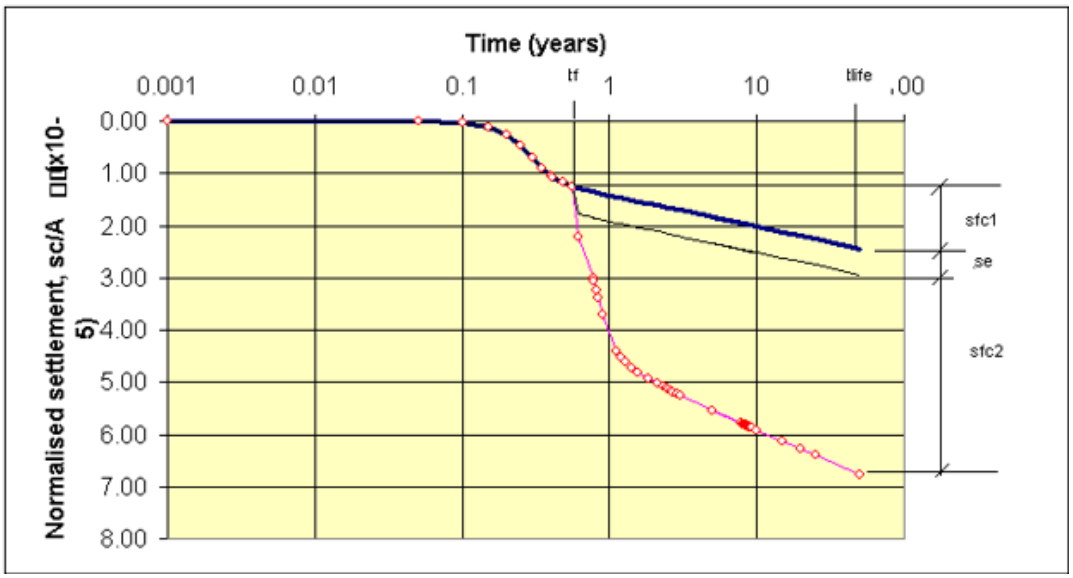

Fig.3.8. Example of results for one foundation point

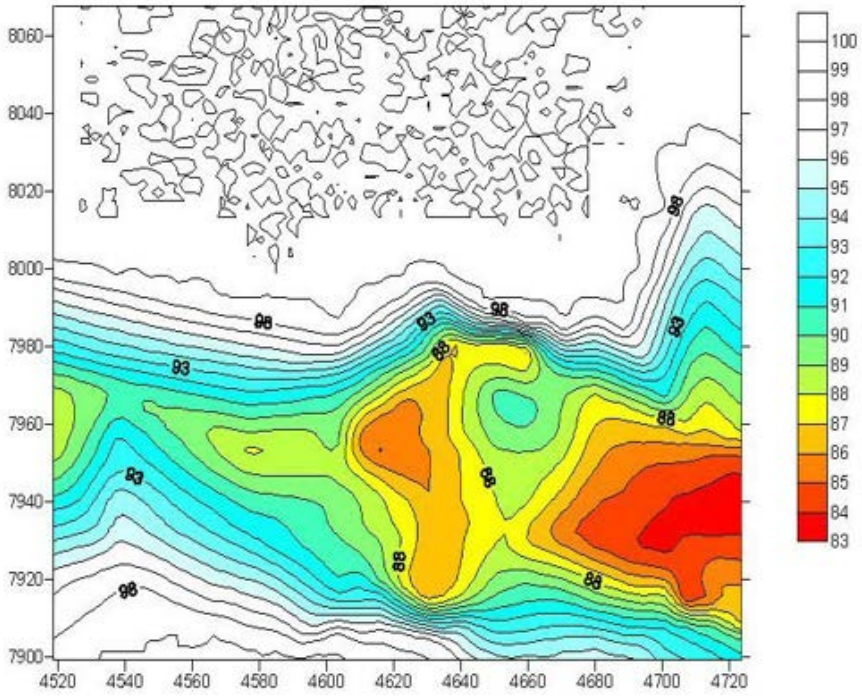

Fig.3.9. Slag Catcher Area Elevations to bedrock.

The results from analyses with the program **ROCKFILL** for one foundation location are presented in Fig.3.8. The creep settlements of the rock fill, s_{fc1}, are initiated as soon as the site preparation is finished and the fill redistribute the contact forces between particles towards a more uniform pattern. The elastic settlements due to foundation loads, s_e, starts at the time t_f when the foundation load is applied. Additional creep settlements, s_{fc2}, start also at t_f, due to the new stresses induced by the foundation.

The rock fill settlements for the whole area can then be shown as illustrated in Figs. 3.9 (bedrock elevations), 3.10 (settlement contours) and 3.11 (settlement contour together with the placement of the structures).

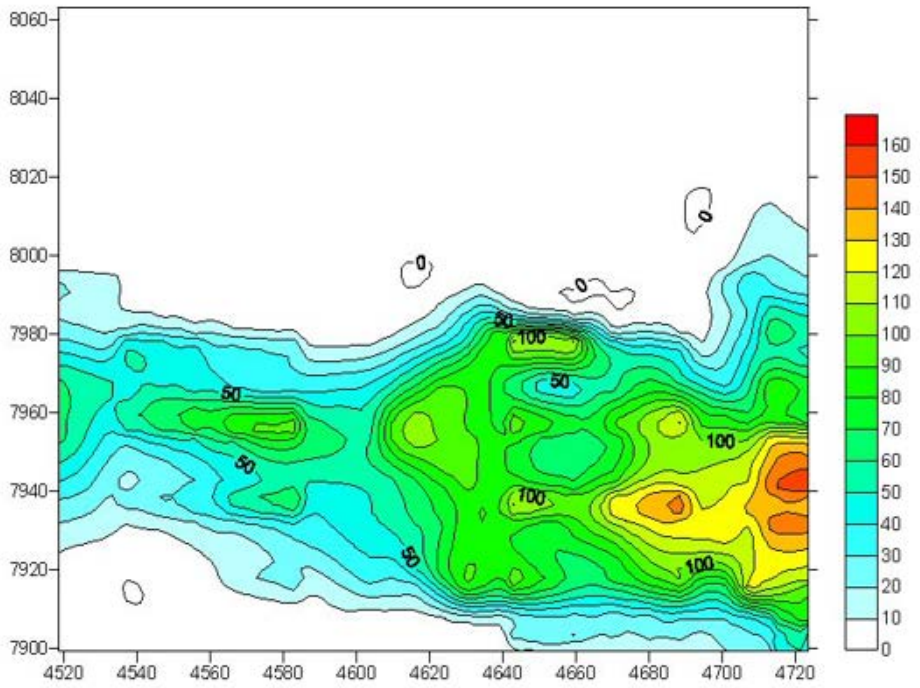

Fig.3.10. Settlements contours (mm).

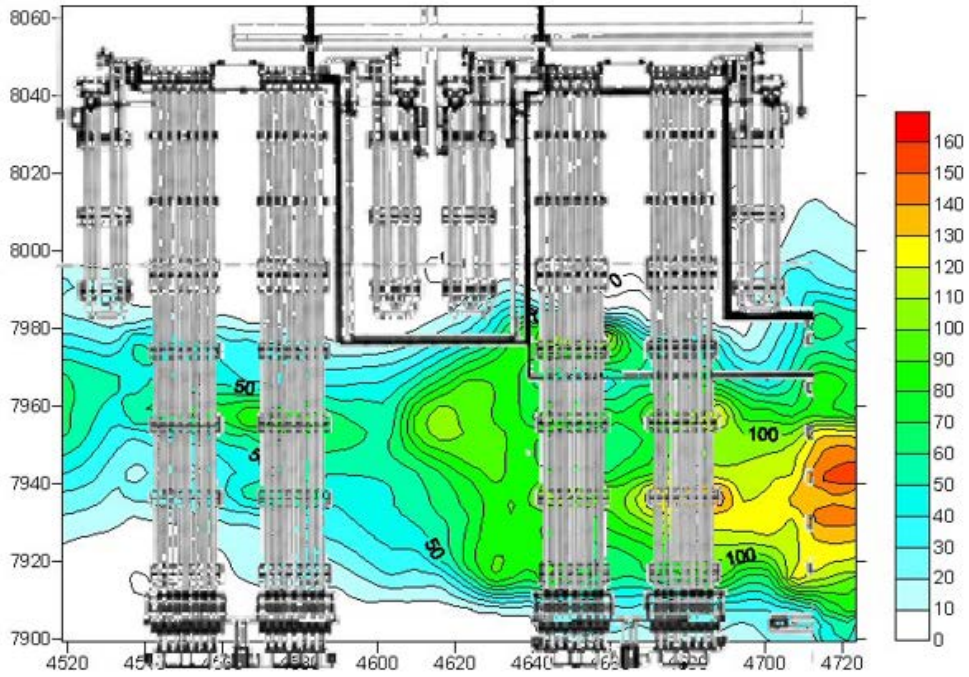

Fig.3.11. Settlement contours with the placement of structures.

CYCLICALLY INDUCED PORE WATER PRESSURES AND THEIR PARTIAL DRAINAGE

Cyclically induced pore water pressures and transient pore pressure analysis.

Cyclic loading will generally tend to break down the soil structure and cause a tendency for volume changes. In undrained conditions, the volume changes are prevented by water incompressibility leading to an increase in pore water pressures and a decrease in effective stresses. The components of cyclically induced pore water pressure and are defined by Andersen, 2009, 2015, Fig.4.1.

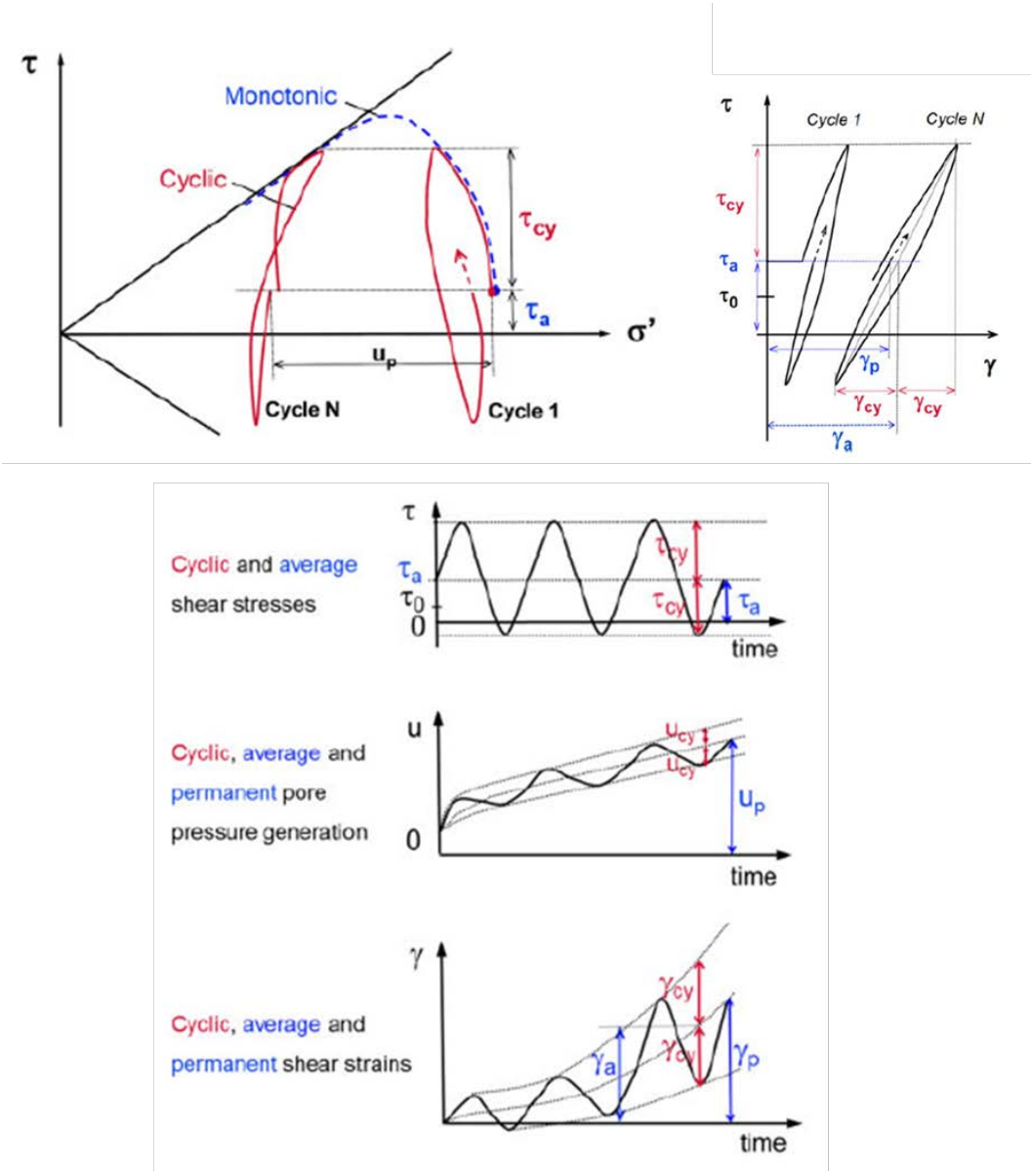

Fig.4.1. Definition pore water pressure and strain components induced by cyclic shear.

Pore water pressures and strains developed during cyclic loading are measured in the laboratory tests, as illustrated in Fig.4.2.

These contour diagrams are used to quantify the cyclic degradation of soil shear loading event such as the wave loading during a storm or earthquake loading.

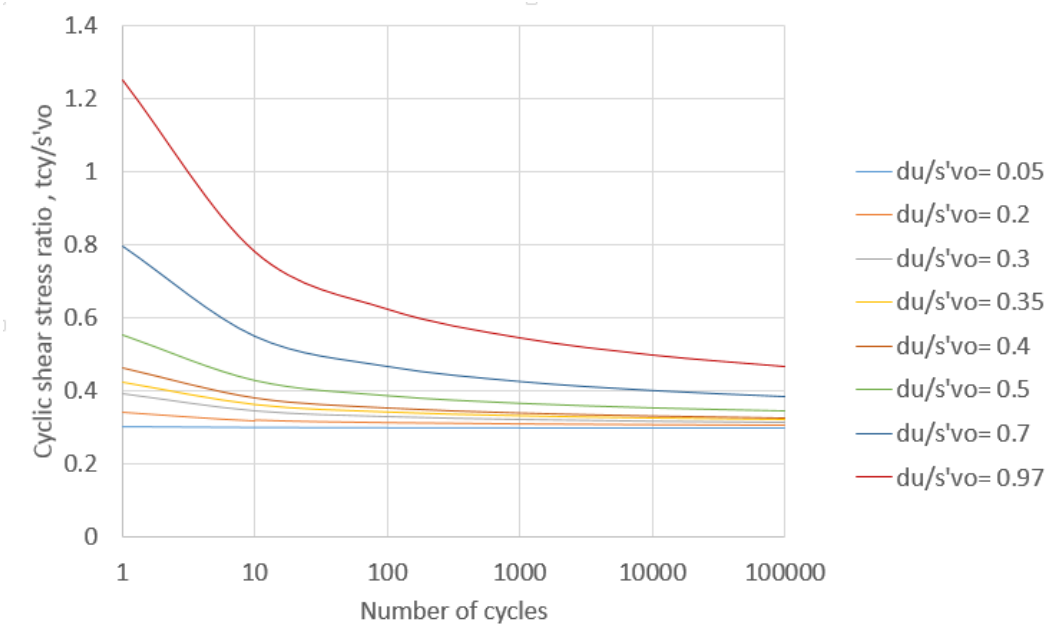

Fig.4.2. Contours of permanent pore pressure measured during cyclic shear test (example).

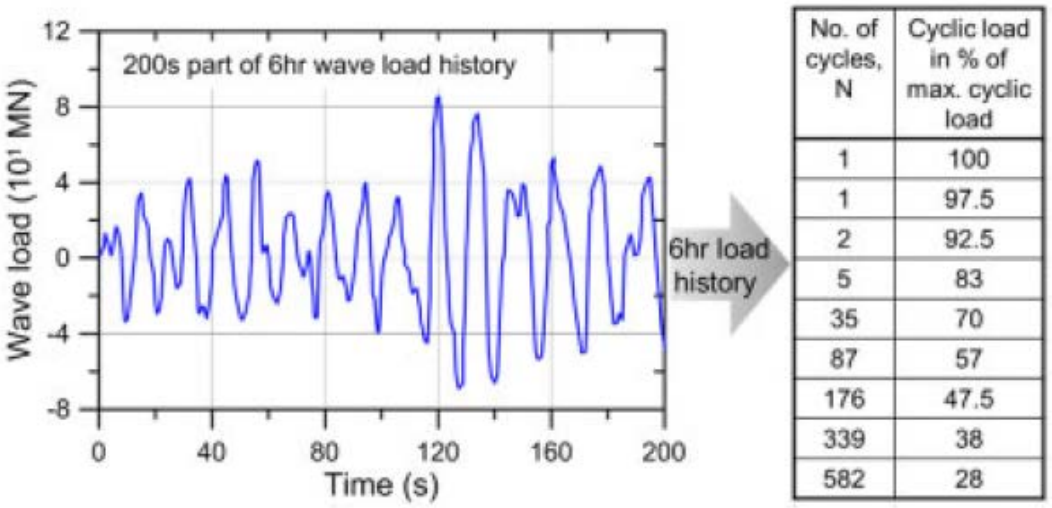

No. of cycles, N	Cyclic load in % of max. cyclic load
1	100
1	97.5
2	92.5
5	83
35	70
87	57
176	47.5
339	38
582	28

Fig.4.3. Actual load history and ordering the loads in batches of equal amplitude (from Andersen, 2015)

Cyclic wave loading during a storm or due to earthquake event consists of cycles with different amplitudes and frequency (periods). If it is assumed that, the permanent pore water pressure generated during the storm is not affected by the order in which the cycles are applied, then the storm can be divided in batches of cycles with the same amplitude starting from the lowest to the highest amplitude (as illustrated in Fig. 4.3).

In order to find the pore pressure development with time during a storm, an accumulation analysis is performed. The accumulation procedure assumes that the pore pressure at the start of one cycle is the same as the pore pressure at the end of

previous cycle. The accumulation analysis is exemplified in Fig.4.4 using the simplified storm history from Fig.4.3.

To each point at the intersection of the load history cyclic stress path with one pore pressure contour corresponds a permanent pore pressure ratio, $\frac{\Delta u_p}{\sigma'_{vo}}$, and a number of cumulative cycles, which multiplied by their period will give the corresponding time from the start of the storm. The undrained permanent pore pressure development in time is shown in Fig.4.5.

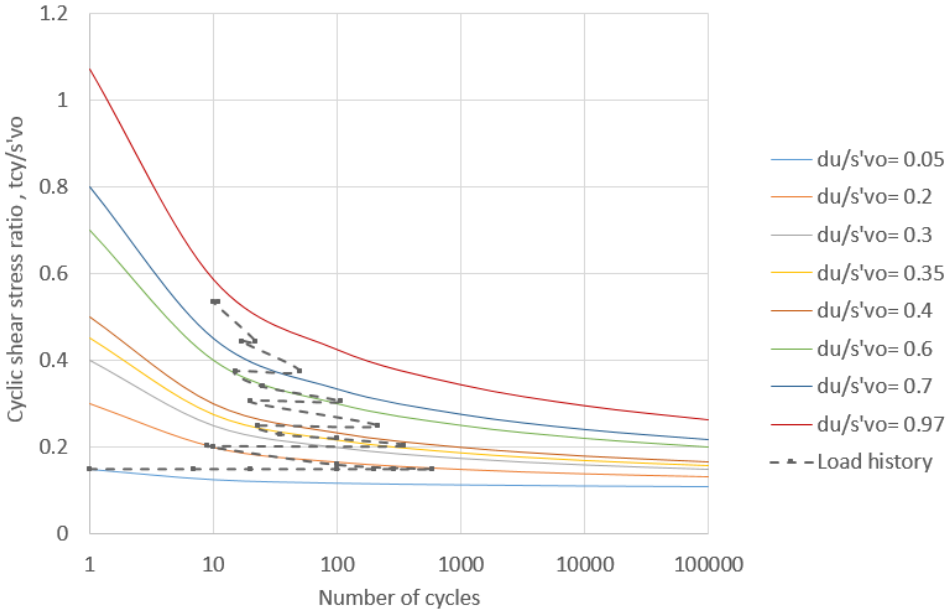

Fig.4.4. Accumulation of permanent pore pressure (undrained conditions).

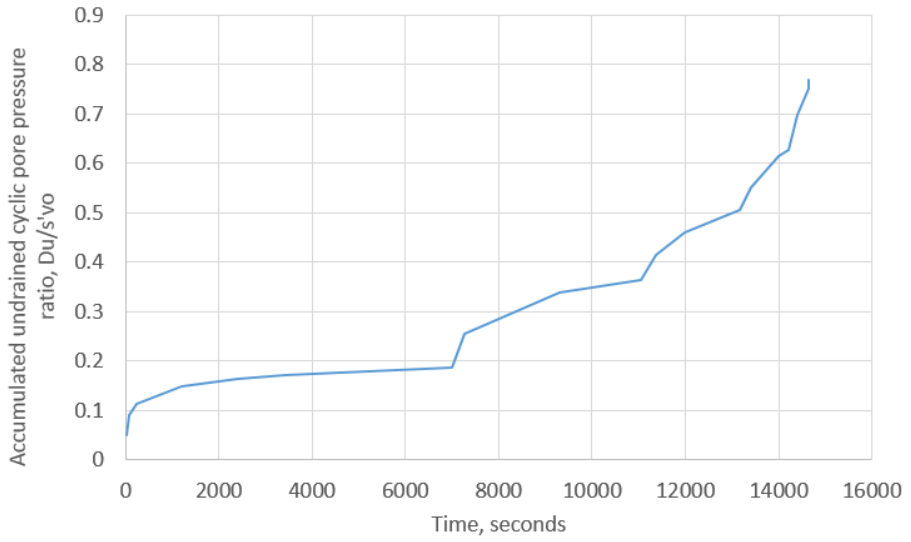

Fig.4.5. Undrained permanent pore pressure development.

Depending on the soil permeability and of the rate of the pore pressure generation during cyclic loading, partial drainage may occur simultaneously with the pore pressure generation. Partial drainage of the permanent pore water pressure will reduce the shear strength and stiffness degradation as the effective stresses will be higher at the end of cyclic loading with partial drainage than at the end of undrained cyclic loading. This is particularly important for accumulated permanent pore pressure due to the wave loading during a storm of several hours for both clay and sand, or for permanent and cyclic pore pressure in silt and sand with higher permeability than that of the clays. It is therefore important to perform a pore pressure dissipation analysis in order to quantify the effect of partial drainage. Most rigorously, the pore pressure dissipation can be determined in finite element consolidation analyses, but difficulties arise from the fact that constitutive relations for soils must be based on the observed behavior under **cyclic loading** which requires advanced models and parameters.

A simplified method for transient pore pressure analysis is developed and incorporated into a computer program, **CYCPORE2,** Athanasiu (1992).

It is based on the parabolic differential equation of consolidation with transient load:

$$\frac{\delta u}{\delta t} = \beta \cdot \nabla^2 u + f_e(x, y, t) \qquad (4.1)$$

Where: $\nabla^2 = \frac{\delta^2}{\delta x^2} + \frac{\delta^2}{\delta y^2}$ for the plane strain case; the function $f_e(x,y,t)$ is the excitation rate function (the increment of undrained pore water pressure during the time interval, δt, and at a point with co-ordinates x and y in the soil volume. The program enables modelling the excitation rate function as a product of the amplitude of the undrained permanent pore pressure ratio, $\Delta u/\sigma'_{vo}$ as a function of co-ordinates x and y in the soil volume and the derivative of an excitation function, f(t), as illustrated in Fig.4.5. The excitation function can be a periodical (harmonic or non-harmonic), or an irregular unit load (varies from 0 to 1) in time. Both, $\Delta u/\sigma'_{vo}$ and f(t) are read as input by the program CYCPORE2 and the excitation rate function is calculated at each time step and element in the transient analysis:

$$f_e(x, y, t) = \frac{\delta f}{\delta t} \cdot \frac{\Delta u_p}{\sigma'_{vo}}(x, y) \qquad (4.2)$$

The equation (4.1) is solved in finite differences and the pore pressure dissipation is calculated at the centre of each element, for each time step, δt.

The excitation function can be specified for different regions in the soil volume.

When using the excitation function with CYCPORE2, care must be taken to enter most conservative excitation function. A time shifting technique is developed to provide the most dangerous time history of the storm, as explained in Fig.4.6. The original excitation function in undrained conditions is denoted as f(t) and is constructed by assuming that the waves in batch 2 come after all the waves in batch 1 have passed over the structure. The line $\mathbf{f(t)_{diss.\,1}}$ is the pore pressure ratio function corresponding to the remnant pore pressure, when dissipation and generation of pore pressure takes place simultaneously. The curve $\mathbf{f(t)_{diss.1}}$ show a maximum value at approximately t=1200 s. (point **A**) and decreases after this time all the way to the end of the batch 1 time. If the transient analysis is continued with the original excitation curve, the dissipation curve will start to increase immediately after the start of batch 2 and a new peak value of the remnant pore pressure will appear after the start of batch 2. As there no restriction on the order of appearance of the waves, the batch 2 of waves is shifted, in time, from

point **B** to point **C**, to occur immediately after the time of maximum remnant pore water pressure from batch 1. The new, shifted excitation curve is $\mathbf{f(t)_{shift}}$. The use of this time shifting technique will produce the next peak on the remnant pore water pressure curve ($\mathbf{f(t)_{diss.2}}$), which will be higher than the second peak from original excitation.

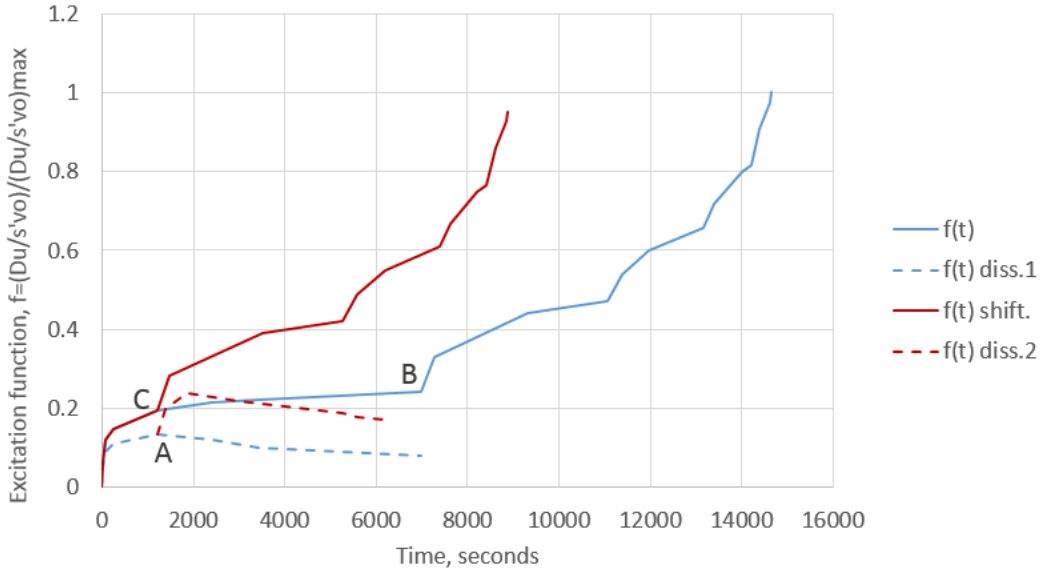

Fig.4.6. Time shifting technique to ensure conservative evaluation of remnant pore pressure after partial drainage.

Example 6. Pore pressure transient analysis for the top sand layer at platform Sakhalin LUN-A (Hamre et al. 2005).

MULTICONSULT AS has been engaged by AkerKværner to study the geotechnical stability of two concrete platforms to be installed outside the Sakhalin Island (Fig.4-7). The description of the analyses performed for LUN-A platform is found in Hamre et al., 2005.

Fig.4.7.Sakhalin Island

The soil conditions at the LUN-A field consists of an approximately 1 m thick loose to medium dense sand layer overlying overconsolidated clay (Fig.4.8).

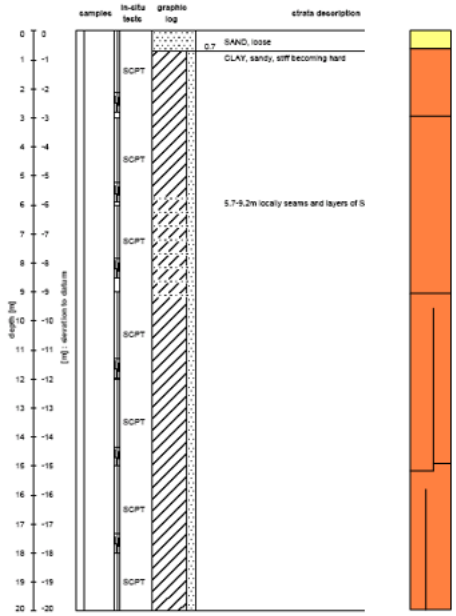

Fig.4.8. Soil conditions at LUN-A location.

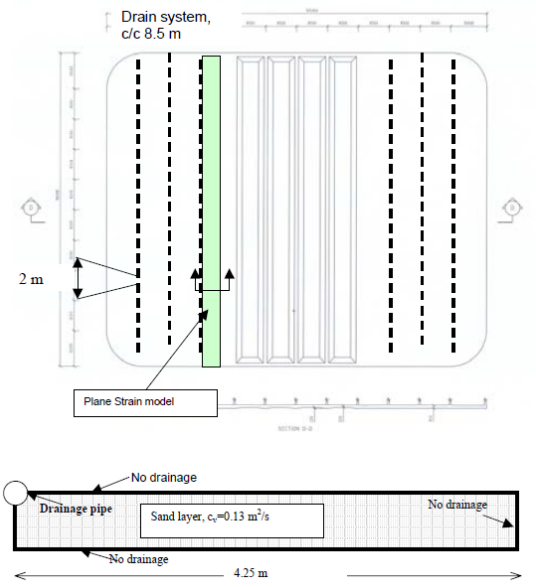

Fig.4.9. Foundation model.

The concept solution from the feed phase consisted of a bottom plate with 2 m deep steel skirt in order to transfer the loads to the over consolidated clay. The skirts were placed in a dense grid in order to ensure a proper transfer of the horizontal loads. The skirts were included as pore pressure development from cyclic loading in the sand layer was considered to be a problem. During the preliminary stages of the detail design, it became obvious that the skirts lead to numerous practical and economical challenges, and other solutions were considered. The final foundation design includes a bottom slab rib system and a soil drainage system that will ensure pore pressure dissipation in the sand layer during cyclic loading. The drainage consists of drainage pipes, with c/c 8.5 m. The dissipation of the permanent pore water pressures build up during the design storm was calculated by a transient pore pressure analysis with program CYCPORE2. The foundation model is shown in Fig.4.9. Due to symmetry, only one 4.25 m long zone, adjacent to the drainage pipe, is analyzed in plane strain conditions.

Table 4.1. Cyclic shear stress history.

Cycle N	τ/σ_a'	Period T [s]
1	0.22	12
2	0.21	12
4	0.20	12
8	0.18	12
15	0.17	11
30	0.16	11
50	0.15	10
90	0.13	9
200	0.11	8
500	0.09	7
900	0.05	5

The governing situation for the generation and dissipation of permanent pore water pressure was found to be the first winter 10 years storm, with no top side load for which $\tau_{cymax}/\sigma'_{vo}$=0.22. The 6 hour Hansteen storm history is transformed in cyclic shear stress history (Table 4.1.).

The undrained excitation function is found by accumulation analysis, using the pore water pressure contours from DSS cyclic shear tests for LUN-A (Fig.4.10).

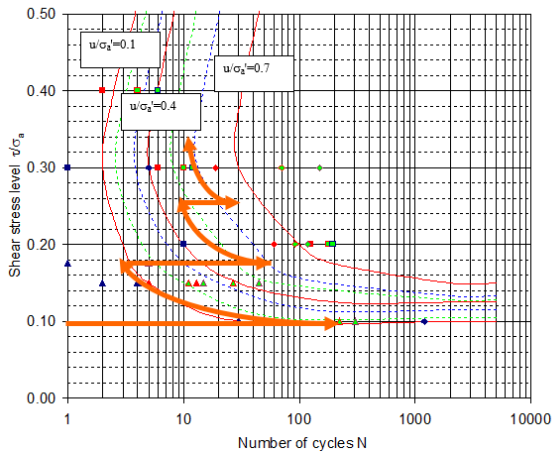

The pore pressure dissipation at different stages of the transient loading, as resulted from CYCPORE2 runs is illustrated in Fig. 4.11.

The accumulated permanent pore water pressure stress path including partial drainage, after applying the time shifting technique is shown in Fig.4.12.

Fig.4.10. Accumulation of permanent pore water pressures.

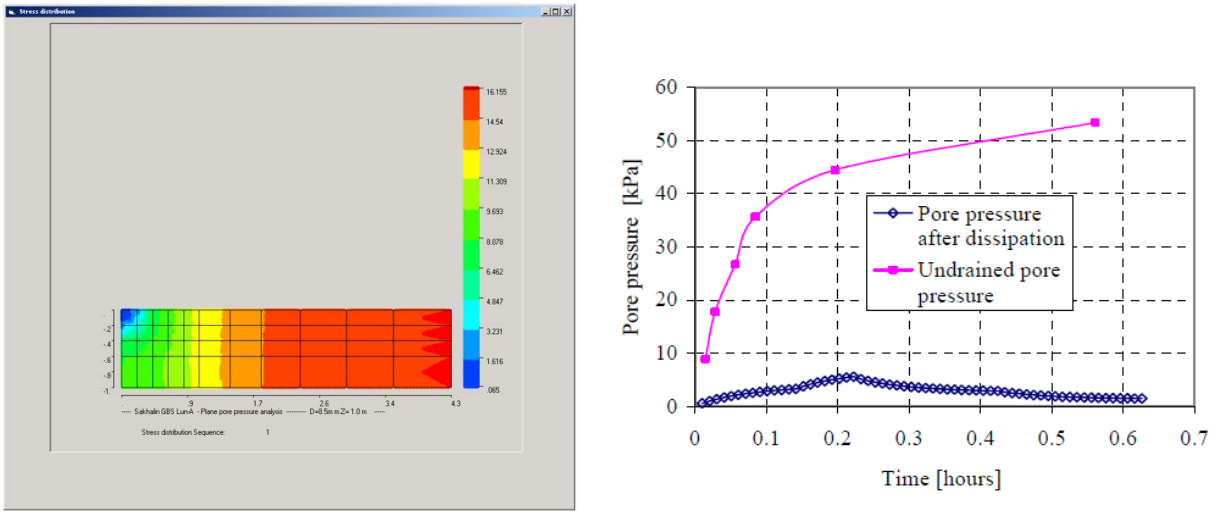

Fig.4.11. Results from CYCPORE2 analysis. Permanent pore pressures with partial drainage (left). Typical pore pressure development after 900 cycles (right).

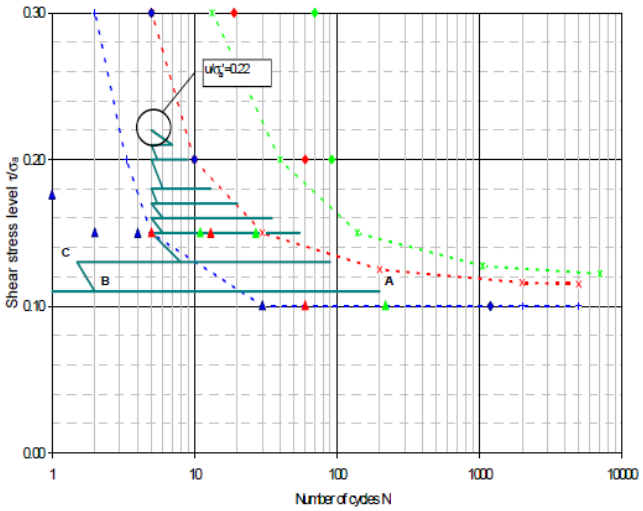

Fig.4.12. Accumulation stress path including partial drainage.

The transient analyses performed with the simplified model in CYCPORE2 have shown that the safety against sliding due to cyclically induced permanent pore water pressures is satisfactory when partial drainage is considered and the solution without skirts could be used.

SOIL STRUCTURE INTERACTION

Soil structure interaction analysis is always an issue of interest in geotechnical design either inland or offshore. This is because the actual soil reactions on a structure depend on the relative flexibility of structure and soil and on their interaction. Even if the structure is stiff, the soil reactions depend on the degree of mobilization of soil response capacity against different parts of the structure. One of the simplified models used in Multiconsult is the discrete element method in which the structure is divided into a number of rigid macro-elements. Each macro-element has a defined form, plan or circular, and a defined position in the soil mass (Fig.5.1).

The macro-elements are rigidly connected to the structure centre. The soil reactions are modelled by non-linear springs. The macro-elements are divided in elements and each element is supported by three non-linear springs, one normal and two tangential to the element plane. As the structure is rigidly connected to the structure centre, the equilibrium equations can be written in terms of six unknown displacement components at the centre of the structure. The simplified method uses a variable secant modulus technique. It is based on stiffness degradation expression that fits the measurements, Athanasiu (1993), Fig.5.2:

$$\frac{K}{K_{\max}} = \left[1 - c_1 \cdot \tan^{-1}(\exp(c_2 \cdot \log(\frac{\delta}{\delta_i}))\right] \quad (5.1)$$

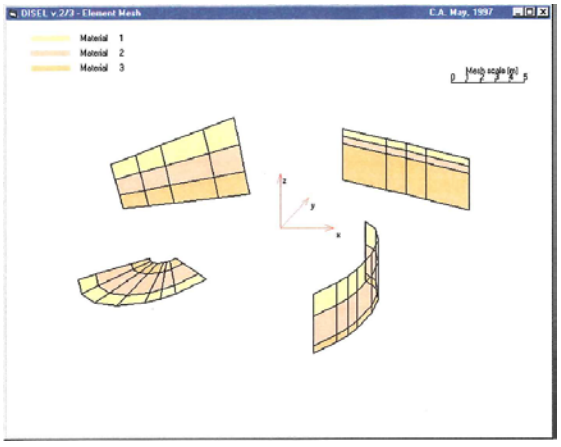

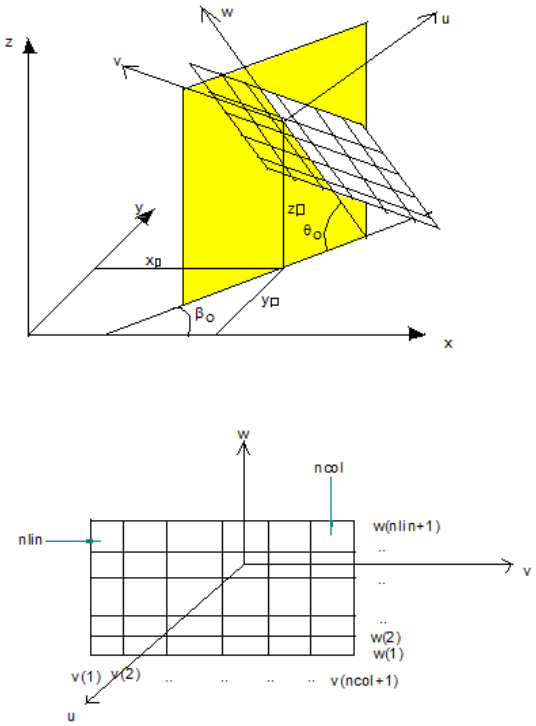

Fig.5.1. Types of macro-elements (left) and global and local co-ordinates of a macro-element (right).

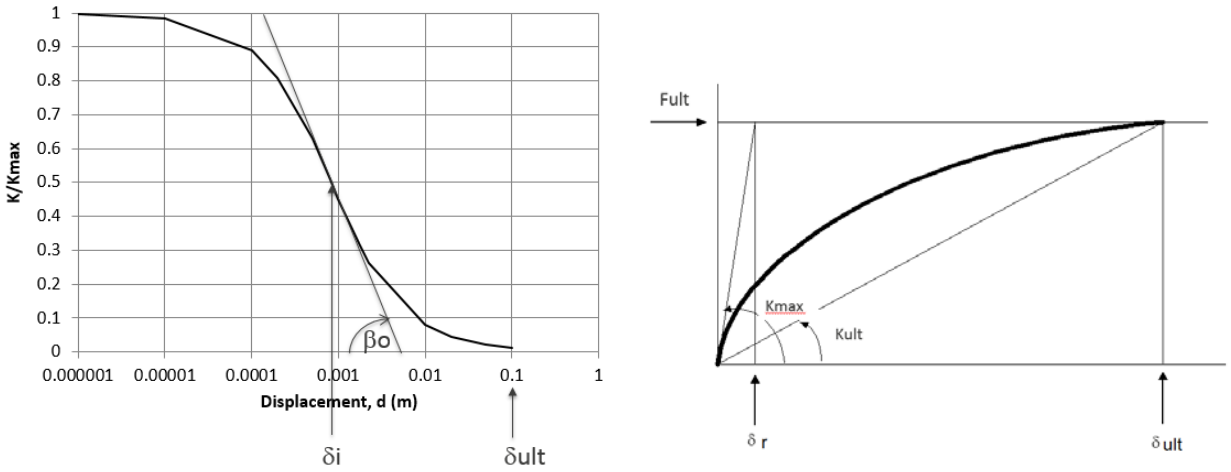

Fig.5.2. Stiffness degradation (left) and force-displacement curve (right).

The resulting force-displacement relationship is :

$$\frac{F}{F_{ult}} = \frac{\delta}{\delta_r} \cdot \left[1 - c_1 \cdot \tan^{-1}(\exp(c_2 \cdot \log(\frac{\delta}{\delta_i})) \right] \quad (5.2)$$

where δ is the displacement; δ_i is the displacement at the inflection point of K/K_{max} vs log (δ) curve; δ_r is reference displacement (Fig.5.2.right); β_o is the slope of stiffness degradation curve at inflexion point; c_1 and c_2 are constants determined from the conditions that, at failure, $\delta = \delta_{ult}$ and $K=K_{ult}$:

$$c_1 = \frac{1 - \frac{K_{ult}}{K_{max}}}{\tan^{-1}(\exp(c_2 \log(\frac{\delta_{ult}}{\delta_i}))} \quad (5.3)$$

and that the slope of the curve K/K_{max} vs log (δ) at the inflection point is β_o:

$$c_2 = \frac{2 \cdot \beta_o}{c_1} \quad (5.4)$$

The method of solution is described in Appendix 5. The simplified method is incorporated into a discrete element program, **DISEL**, Athanasiu (1993).

Example 7. Use of DISEL for soil-structure interaction analyses.

Use of DISEL to study the displacements and contact stresses on different parts of foundation structure is particularly versatile when parametric studies are required in concept phases of offshore subsea structures. Fig. 5.3 shows a four caisson manifold foundation, modelled with discrete elements.

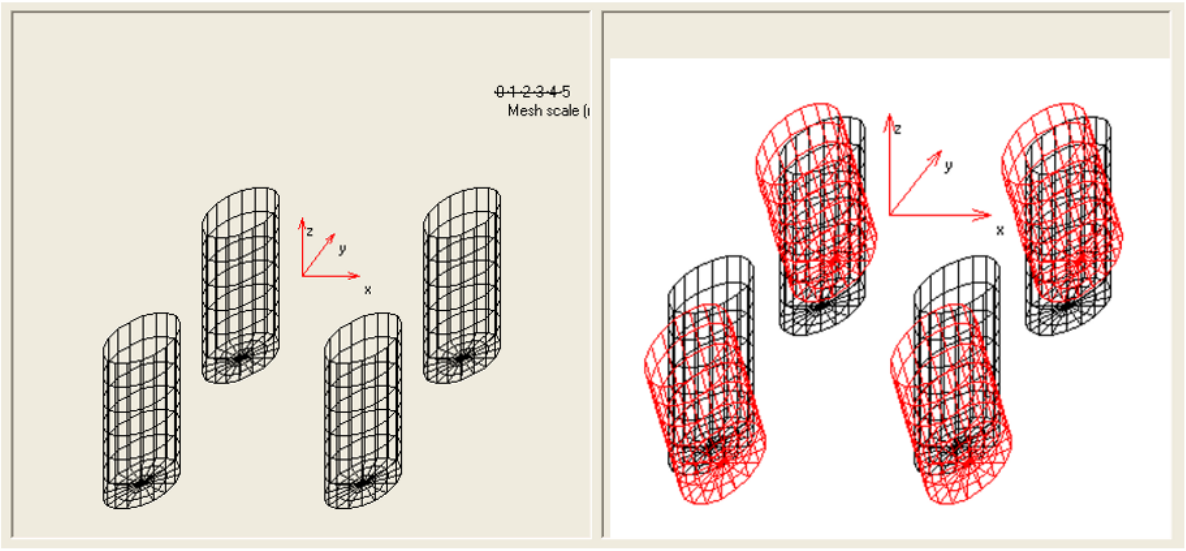

Fig.5.3.a/ Discrete element model of four-caisson foundation (left) and b/ Displaced foundation (right).

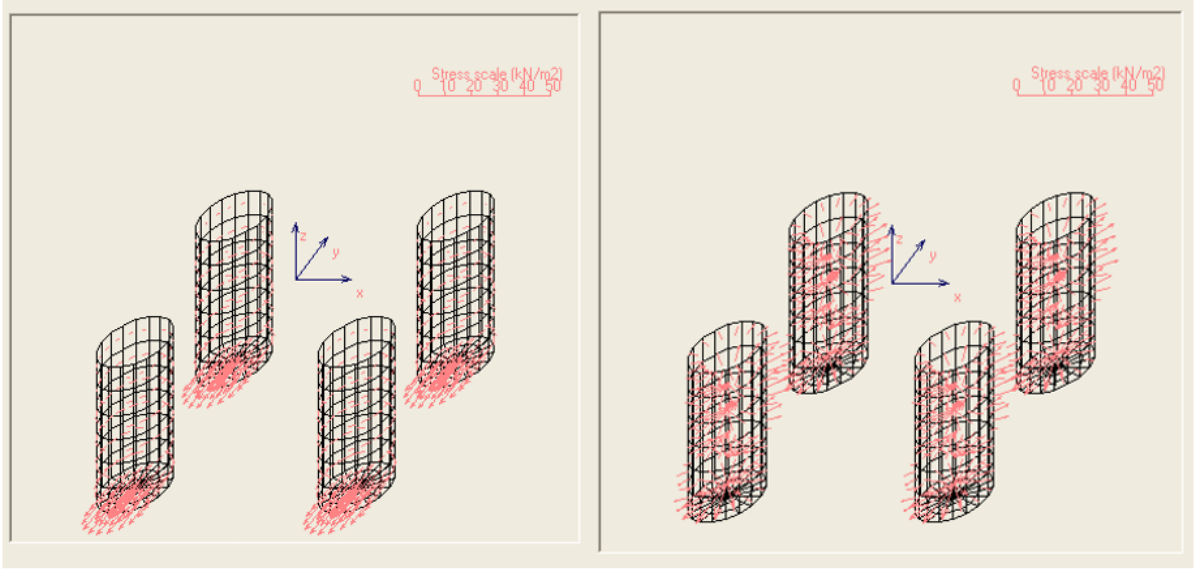

Fig.5.4. Results from DISEL analysis. a/ contact shear stresses(left) and b/ contact normal stresses (right).

The input consists of foundation geometry, soil parameters and load vector, which can be either specified force/moment or specified displacement/rotation for each degree of freedom. Fig.5.4 illustrates the results of analysis.

Example 8. Calibration of DISEL soil parameters with PLAXIS analyses.

One limitation of the simplified method used with DISEL is that the generation of each spring curve does not account for the

presence of neighbouring structure elements.

In order to improve the parameters for curve generation, PLAXIS analyses were carried out for typical vertical cross section of sub-sea structure, treated as plane strain problem, Athanasiu, Bogen and Prestegarden (1999).

Fig.5.5 shows the subsea mud mat foundation with skirts modelled with DISEL and with PLAXIS.

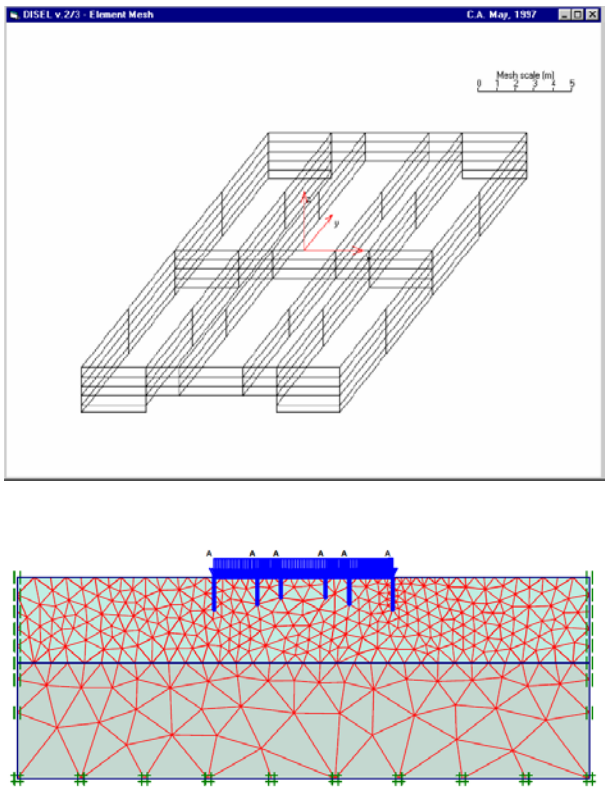

Fig. 5.5. Mud mat foundation model a/ DISEL (upper) and b/ PLAXIS plane strain (lower).

The finite element mesh consists of 15-nodes elements modelling the upper soft clay layer dawn to 6.3 m and the stiff dense sand below 6.3 m depth dawn to 15 m depth. Below the depth of 15 m the very stiff clay is considered as a rigid boundary. The undrained shear strength profile, down to 2.5 m is shown in Fig.5.6.

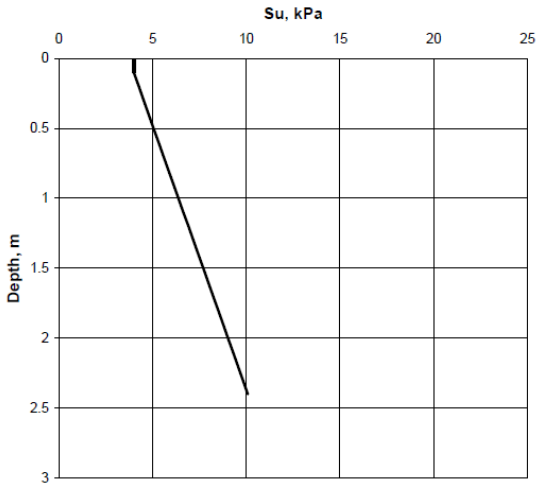

Fig.5.6. Undrained shear strength profile

The upper soft clay is modelled by the Soft Soil Model while the dense sand behaviour is modelled by Mohr-Coulomb model (Brinkgreve et al.,1998). The parameters for Soft-Soil Model were determined from consolidated undrained triaxial test results and from oedometer test results. It is found that the predicted friction angle using the correlations between undrained active shear strength and the angle of shearing resistance based on Cam clay model (Wood, 1996) is about 35 °. It agrees well with the measured friction angle in traixial tests. A lower friction angle is however used with Soft-Soil Model (30°), in order to obtain an average undrained shear strength equal to approximately 0.85 of suA. Table 5.1 shows a summary of soil parameters used with PLAXIS.

Two PLAXIS analyses are run, one for horizontal force-displacement relationship and one for vertical force-displacement. In the first run, the horizontal load is increased to failure while the vertical displacements are restrained. The analysis for horizontal loading shows that, at failure, the shear zone under skirt tip level is approximately 1m thick (Fig.5.7 shows the displacement pattern) and that the presence of the sand layer does not influence the results.

Table 5.1. Summary of soil parameters

Layer	γ (kN/m^3)	λ^*	κ^*	ν_{ur}	K_o^{nc}	M	C_{ref} (kN/m^2)	φ (°)	ψ (°)	R_{inter}	Type	
Very soft clay	17.8	0.08	0.02	0.15	0.5	1.56	1	30	0	0.1	Undrained	
Layer	γ (kN/m^3)	E_{incr} (kN/m^2)	C_{incr} (kN/m^2)	ν	E_{ref} (kN/m^2)	T-strength (kN/m^2)	C_{ref} (kN/m^2)	φ (°)	ψ (°)	R_{inter}	Type	Y_{ref}
Very dense sand	19.8	0	0	0.35	38000	0	1	35	0	1.0	Drained	0

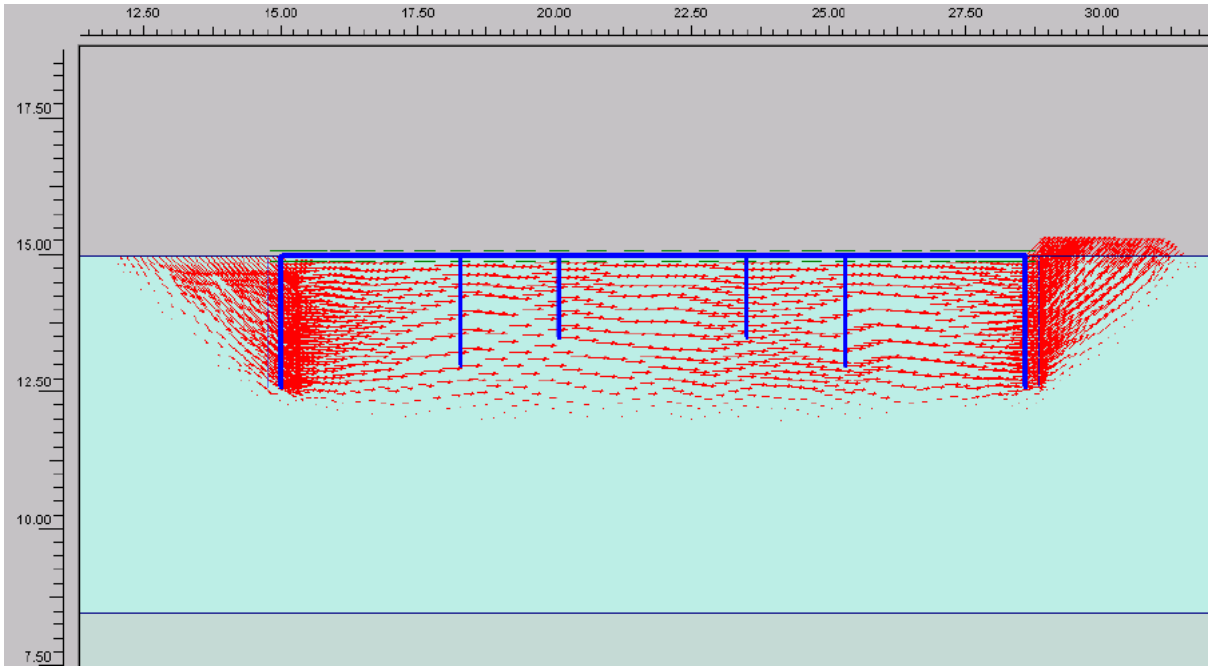

Fig.5.7. Displacements for horizontal loading.

The force-displacement curves from DISEL and PLAXIS agree well if the initial shear modulus, Go i DISEL is taken as 250*s_{uA} and the ratio G_{ult}/G_o as 0.05. The comparison between the two curves is shown in Fig.5.8.

The PLAXIS run for vertical loading show that the presence of sand layer influence both, the vertical displacements and the ultimate, bearing capacity force. The failure mechanism revealed by the displacement pattern (Fig. 5.9 shows the displacements for half of the structure) is typical for a clay layer with linearly increasing shear strength with depth and agrees well with failure mechanism assumed by Davis and Brooker, Ref.[5].

The calibration of DISEL parameters by PLAXIS analyses shows that the ultimate capacities calculated with DISEL agree well with those from PLAXIS. It also shows that different deformation parameters must be used with DISEL for horizontal loading (Go=250*s_{uA} and Gult/Go=0.05) and for vertical loading (Go=1000*s_{uA} and Gult/Go=0.35) in order to obtain comparable displacements in the two analyses.

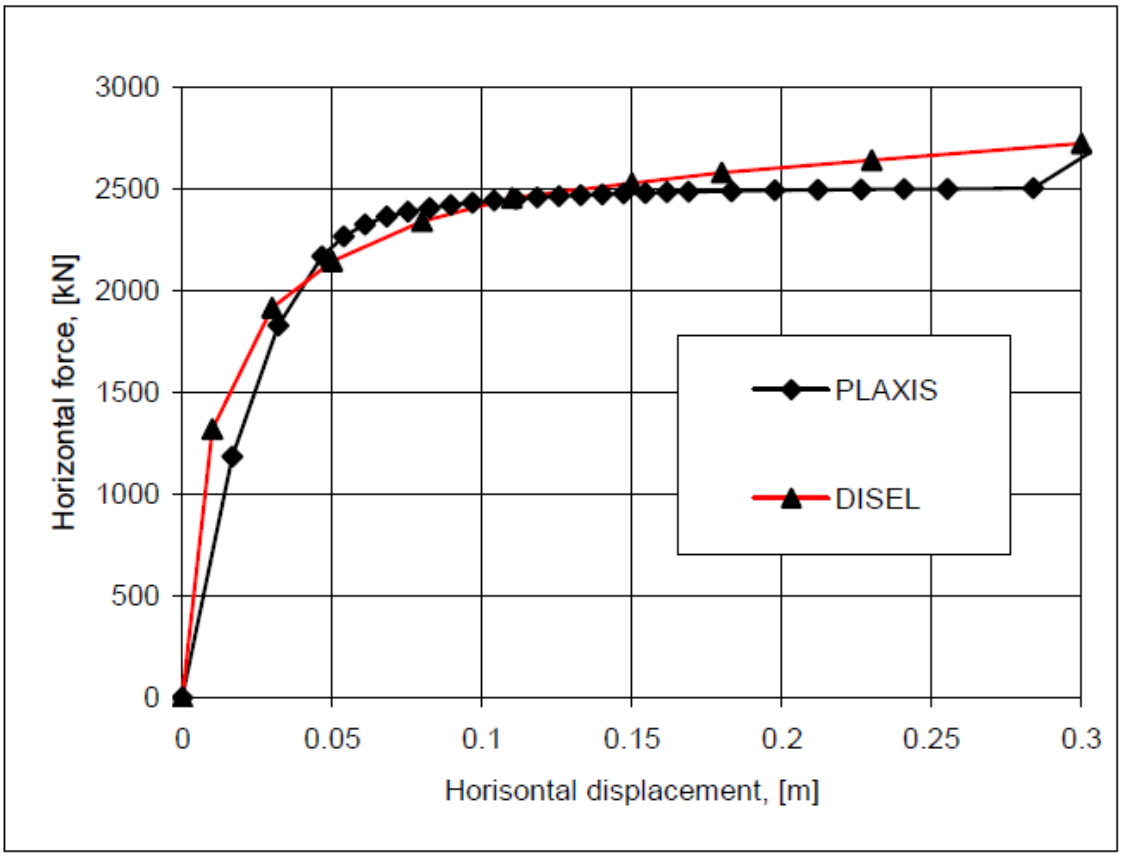

Fig.5.8. Comparison between PLAXIS and DISEL analyses. Horizontal force-displacement relationship.

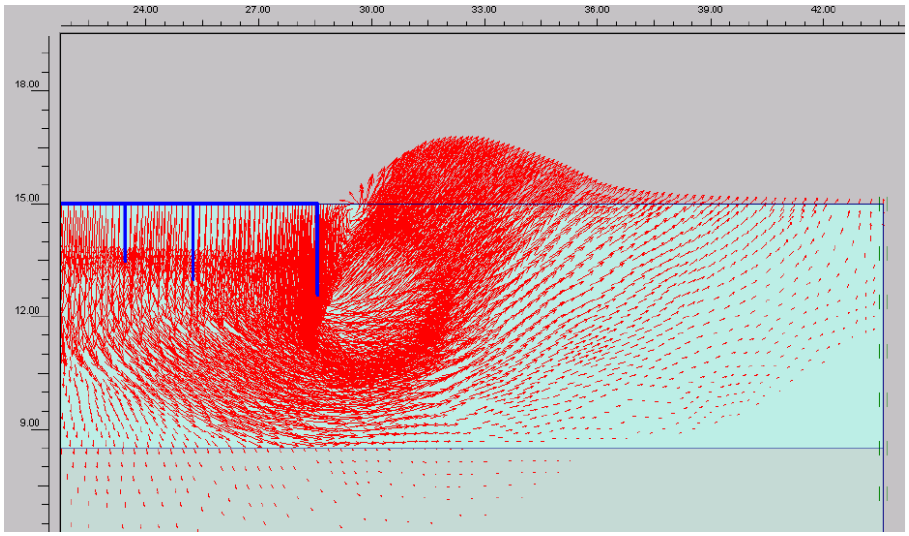

Fig.5.9. Displacements for vertical loading.

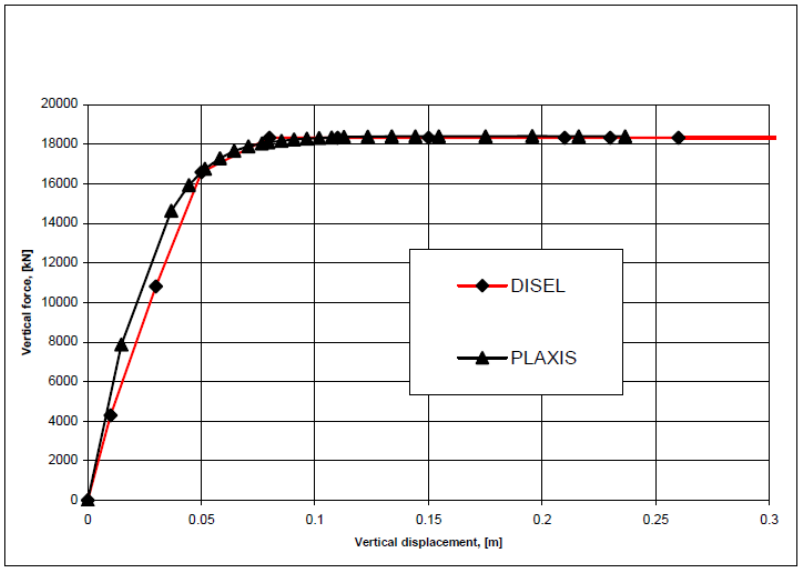

Fig.5.10. Comparison between PLAXIS and DISEL analyses. Vertical force-displacement relationship.

Example 9. Levelling analysis of a template foundation (Athanasiu and Guttormsen, 1998)

The foundation soil beneath a Template bottom can locally be washed away during drilling operations. The washing out may cause uneven settlements of the structure, with the risk of loading the subsea tree flowline connector. In order to immediately secure the situation, uplift forces must be applied by attaching buoyancy elements to the structure lifting trunnions in a levelling operation. The estimation of the required levelling forces by a soil-structure interaction analysis using the program **DISEL** is illustrated in this section.

The plan of bottom frame, with the four wells, B1 to B4, showing the assumed "washed out" zone and DISEL model of the skirts, where part of the skirts in "wash out" zone is de-activated, are presented in Fig. 5.11.

The levelling analysis is a typical loading/unloading problem, which requires modelling of hysteretic behavior upon reversal of the load. This is done by two separate analyses: in the first analysis the "as-is" situation after "wash-out" is modelled, where the vertical displacements and corresponding vertical shear stresses mobilized along the skirts are determined. In this analysis, one element on the skirt wall shown in Fig.5.12. has moved from point 1 to point 2. During levelling, the shear stress acting on this element will be reduced (the shear stress will move from 2 to 3) and, for large upward displacements, the undrained shear strength will be mobilized in the opposite direction. In the second analysis, the ultimate shear strength for the element is set equal to the sum of the mobilized shear stress from the first run and the undrained shear strength. The uplift forces are gradually increased and the upward movements at the wellhead calculated as shown in Fig.5.13.

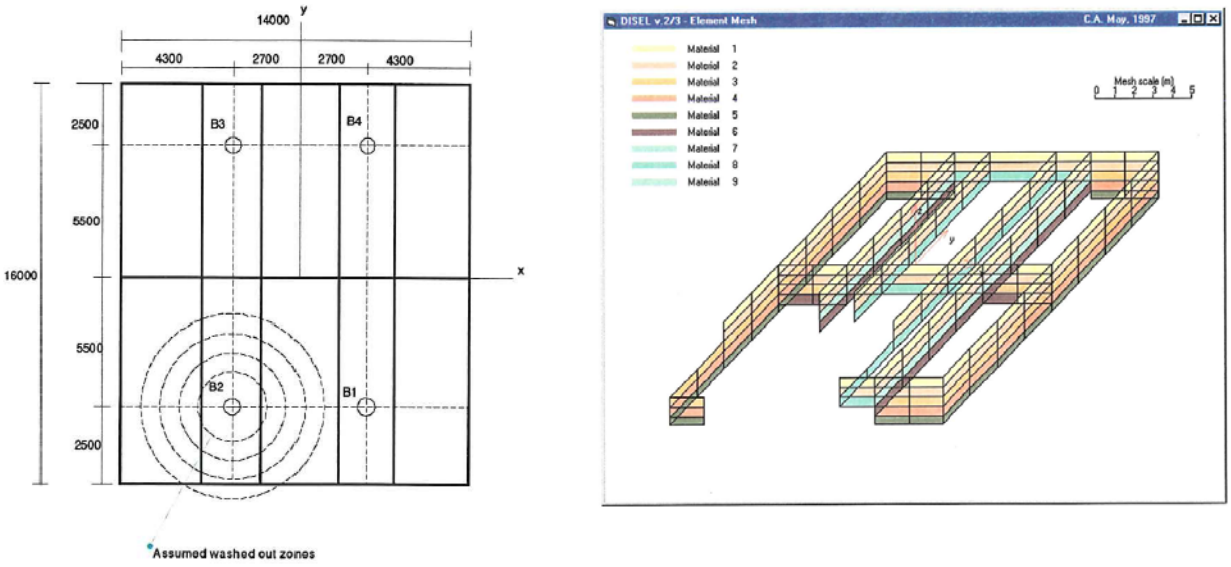

Fig.5.11.The plan of bottom frame (left) and the DISEL model (right).

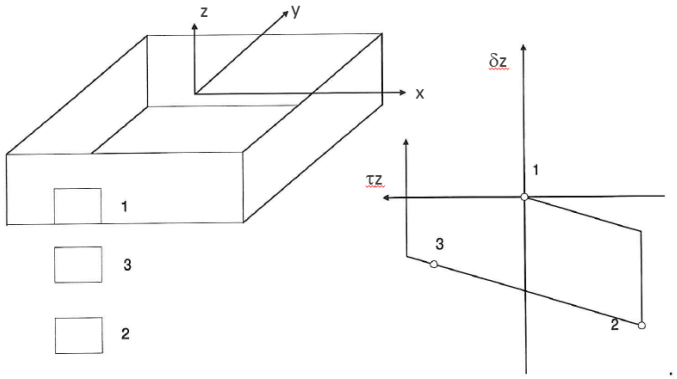

Fig.5.12.Mobilization of shear stresses upon reversal of the load

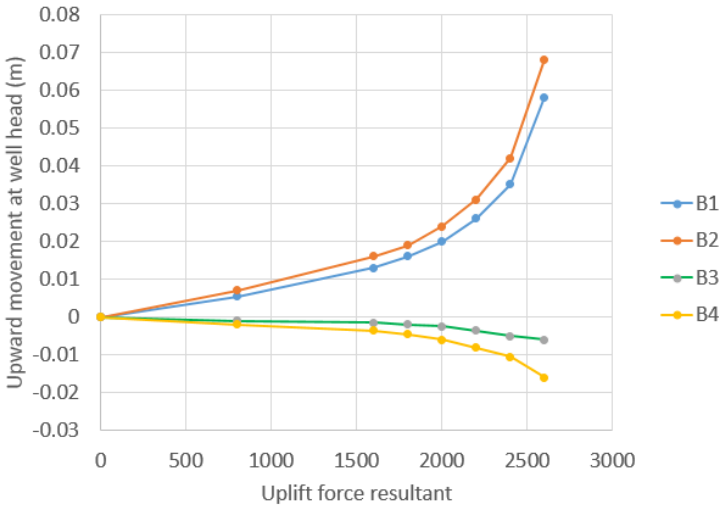

Fig.5.13.The relation between applied uplift forces and resulting upward displacements.

MONOTONIC AND CYCLIC UNDRAINED SHEAR STRENGTH OF DENSE SAND

Undrained shear strength of sand using Janbu's dilatancy parameter

Stability analyses of caisson or pile foundations for offshore structures require (when dense sand is present in the seabed soil profile) the use of undrained shear strength of sand. A simplified expression for estimating the undrained shear strength of sands is based on Janbu's secant dilatancy parameter, Df, at failure, defined as the slope of the effective stress path in undrained loading:

$$Df = \frac{\Delta p'}{\Delta q} = \frac{p'_f - p'_o}{q_f - q_o} \qquad (6.1)$$

where p' is the mean effective normal stress, p'=(σ'1+σ'2+σ'3)/3; q is the deviatoric stress, q=σ1-σ3; p'o and qo are the effective "in situ" stresses, including the effective stresses from the own weight of the structure, existing in the ground prior the undrained loading is applied; p'f and qf are effective stresses at failure.

The undrained shear strength is expressed in terms of effective stress parameters as:

$$s_u = \frac{1}{2} \cdot \frac{(p'_o - f_D \cdot q_o \cdot D_f)}{(1 + f_D \cdot f \cdot M \cdot D_f)} \cdot M \qquad (6.2)$$

Where:

$$M = \frac{6 \cdot \sin(\varphi')}{3 + (2 \cdot b - 1) \cdot \sin(\varphi')} \qquad (6.3)$$

$$b = \frac{\sigma_2 - \sigma_3}{\sigma_1 - \sigma_3} \qquad (6.4)$$

The factor f=-1 for **Compression** and **DSS** type of loading and f=+1 for **Extension** type of loading; f_D=+1 for **Compression** and **DSS** type of loading and f_D=-1 for **Extension** type of loading; D_f is the secant failure dilatancy parameter. The different stress path for the different loading types are shown in Fig.6.1.

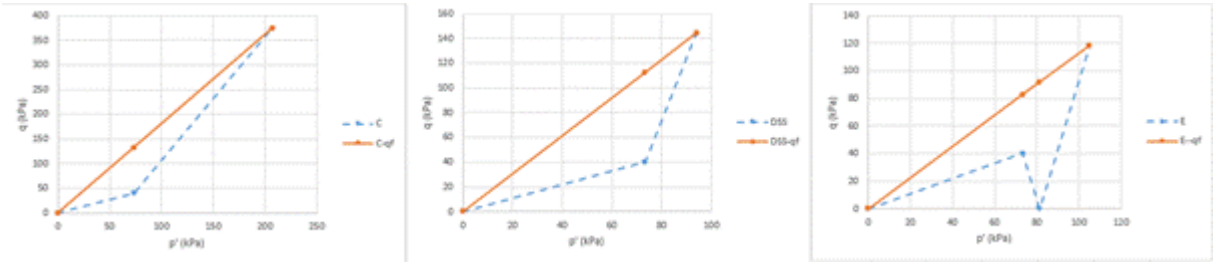

Fig.6.1. Effective stress paths in different types of test.

The secant dilatancy parameter at failure can be estimated based on Elasto-Plasticity assuming two yield surfaces, one for plastic shear strain hardening and one for plastic volumetric strain hardening, using the effective stress friction angle, φ', and dilation angle at failure, Ψmax. The derivation of dilatancy parameter is explained in Appendix 6.

Undrained cyclic shear strength of dense sands

The effect of permanent pore water pressure

The results of cyclic shear tests show that permanent pore water pressure, up, develops during cyclic shearing. The permanent pore water pressure increases

both with the number of cycles for the same cyclic shear stress and with the magnitude of cyclic shear stress for the same number of cycles. During the cyclic loading the effective stress will be reduced from p'_o to (p'_o-u_p). Assuming that the ultimate D-parameter remains unchanged, the cyclic undrained shear strength of sand can be evaluated with the same Equations as for static strength but with reduced initial mean effective stress:

$$p'_{op} = p'_o \cdot \left(1 - \frac{u_p}{\sigma'_{vo}}\right) \quad (6.5)$$

The permanent pore water pressure, u_p, and the equivalent number of cycles, N_{eq}, are determined by using the accumulation procedure for the given load history.

- **The effect of cyclic pore water pressure**

The assumption that the pore pressure at the start of a cycle is the same as the pore pressure at the end of the previous cycle may not be valid in all cases, such as in dense dilatant sand. The sand will tend to dilate when the cyclic shear stress is increased from τcy,a to τcy,b (Figure 6.2), introducing a negative change in the pore pressure, -up. When the shear stresses before and after the change in cyclic shear stress are on the failure envelope, the change in pore pressure can be expressed as (Jostad et al. 1997), generalized in q-p space as:

$$\Delta u_{cy} = (1 - \frac{q_b}{q_a}) \cdot (p'_o - \frac{q_o}{M}) \quad (6.6)$$

In undrained conditions, the effect of cyclic pore pressure can be evaluated by reducing the initial mean effective stress:

$$p'_{op} = p'_o \cdot (1 - \frac{\Delta u_{cy}}{\sigma'_{vo}}) \quad (6.7)$$

- **The effect of partial drainage of permanent pore water pressure**

When the numbers of cycles for each bin of cyclic shear stress applied during the load history and when the average period of each cycle in a bin are such that some partial drainage may occur, the accumulation procedure must account for the partial drainage as illustrated in *Figure* 6.2.

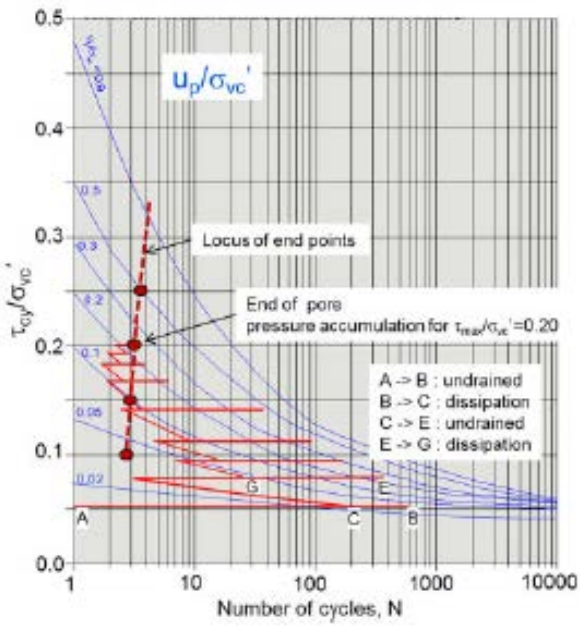

Figure 6-2 Example of pore pressure accumulation for partly drained conditions (from Andersen 2015).

The corrected initial effective mean stress will be:

$$p'_{0ppd} = p'_o \cdot (1 - \frac{u_{ppd}}{\sigma'_{vo}}) \quad (6.8)$$

where u_{ppd} is the permanent pore water pressure for partly drained conditions:

$u_{ppd} = u_p \cdot (1 - U_p)$ where U_p is the degree of consolidation of permanent pore water pressure.

To determine Up, a transient dissipation analysis must be performed where the loads (or the undrained pore water pressures) are applied following the load history.

- **The effect of partial drainage of permanent and cyclic pore water pressure**

Cyclic pore water pressures, as measured in undrained cyclic shear tests, may be partly drained during the cyclic loading of the soil in the field if the time required for the load to reach the first half amplitude of the cycle (a quarter of the load period) is large enough to allow some partial drainage to occur.

The initial effective mean stress must be corrected also for partial drainage of cyclic pore water pressure:

$$p'_{oppdcy} = p'_o \cdot \left(1 - \frac{u_{ppd}}{\sigma'_{vo}} + \frac{u_{cypd}}{\sigma'_{vo}}\right) \qquad (6.9)$$

where $u_{cypd} = u_{cy} \cdot (1 - U_{cy})$, U_{cy} is the degree of consolidation of the cyclic pore water pressure during the first quarter of the final cyclic load.

If u_{cyc} is positive as may be the case for compression caisson, the partial drainage will increase the undrained cyclic shear strength. If however the u_{cyc} is negative (suction) as may be the case for tension caisson, the consolidation will reduce the strength.
Determination of U_{cyc} will also require a transient dissipation analysis conducted for a quarter of one cycle with the maximum load amplitude.

Example 10. The use of undrained shear strength of sand formulation in stability analyses of caisson foundations.

Stability analyses of caisson foundations of a steel jacket under the environmental loads require determination of undrained, cyclic shear strength of sand along the critical slip surface. The main challenge is the estimation of undrained pore water pressures, both permanent and cyclic, and of their dissipation during the design storm and during the last wave load. The problem is illustrated in Fig.6.3.

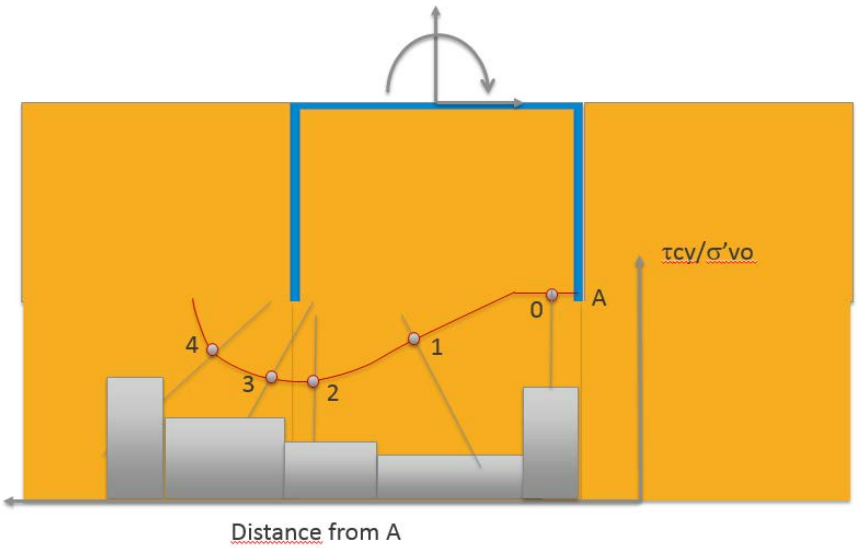

Fig.6.3. Cyclic shear stress distribution along the sliding surface.

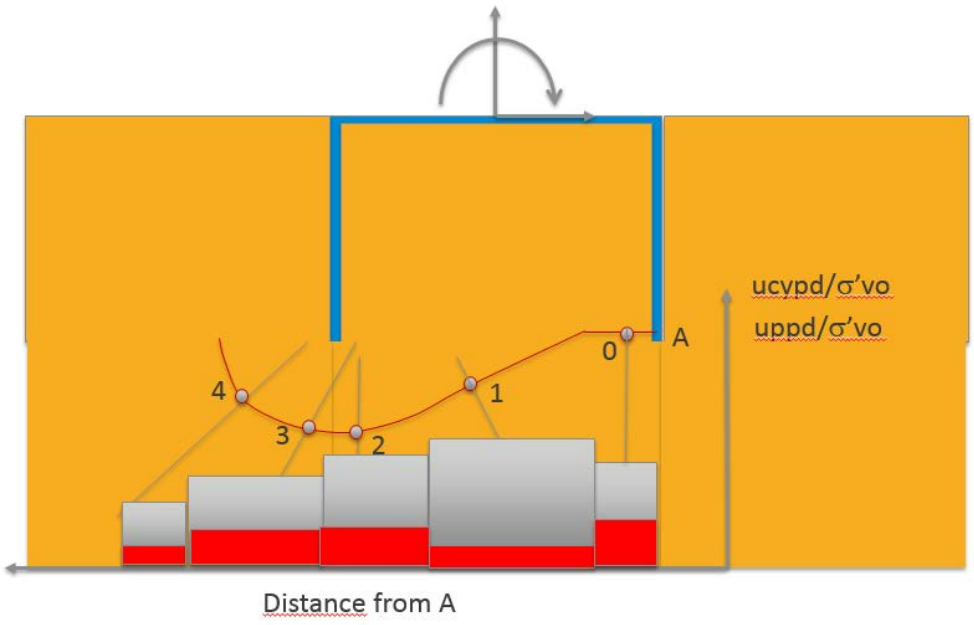

Fig.6.4. Remnant cyclic (grey) and permanent (red) pore water pressures with partial drainage along the sliding surface.

The method of solution for assessing the foundation capacity is described as follows and is illustrated for tension load case of the caisson foundation.

- A finite element analysis is first performed to determine the cyclic shear stresses that occur when the highest wave hits the structure. These are input for CYCPORE2 analysis as the amplitude function of x and y co-ordinates in the same element mesh as used in finite element analysis.
- The accumulation procedure is used to determine the undrained excitation functions of time during the design storm as described in Section 4.1.
- Transient analysis is performed using CYCPORE2 program to determine the remnant permanent pore water pressures, u_{ppd}/σ'_{vo}, along the sliding surface (Fig.6.4).
- The cyclic pore water pressure generated in undrained conditions is scaled as a function of cyclic shear stress applied by the last wave to determine the undrained excitation function for cyclic pore pressures.
- Transient analysis is performed with the new excitation function to determine the remnant cyclic pore pressure (suction), with partial drainage, u_{cypd}/σ'_{vo}, (Fig.6.4).
- Bearing capacity analyses are performed using the undrained shear strength corrected for permanent and cyclic pore water pressure with partial drainage.

The procedure described above was used to determine the compression and tension capacity of caisson foundations of Draupner E Jacket (Bye et al. 1995, Tjelta, 2015).

The design of caisson foundations for Draupner E Jacket showed that partial drainage will increase the vertical capacity in compression and will reduce the vertical capacity in tension and the horizontal capacity.

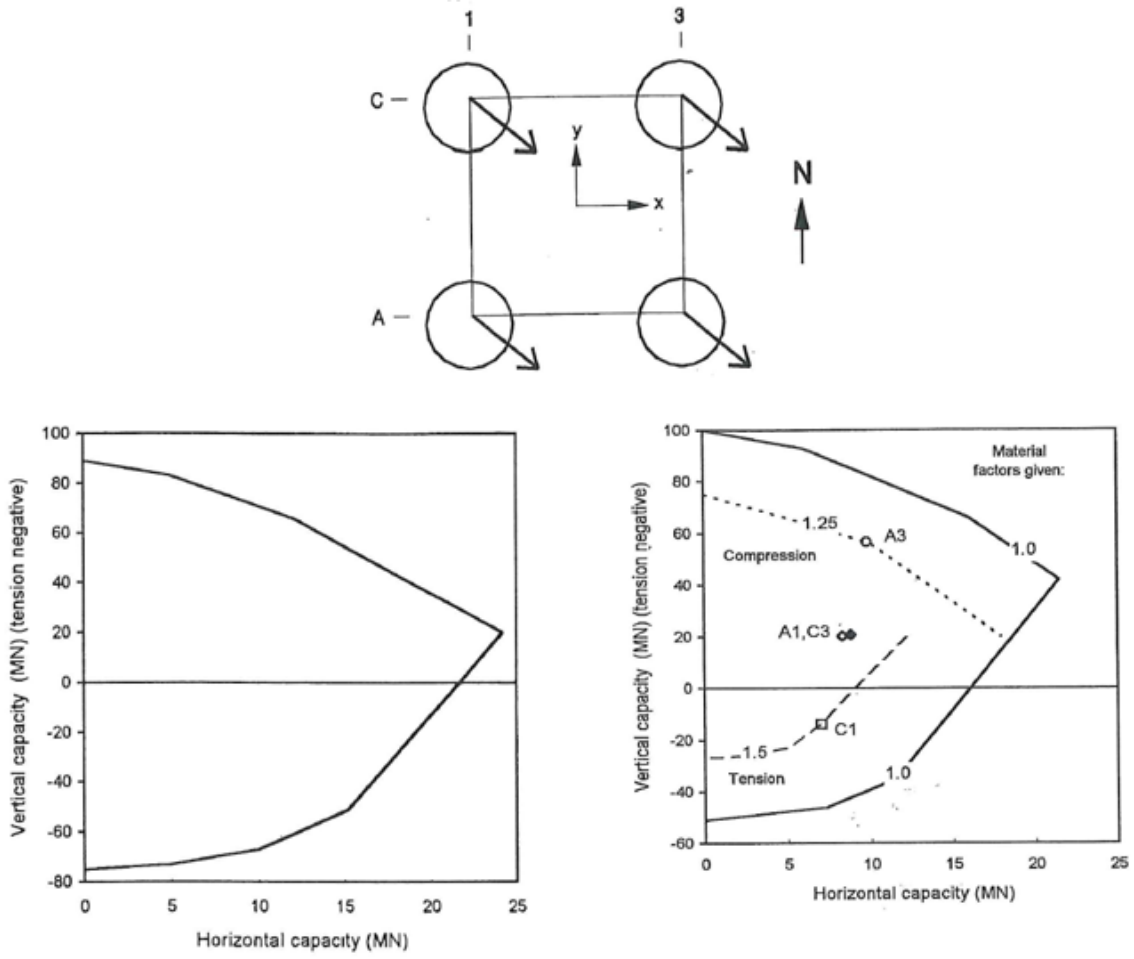

Fig.6.5. Comparison between undrained compression and tension capacity of the caisson and resulting capacities when partial drainage is accounted for.

THE NEED FOR A GEOTECHNICAL DATA BANK

One of the most complex problems the geotechnical designer is faced with is the selection of soil parameters. We witness a gradually increasing use of advanced computer programs with complex soil models, based on Elasto-plasticity. The use of these computer programs makes it possible to analyze complex problems of soil-structure interaction, with a variety of soil conditions, geometry and loads.

However, the results are not better than the input soil parameters are able to properly simulate the soil behaviour. Even if we use simplified methods and models, the results depends entirely on the use of reliable soil parameters. Costly soil investigations, including field and laboratory tests and engineering judgement and experience are required to select soil parameters.

On the other hand, the tremendous amount of data, accumulated from soil investigations and from research projects, opens the possibility of reusing existing information to predict parameters for a new soil with known identification properties

from the parameters of soils with similar identification properties.

A geotechnical data bank for soil parameters is therefore needed. It could be used to store the existing information on soil behaviour, to perform a systematization of data and to “retrieve”, i.e. predict the parameters for a soil, specified only by its identification properties, by using the soil properties stored in data bank.

The proposed system is not meant as a substitute for soil investigations, but as a tool to evaluate soil parameters in early feasibility studies, as a guide in planning field and laboratory testing programmes and as a guide in interpreting the results from laboratory tests at new sites (Andrei and Athanasiu, 1979).

The soil behavior is determined by its nature and composition (i.e. the type of constituent material) and by its state (water content and void ratio, i.e saturation degree and relative density).

Soil identification and classification

Three types of soil print are proposed for soil nature and composition: “A-print”, “Ch-print” and “M-print” as illustrated in Fig.7.1. , and 7.2.

The details of constructing soil prints for identifying its nature and composition are described by Andrei and Athanasiu, 1979, Athanasiu, Andrei and Jianu, 2004 and Athanasiu and Jianu, 2005. The identification properties can be used for soil classification according to different classification systems as illustrated in Fig.7.3.

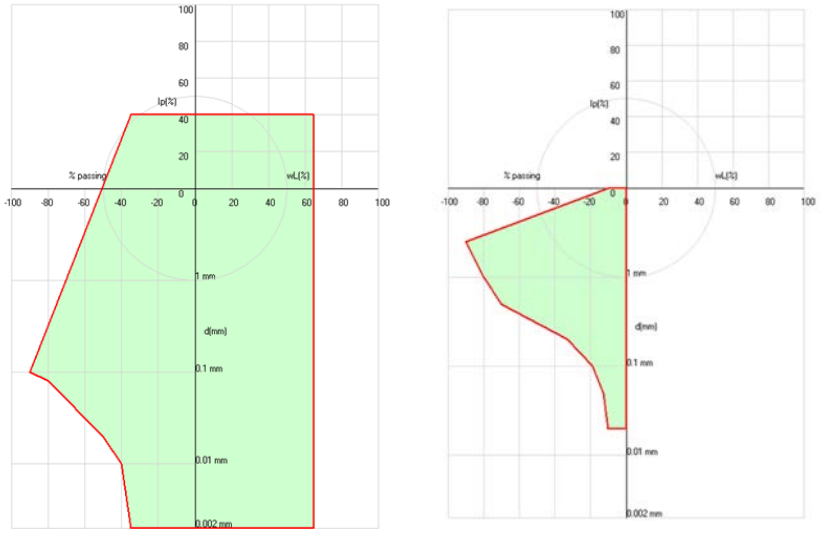

Fig.7.1. Soil «A-print» a/ clay (left) b/ sand (right).

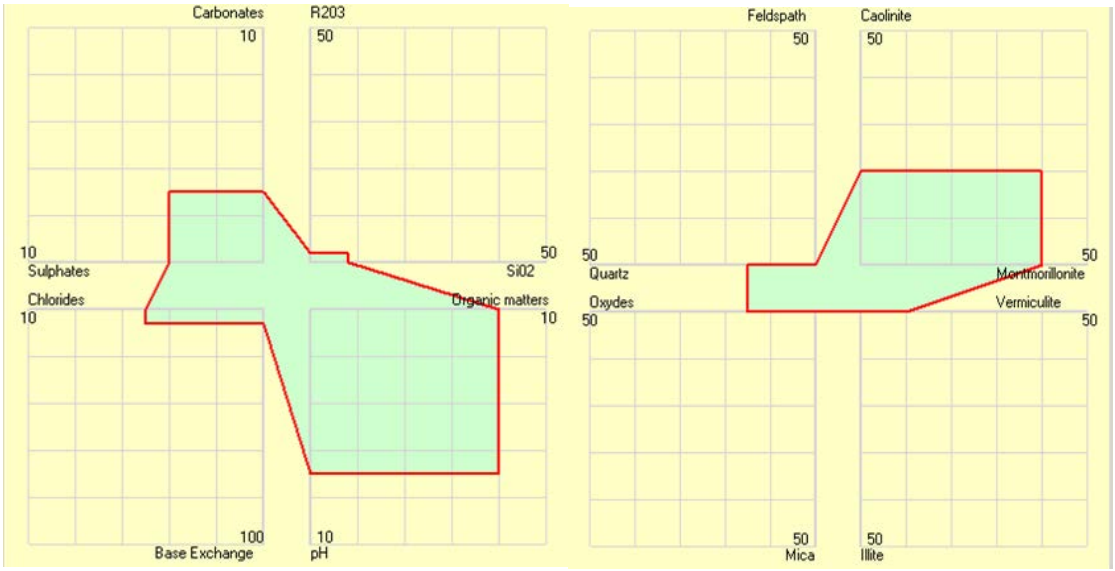

Fig.7.2. a/ Soil "Ch-print" (left) and b/ Soil "M-print" (right)

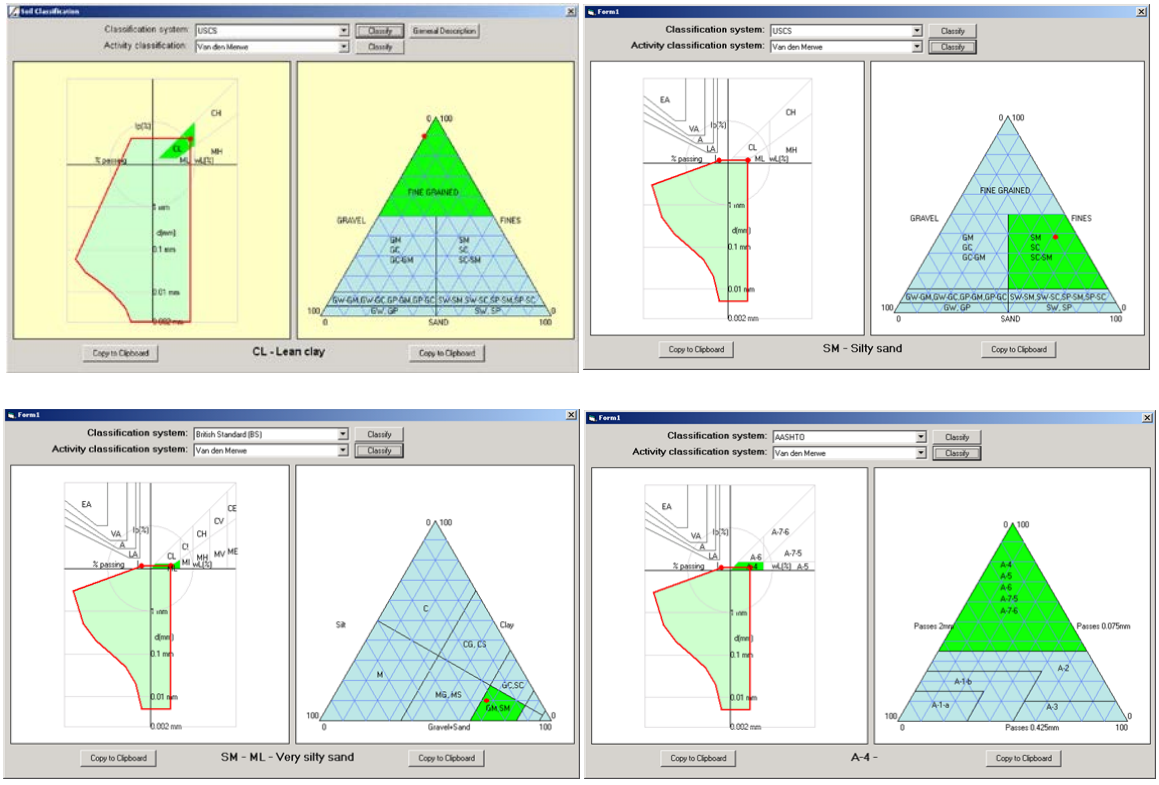

Fig.7.3. Soil classification

The soil behaviour is influenced not only by its nature and composition but also by its state (water content and density). It is therefore important that all soil parameters must be recorded together with the state in which the parameter was measured. A convenient way of representing the soil parameters is to draw the soil state in a "state diagram" as a point and to note the value of soil parameter at this state. A point in the state diagram has the water content, w (%), in abscissa and the volume of soil, V100, corresponding to a weight of solid particles equal to the weight of 100 volume units of water:

$$V_{100}=100\cdot\gamma_w/\gamma_d \qquad (7.1)$$

where : γw - unit weight of water, γd – dry unit weight of soil.

The advantage of V100 representation is that the water volume is equal to water content expressed in percentage of solid skeleton weight and that straight lines are obtained for constant degree of saturation, as shown in Fig.7.4.

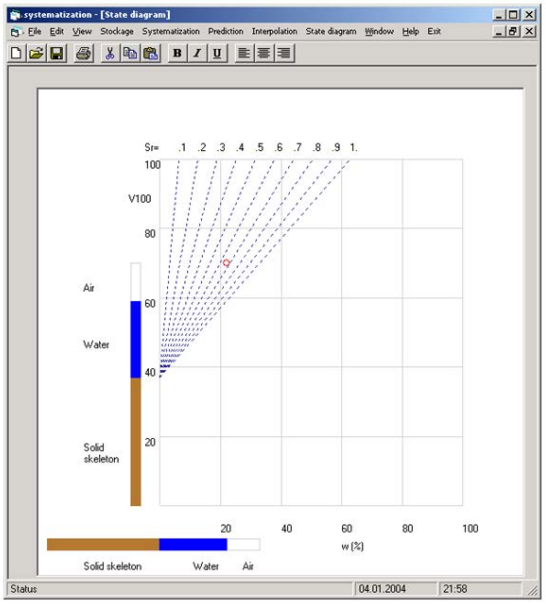

Fig.7.4. State diagram

Parameter data storage

The soil properties data stored in data bank can be presented as values of a parameter on the state diagram as illustrated in Fig.7.5.

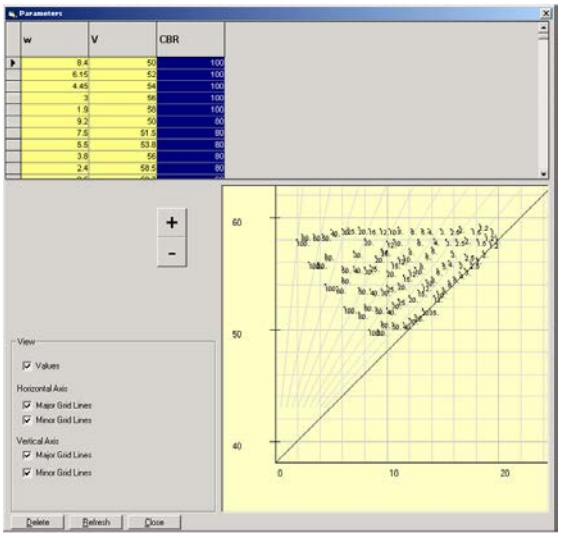

Fig.7.5. Storage of parameter (CBR) on state diagram

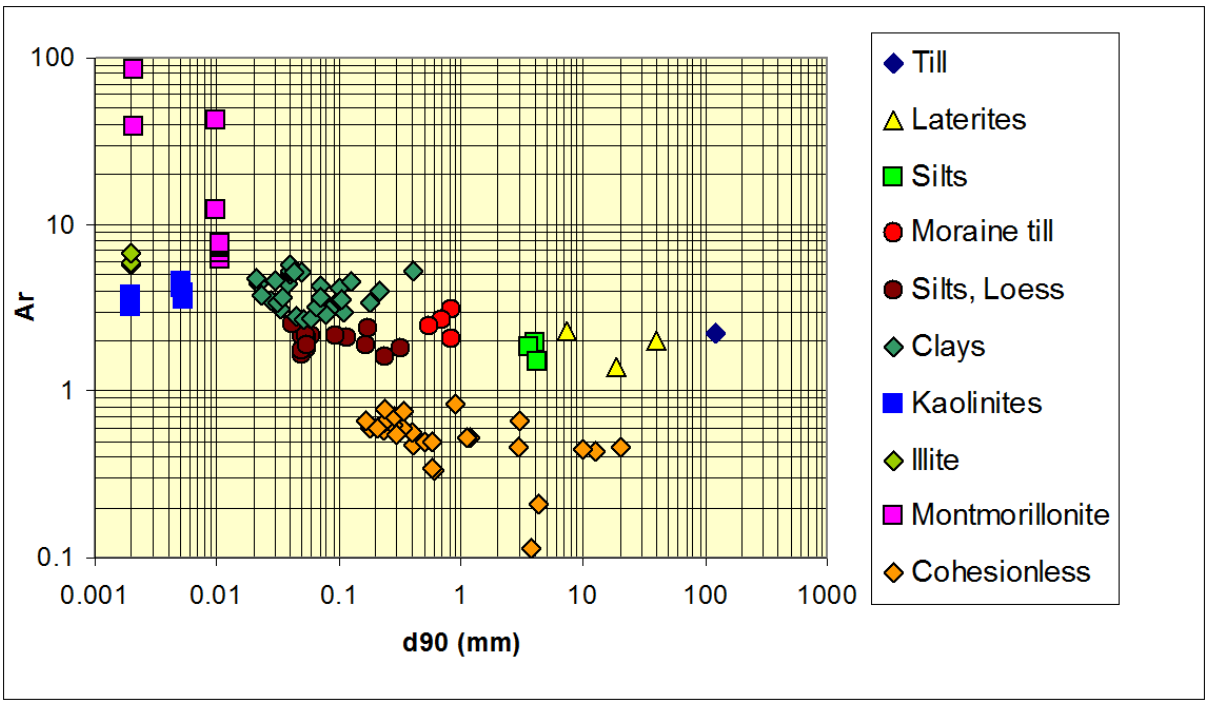

Fig.7.6. Nature diagram

Soil data systematization

All soil records stored in Data Bank are systematised in a nature diagram, having d_{90} in abscissa and A_r (A-print area) in ordinate, both in log scale. All soils are plotted on nature diagram as clouds of points, (Fig. 7.6). As can be seen from Fig.7.6 in which a series of 78 soils has been recorded, (Andrei & Manea, 1995), soils having similar nature can be detected as belonging to the same cloud of points in nature diagram.

Soil data systematization using the "nature diagram" helps finding the degree of analogy between two soils by expressing it as the distance between their points on the diagram. Based on this assumption, the nature diagram can be used to find out which soils have similar properties to a soil for which only relative area, A_r, and d_{90} are known.

Data retrieval to predict soil parameters

Prediction of soil parameters from data bank can be performed either by retrieval operation or by use of correlations.

The **retrieval operation** to predict soil parameters is based on a "double kriging technique" (Athanasiu, Andrei and Jianu, 2004), to determine the value of required parameter at given state, in state diagram, and one to select the soil with highest degree of analogy with the given soil, in nature diagram.

One example of kriging in state diagram is illustrated in Fig.7.7 where the value of constrained modulus between 2 and 3 daN/m^2 applied pressure, M2-3, is predicted for a given soil state.

Example of kriging technique applied to select the soil with highest degree of analogy with the given soil is presented in Fig.7.8.

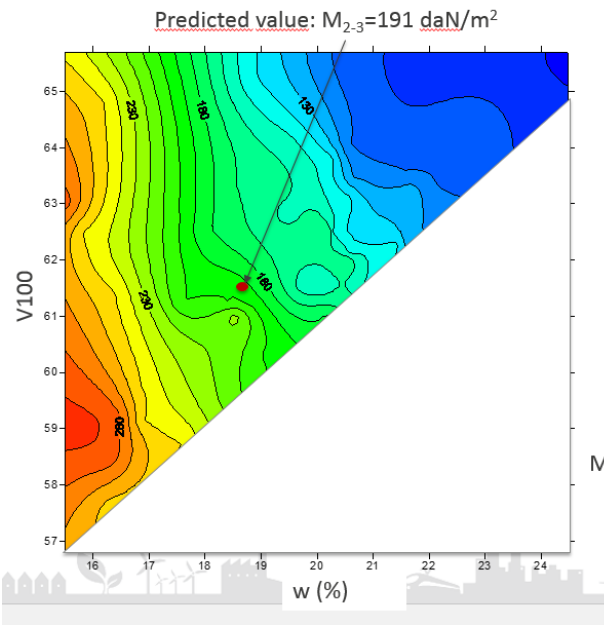

Fig.7.7. Selecting the parameter value, M2-3, for the state of given soil from the parameters known for other states

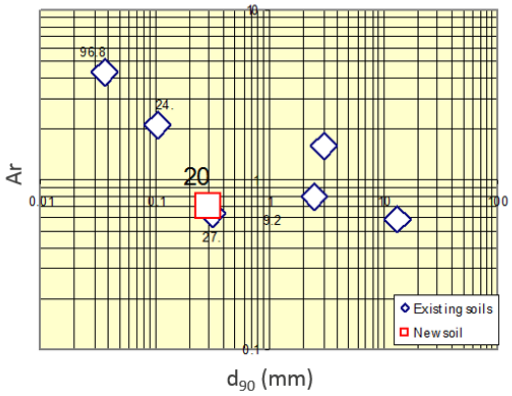

Fig.7.8. Selecting the soil with highest degree of analogy with the given soil.

Prediction based on correlations is the most common method to predict soil parameters and can be performed only for soils for which the necessary data, required by correlation (w, Ip, OCR, etc.), are in the data bank. Examples of such correlations are shown in Fig.7.9. Fig.7.10 shows a comparison between values of G50/su measured in triaxial and DSS tests as compared to predicted values from Data Bank.

The necessity of a data bank for soil parameters is one of the challenges in geotechnical design (e.g. Lacasse et al., 2013, Karlsrud, 2014). That is why we, in Multiconsult, plan to invest more in developing the existing Data Bank in the coming years.

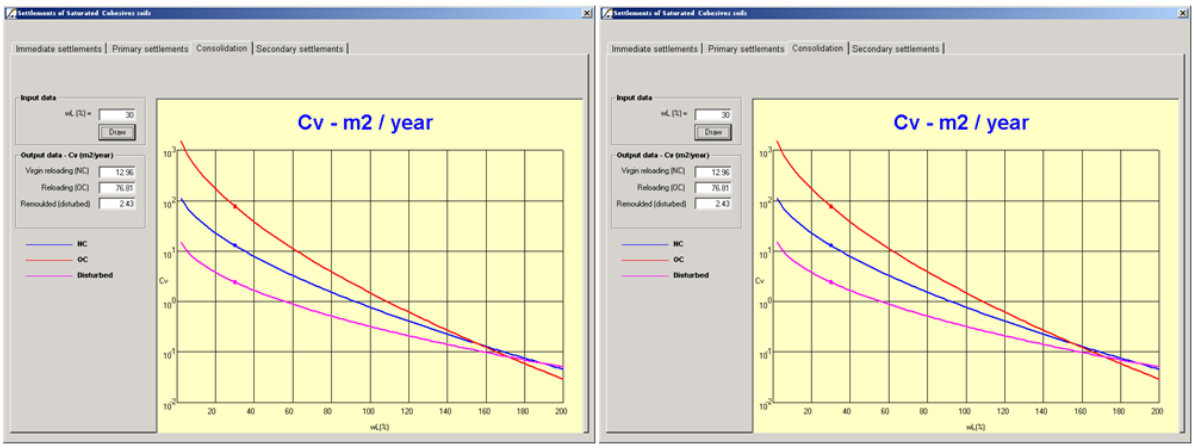

Fig.7.9a. Examples of prediction using correlations (c_v).

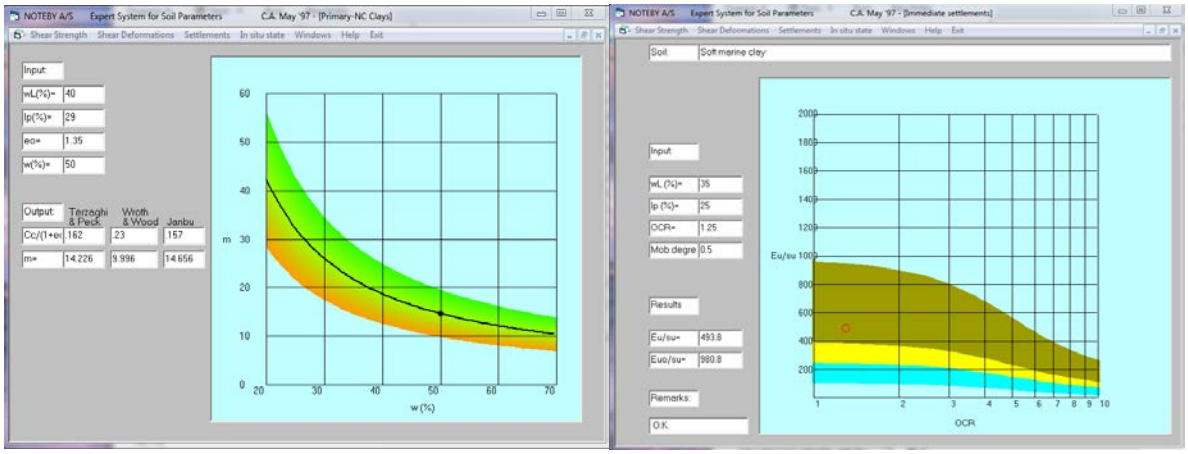

Fig.7.9b. Examples of prediction using correlations (m,Eu/su).

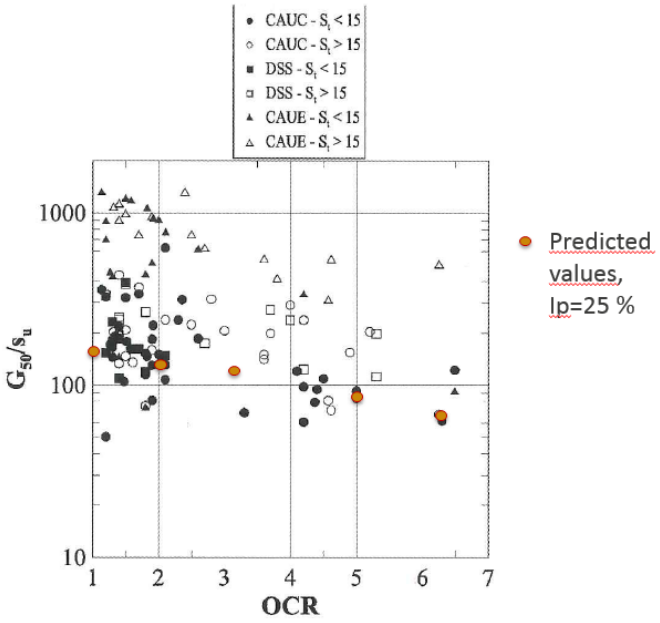

Fig.7.10. Values of shear modulus at 50% mobilization normalized to undrained shear strength (G50/su) in relation to OCR (Karlsrud, 2014) compared to predicted values from data bank.

CONCLUDING REMARKS

- Some examples are presented to illustrate the use of simple models in geotechnical design.

- These models are useful particularly in the early design phases where many parameter studies are to be performed in a limited period of time and with little information about the ground conditions and parameters;

- The students attending Courses on Computational Geotechnics at NTNU are told to not start a finite element analysis until they have an idea of what answer can be. The simple models can help to find an approximate answer;

- As many times as possible, the results from simplified methods should be compared to in situ measurements or to

laboratory tests in order to continuously improve their degree of accuracy;

- When the type of problem or the parameters are changed as compared to the situation for which the simplified methods were conceived, the methods must be validated and parameters calibrated by theoretical solutions or by finite element analyses;

- Detailed analyses using more complex modelling and parameters remain the right tools to perform detail design in Geotechnical Engineering;

- As Duncan (2013) expressed in his key note at ASCE Geo-Congress, although the tools in use today are much more sophisticated than in 60s and 90s, experience, judgement and thorough quality control remain as important as ever.

ACKNOWLEDGEMENTS

The work with contact stress models started during my PhD studies at Technical University in Bucharest, Romania. My supervisor, Prof. Stanculescu has guided me through the small- and large-scale model tests. Prof. Andrei Silvan, from the same University, inspired the work with geotechnical data bank. I am indebted to both of them.

Many of the examples presented in this lecture are selected from the design and consulting activity at MULTICONSULT ASA where I worked together with my colleagues to develop some of the simplified methods and computer programs. I would like to thank all of them and particularly to Anders Bye from whom I learn that, in theory, the difference between theory and practice is small, but in practice, it can be significant.

I would like to express my thanks to Gunn Ralle from NGI who meticulously reviewed the manuscript and made the small but important corrections to the text.

The fundamentals of undrained shear strength and of the behavior of soft marine clays comes from weekly meetings at NGI in 1971-1972 and fruitful discussions with Dr. Bjerrum during my work with plane strain apparatus at NGI. I will always be indebted to Dr. Bjerrum for opening the geotechnical window for me. During our first meeting at NGI he asked me something and I answered:

- Yes Sir.
- Do not “sir” me! I am Laurits you are Corneliu – came the answer from the former President of the International Society of Soil Mechanics and Foundation Engineering. Thus, I have the first lesson of democracy from him.

Many of ideas back the models come from fruitful discussions within the Geotechnical Group at NTNU, particularly with the late Prof. Nilmar Janbu and Prof. Steinar Nordal to whom I am indebted for the inspiration towards respect for theory and for clear and pedagogical presentations.

So you see, Technical University of Bucharest, NGI, NTNU and Multiconsult have co-operate in inspiring this presentation. I think this illustrates that, in Geotechnical Engineering, the co-operation between different Companies is of vital importance. Once again, Bjerrum was right when he proposed at the closing banquet of Mexico Conference in 1969 a new principle in Soil Mechanics: “To reduce the friction and increase the cohesion among the participants”. Let us follow his advice!

REFERENCES

Andersen, K.H. -2009-. Bearing capacity of structures under cyclic loading; offshore, along the coast and on land. 21st Bjerrum

Lecture presented in Oslo 23 November 2007. Can. Geotech. J. 46: 513.535. Also: Norsk Geoteknisk Forening, Bjerrums Foredrag Nr. 21.

Andersen, K.H. & Schjetne, K. -2013-. Data base of friction angles of sand and consolidation characteristics of sand, silt and clay. ASCE J. of Geotech. & Env. Engrg., 139 (7), 1140–1155.

.**Andrei, S. and C. Athanasiu – 1979 –** Test data systematization and storage to predict the parameters describing the behavior of unsaturated soils. Proc. of the VIIth European Conf. On Soil Mechanics and Found. Engineering, Brighton. England.

Andrei, S. & S. Manea. **-1995-**. Moisture and volume changes in unsaturated soils. Proceedings of the 1st Int. Conf. on Unsaturated Soils, "UNSAT'95", Paris, 6-8 September.

Athanasiu, R., S. Andrei and L. Jianu – 2004- Storage, Systematization and Retrieval of Geotechnical Data to Predict Soil Parameters for Design. Nordic Geotechnical Meeting, NGM2004, Ystad, Sweden.

Athanasiu, R. and L. Jianu – 2005- The use of Geotechnical Data Bank for foundation design. Romanian Geotechnical Conference. Bucharest. Romania.

Athanasiu C. -1978-. *"Contributions to the Problem of Contact Pressures between Structures and their Supporting Soil*". (in Romanian). Ph.D Thesis. Technical University. Bucharest, Romania, 1978, 174 p.

Athanasiu, C. – 1993 – DISEL- Discrete element analysis program. User's Manual. NOTEBY Report 39153 No.1. Jan. 1993, Rev. 2-1999.

Athanasiu, C. - 1994- FPLATES User's Manual. NOTEBY Report 39108 May 1994.

Athanasiu, C., Simonsen, A. Schram, Soereide, O., K. and J. Tistel – 2005 – Elastic and creep settlements of rock fills. 16th Int. Conf. on Soil Mechanics and Foundation Engineering. Osaka, Japan.

Athanasiu, C. and T. Guttormsen – 1998 – 3-D Discrete Element Analysis of Rigid Structures resting on non-linear Soil. 4th European Conference on Numerical Methods in Geotechnical Engineering, Udine, Italy.

Athanasiu, C., T. Alm and A. Bye-1989- Soil structure interaction and stability analysis of gravity platforms with discontinuous/irregular foundations.12th Int.Conf. on Soil mechanics and Found. Engineering. Rio de Janeiro. Brasil.

Athanasiu, C., L. O. Bogen and J. H. Prestegarden – 1999- PLAXIS analyses of sub-sea structures.3rd Norwegian PLAXIS-user Meeting. Oslo. Nov.1999

Athanasiu, C. -2000- Proposal for anisotropic, soft clay model to be incorporated in future developments in PLAXIS, Beyond 2000 in Computational Geotechnics.

Burland, J., B., B., B., Broms and V., F., B., DeMello – 1977- Behaviour of Foundations and Structures. State of the Art Report. Proc. Of the IXth Int. Conf. of Soil Mechanics and Foundation Engineering. Tokyo, Japan.

Brinkgreve, R. B. J. and P. A. Vermeer-1998- .PLAXIS- Complete set of manuals – version 7.

Bye, A., C. Erbrich, B. Rognlien and T.I. Tjelta-1995- Geotechnical Design of Bucket Foundations. 27th Annual Offshore Technology Conference, Houston, Texas.

Caselunghe, A. and J. Eriksson – 2012 - Structural Element Approaches for Soil-Structure Interaction. M. Sc. Thesis. Chalmers University of Technology. Göteborg. Sweden.

Davis, E. H. and J. R. Brooker – 1973 – The effect of increasing strength with depth on the bearing capacity of clays. Geotechnique 23, No.4, 551-563.

Duncan, J., M. – 2013 – Slope stability then and now. ASCE GeoCongress. San Diego CA USA. Invited Lecture. Pp. 2191-2210.

Hammah, R., E. and J., H. Curran – 2009 – It is better to be Approximately Right than Precisely Wrong: Why Simple Models Work in Mining Geomechanics. 43rd US Rock Mechanics Symposium and 4th U.S.-Canada Rock Mechanics Symposium, held at Asheville NC June 28th- July 1, 2009.

Hamre, L., Bye, A., Soereide, O., K., and C. Athanasiu – 2005 – Study of transient pore pressures due to cyclic loads to optimise the foundation concept for Sakhalin platforms. 16th Int. Conf. on Soil Mechanics and Foundation Engineering. Osaka, Japan.

Houser, C. and K. Karlsrud – 2014 – Bestemmelse av ekvivalente jordfjærer for bruk i statiske beregninger og behov for felles forståelse mellom RIG og RIB. Fjellsprengningsteknikk Bergmekanikk/ Geoteknikk Konferanse, Oslo, Norway.

Janbu, N. –1970- Grunnlag i Geoteknikk, Tapir.

Janbu, N., L. Grande and K. Eggereide – 1976 – Effective stress analysis for gravity structures. BOSS'76. NTNU.

Janbu, N. -1985- Soil Models in Offshore Engineering. 25th Rankine Lecture, Geotechnique 35(3): 241-281.

Jostad, H.P., Andersen, K.H. & Tjelta, T.I. -1997-. Analyses of skirted foundations and anchors in sand subjected to cyclic loading. Proc., Int Conf on Behavior of Offsh Structures, 8. Delft,The Netherlands, (1): 49–162.Also NGI Pub 199.

Jostad, H.P., Grimstad, G., Andersen, K.H., Saue, M., Shin, Y. &You, D. -2014- . A FE procedure for foundation design of offshore structures – applied to study a potential OWT monopile foundation in the KoreanWestern Sea. Geotech. Engrg. J. of SEAGS &AGSSEA, Vol. 45 (4), Dec 2014.

Jostad, H.P., Grimstad, G., Andersen, K.H. & Sivasithamparam, N. -2015-. A FE procedure for calculation of cyclic behaviour of offshore foundations under partly drained conditions. Proc., Int. Symp. on Frontiers in Offshore Geotechnics, ISFOG, Oslo, Norway.

Karlsrud, K.-2014- Strength and deformation properties of Norwegian clays from Laboratory tests on high quality block samples. 23th Bjerrum Lecture. Norwegian Geotechnical Society, Oslo.

Karlsrud, K. & Nadim, F. -1990-. Axial capacity of offshore piles in clay. Proc., 22nd OTC, Houston, Paper 6245, pp. 404–416.

Leussink, H. and K. Schweickert -1963- Versuche uber Setzungsverhalten und Sohldruckverteilung am Übergang vom elastischen zum plastischen Zustand einer sehr dicht gelagerten Sandunterlage bei Belastung durch ein stares Fundament. Proceedings of European Conf. On Soil Mech. and Found. Engineering, Wiesbaden, Germany.

Lacasse, S., H., P. Jostad, C. Athanasiu, J-S. L'Heureux, T. Sandene, and Z. Liu – 2013 – Assistance for the calculation of settlement. Geo Montréal.

Marsal, R., J. – 1965 – Stochastic Process in the Grain Skeleton of Soils. 6th Int. Conf. on Soil Mechanics and Foundation Engineering, Montreal, voll.2, pp.303-306.

Marsal, R. J. – 1973 – Mechanical Properties of Rock-fill. "Embankment Dam Engineering", John Willey & Sons, New York.

Poulos, H., G. and E., H. Davis –1974 - Elastic solutions for Soil and Rock Mechanics. John Wiley & Sons, Inc. New York, London, Sydney, Toronto. Series in Soil Engineering.

Schanz, T., P. A. Vermeer and P. G. Bonnier – 2000- The hardening soil model: Formulation and verification, Beyond 2000 in Computational Geotechnics.

Stanculescu, I., C., Athanasiu and M. Popescu – 1979 – Measurement and use of relevant parameters for collapsible and expansive soils in Romania. National Paper. Proc. of the VIIth European Conf. On Soil Mechanics and Found. Engineering, Brighton. England.

Stordal, A.D. – 1980 – Back-calculation of the bearing capacity factor, Nu. Soil Mechanics and Foundations Division. NTNU.

Wibel, A., R. – 1971 – Spannungs verteilung unter flachgegründeten Kreisfundamenten auf trocknen Sand. Veröffenlichungen des Isntitutes für Bodenmechanik und Felsmechanik der Universität Fridericiana in Karlsruhe.

Winkler, E. – 1867 – Die Lehre von der Elastizität und Festigkeit, Prague.

Wood, D.M.-1996- Soil Behaviour and Critical State Soil Mechanics. Cambridge University Press, 1990. Reprinted 1996.

Appendix 1. Method of solution used with SPLATE

The settlement of a stiff plate resting on ground surface can be expressed in terms of a vertical translation, s_o and the rotations about co-ordinate axes x (α) and y (β), Fig.A.1.1:

$$s_i = -s_o - \alpha \cdot x_i - \beta \cdot y_i \qquad \text{(A.1.1)}$$

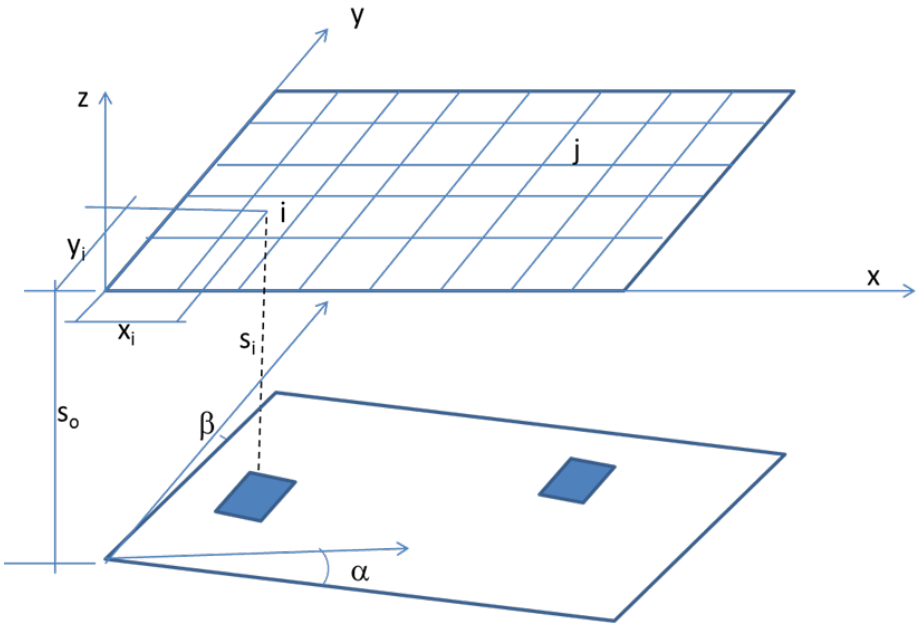

Fig.A.1.1. Geometry of the displaced plate.

From the Theory of Elasticity, the settlement of the elastic half space at the centre of element "i" can be calculated by superposition of the settlements from all evenly distributed loads, p_j, at each element "j", on the surface of half space:

$$s_i = \sum_{j=1}^{n} c_{ij} \cdot p_j \qquad \text{(A.1.2)}$$

where c_{ij} are flexibility coefficients (the settlement at centre of element i due to unit evenly distributed load at element j), functions of soil Elasticity modulus, E_s, and Poissons ratio, ν_s, of the dimensions a_i and b_i of element i and of the distance between centre of element i and centre of element j. Equating the expressions of s_i from eqs. (A.1.1) and (A.1.2), we obtain a system

of **n+3** equations with **n** unknowns, uniformly distributed loads on each element, $p_1..p_n$, and **3** unknowns displacements, s_o, α and β. The last three equations represent the equilibrium conditions:

$$\sum_{j=1}^{n}(c_{ij} \cdot p_j) - so - \alpha \cdot x_i - \beta \cdot y_i = 0$$

$$\sum_{i=1}^{n}(a_i \cdot b_i \cdot p_i) = Q_v$$

$$\sum_{i=1}^{n}(a_i \cdot b_i \cdot p_i \cdot x_i) = M_y \qquad \text{(A.1.3)}$$

$$\sum_{i=1}^{n}(a_i \cdot b_i \cdot p_i \cdot y_i) = M_x$$

The system of equations (A.1.3) is solved and the contact stresses, $\mathbf{p_i}$, are determined, at each element centre as well as the settlement and rotations, $\mathbf{s_o}$, $\boldsymbol{\alpha}$ and $\boldsymbol{\beta}$.

The contact stresses obtained from elastic distribution, p_j, are checked against the limit contact stresses, p_{jf}. If the elastic contact stress in an element k, $p_k > p_{kf}$, a new iteration is required to redistribute the excess stress (p_k-p_{kf}) to non-failed elements while the failed element k is assigned the contact stress p_{kf}. This is done by modifying the flexibility matrix and the load vector.

Appendix 2. Method of solution using non-linear soil reaction coefficient.

The initial soil reaction coefficient, k_i and the exponent were determined from "in situ" plate loading tests on natural loess and on inundated loess and from triaxial tests as follows.

Triaxial compression tests carried out on samples at natural water content and on saturated samples before testing have shown that the tangent Young modulus (defined as the slope of the tangent at the stress-strain curve with strain axis) is strongly dependent on the stress level the sample is loaded (Fig.A2.1):

$$E_t = \frac{\Delta(\sigma_1-\sigma_3)}{\Delta\varepsilon_{ax}} = E_{t,i} \cdot (1 - \frac{(\sigma_1-\sigma_3)}{(\sigma_1-\sigma_3)_f})^m \qquad \text{(A.2.1)}$$

were:

E_t is the tangent Young modulus

E_{ti} is the initial Young modulus

$(\sigma_1-\sigma_3)_f$ is the deviatoric stress at failure

m modulus exponent

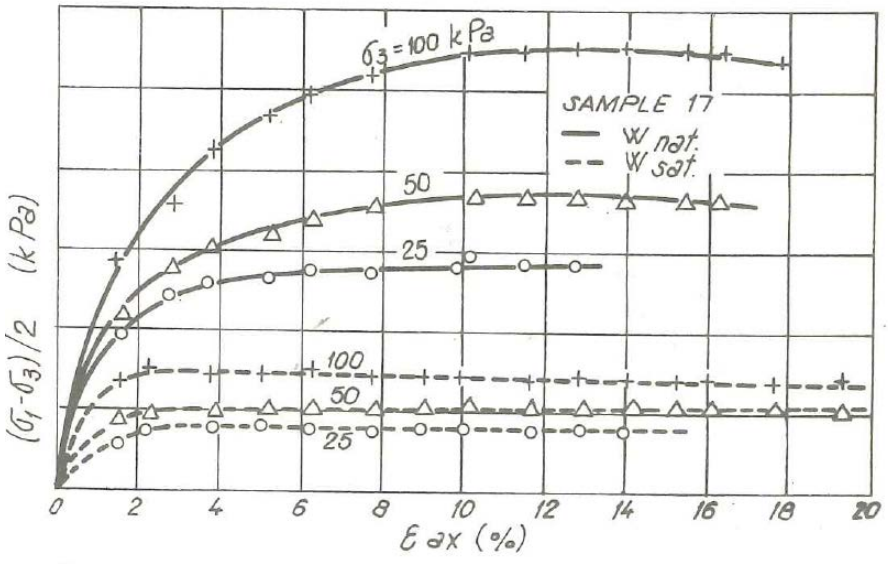

Fig.A.2.1. Stress-strain relations for loess.

The triaxial tests have also shown that the effect of confining pressure on the value of initial Young modulus can be expressed by the equation proposed by Dunlop, Duncan and Seed (1968):

$$E_{t,i} = K_m \cdot \sigma_{3c}^{n} \qquad \text{(A.2.2)}$$

Were:

σ_{3c} is the confining pressure the sample was consolidated for before drained shearing phase;

n is stress exponent

The values of the parameters K_m and n, both at natural water content and of saturated samples were determined by plotting E_{ti} versus σ_{3c} at logarithmic scale (Fig.A.2.2).

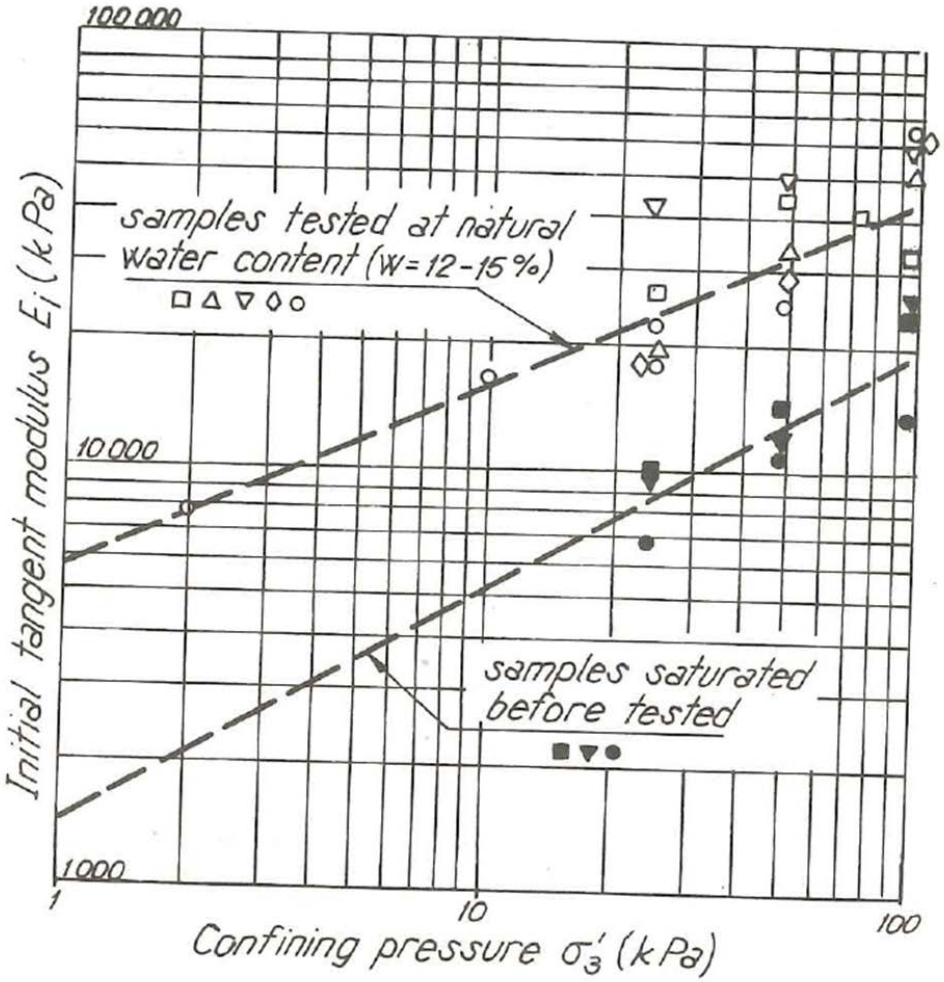

Fig.A.2.2.Inflence of water content and confining pressure on initial modulus.

If the tangent reaction coefficient is defined as the ratio between the load increment and the corresponding settlement increment, then an equation similar to eq. (2.3) could describe the dependency of the reaction coefficient on the degree of mobilization of ultimate load:

$$K_t = \frac{\Delta p}{\Delta s} = K_i \cdot (1 - \frac{p}{p_{ult}})^m \qquad \text{(A.2.3)}$$

The non-linear behavior of the loessial soil (Fig.A.2.1) makes impossible to directly correlate the Young modulus from triaxial tests and reaction modulus from "in situ" plate loading tests. However, if only the initial portion of the load-settlement curve is considered, then from Theory of Elasticity:

$$s = p \cdot B \cdot I_w \cdot \frac{1-\nu^2}{E_i} = p \cdot B \cdot I_w \cdot \frac{1-\nu^2}{K_m \cdot p_m^n} \qquad \text{(A.2.4)}$$

in which:

s- is the settlement of the plate

p is the applied pressure

I_w is an influence factor depending on the shape of the plate

ν is Poissons ratio of loess

E_i initial Young modulus

p_m is the mean effective stress acting in the active zone of the loess beneath the plate.

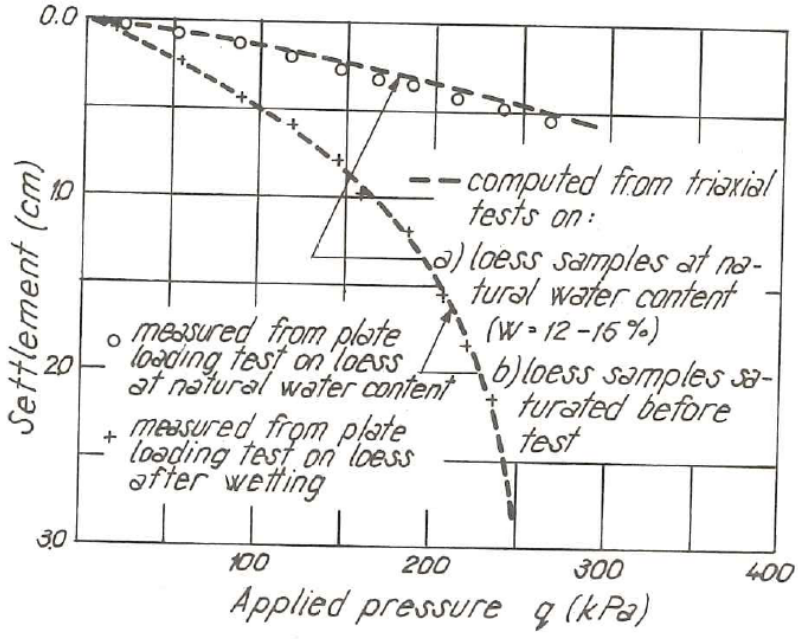

Fig.A.2.3. Load-settlement curves from plate loading tests.

Following the eq. (2.6), the initial Winkler coefficient, k_i, is correlated with K_m coefficient by:

$$k_i = \frac{K_m \cdot \sigma_m^n}{B \cdot I_w \cdot (1-\nu^2)} \qquad \text{(A.2.5)}$$

The final expression of variable tangent Winkler modulus, eq.(A.2.3), is obtained by assuming that the mobilization degree in plate loading test, expressed as p/p_{ult}, is equivalent to the mobilization degree from triaxial test, $\frac{(\sigma_1-\sigma_3)}{(\sigma_1-\sigma_3)_f}$.

Appendix 3. Undrained, effective stress bearing capacity formulation

The following expressions relating the shear stress, the total normal stress and the mobilized friction, tanρ, can be written (Janbu et al., 1976):

$$\tau_p = r_p \cdot tan\rho \cdot (\sigma_v + a - \delta u_b) \quad \text{(A.3.1)}$$

$$q_{ult} = N_w \cdot [N_q \cdot p' + (N_q - 1) \cdot a + 0.5 \cdot N_\gamma \cdot \gamma' \cdot B - N_u \cdot \delta u_b] \quad \text{(A.3.2)}$$

where:

$$N_w = (1 + f_w^2)/(1 + f_w^2 \cdot tan^2\left(45 + \frac{\rho}{2}\right)) \quad \text{(A.3.3)}$$

$$f_w = (1 - \sqrt{(1 - r_n^2)}\,)/r_n \quad \text{(A.3.4)}$$

q_{ult} – average total bearing capacity of the element;

δu_b – average excess pore pressure at bottom slab/soil contact;

N_q, N_γ, N_u – bearing capacity factors (Stordal, 1980);

r_p, r_n – roughness factors in failure direction and normal to the failure direction, respectively;

The procedure used by the program to assess the foundation stability is illustrated in the flow chart (Fig.A.3.1).

The material coefficient is thus defined as:

$$\gamma_m = tan\varphi'_u/tan\rho \quad \text{(A.3.5)}$$

The pore pressures acting at the bottom of each discrete element were calculated using Janbu's equation:

$$\delta u_b = \delta p - D \cdot \delta q \quad \text{(A.3.6)}$$

The two roughness factors, one in radial direction, r_p and one in tangential direction, r_n, are defined by the two components, radial and tangential of the shear stress. The radial roughness is defining the vertical component of bearing capacity, q_{ult}, while the resultant (total) roughness factor, r_t is used to assess the critical (ultimate) shear stress, τ_{ult}.

The procedure used in the program DEAP to assess the critical (ultimate) shear and normal stresses is described by the flow chart in Fig. A3.1.

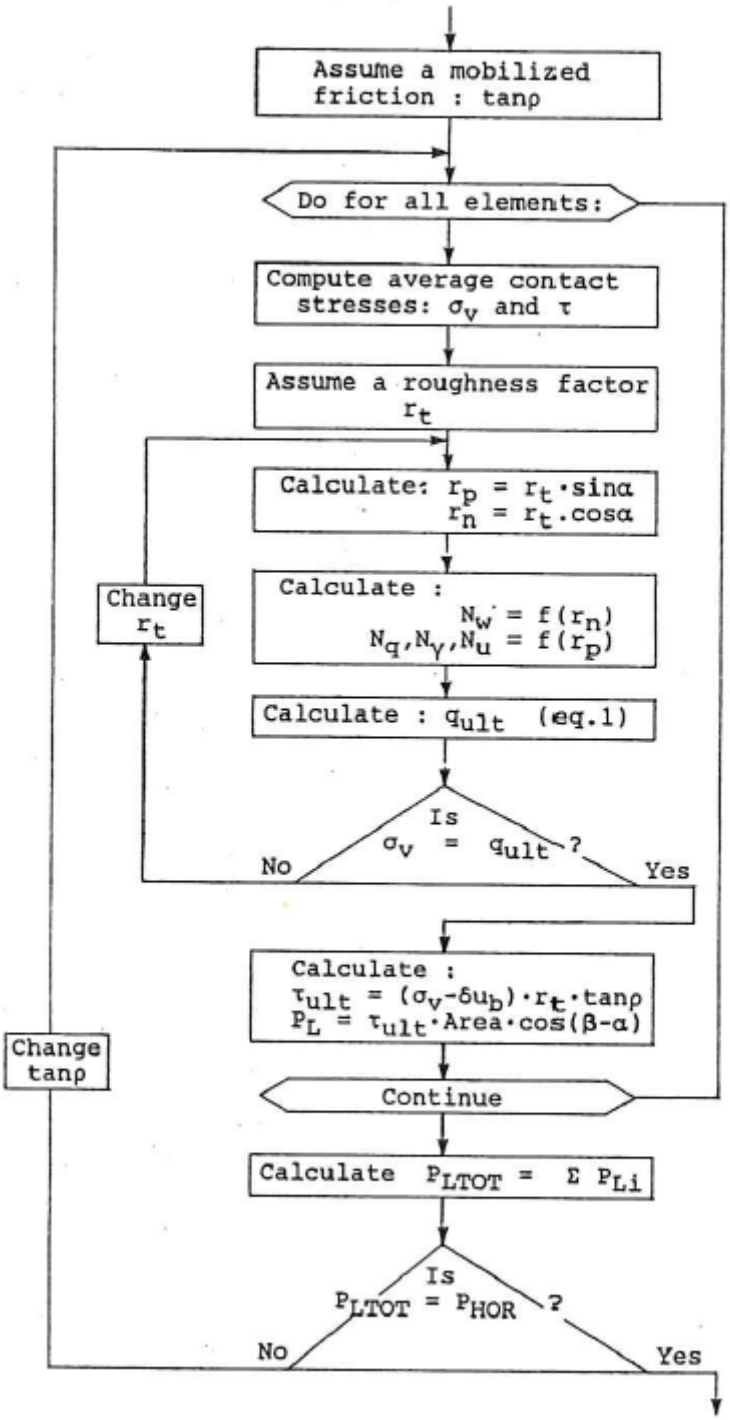

Fig.A.3.1 Flow chart of stability analysis.

Appendix 4. Simplified method for contact stresses and displacements of flexible plates

The flexible plate is modelled by four node isoparametric plate elements. Both concentrated loads at nodal points and distributed loads over the elements can be entered as input loading. The soil is modelled by non-linear springs at nodal points.

The differential equation of thin plates in bending is expresses as:

$$D \cdot \frac{\partial^4 w}{\partial x^2 \partial y^2} = q - k_s \cdot w \qquad \text{(A.4.1)}$$

where:

D is the flexural stiffness of the plate:

$$D = \frac{E_p \cdot h^3}{12 \cdot (1 - \nu_p^2)} \qquad \text{(A.4.2)}$$

E_p is the Elasticity modulus of plate material

ν_p is the Poisson's ratio of the plate material

h is the thickness of the plate

w is the plate deflection

k_s is the soil reaction, variable coefficient (secant modulus of the stress-displacement relationship for soil).

The plate element is shown in Fig.A.4.1. The four degrees of freedom assumed per element are:

$$\{w\} = \begin{Bmatrix} w \\ \theta_y \\ \theta_x \\ \theta_{xy} \end{Bmatrix} \qquad \text{(A.4.3)}$$

The corresponding nodal force vector is defined as:

$$\{F\} = \begin{Bmatrix} F_z \\ M_y \\ M_x \\ M_{xy} \end{Bmatrix} \qquad \text{(A.4.4)}$$

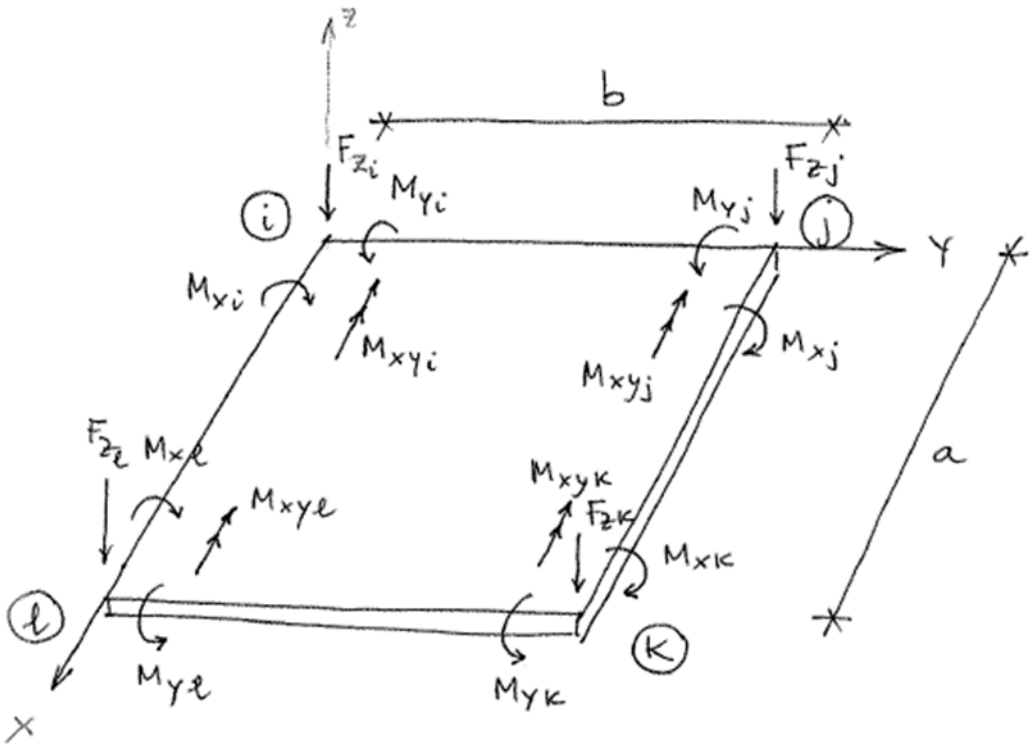

Fig.A.4.1. Four nodes isoparametric plate element.

The system of equations for the equilibrium of the plate subjected to applied loads, normal to its median plan (Fig.A.4.2) is:

$$[K] \cdot \{w\} = \{F\} - [k_s] \cdot \{w\} \qquad \text{(A.4.5)}$$

Where:

$[K]$ is the stiffness matrix of the plate and $[k_s]$ is the stiffness matrix of the supporting springs.

The system is solved for the displacements accounting for the boundary conditions. Nodal point forces for each element are then calculated by multiplication of element stiffness matrix with the vector of nodal displacements.

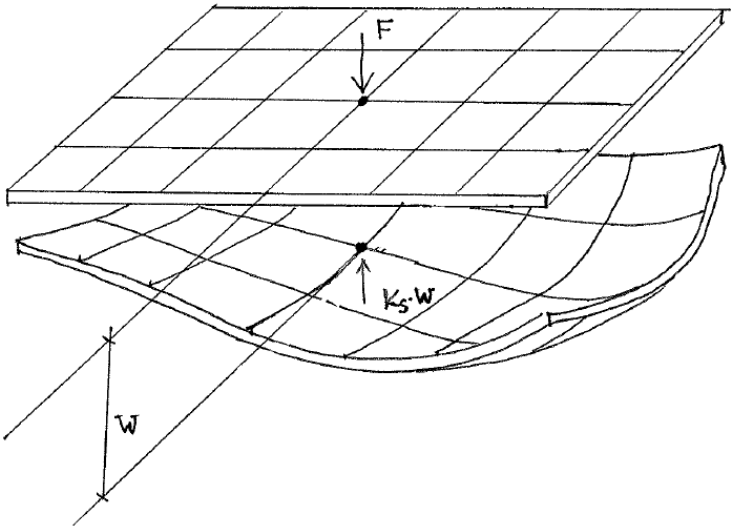

Fig.A.4.2. Equilibrium of the plate.

The plate thickness and material properties can vary from element to element (Fig.A.4.3). Holes in the plate can also be modelled by assigning material number=0 to the elements over the hole.

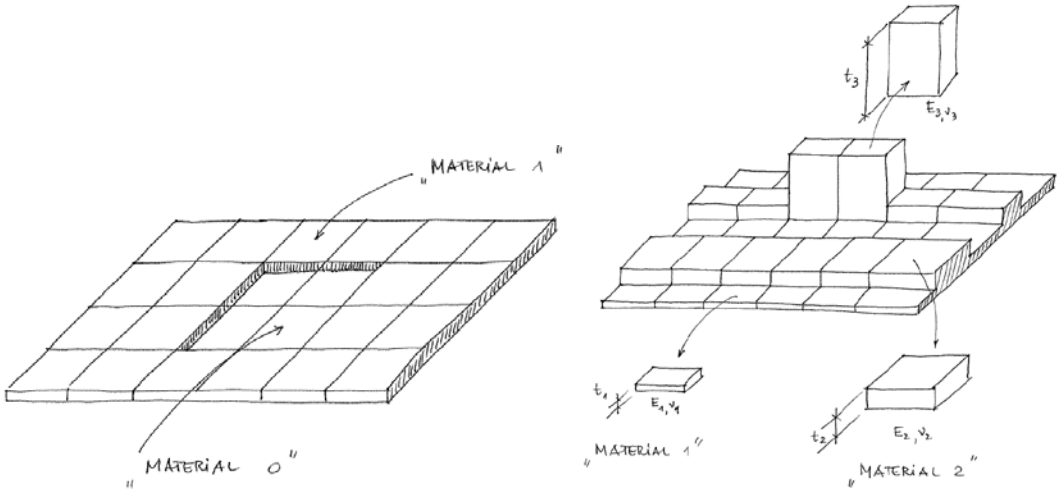

Fig.A.4.3. Modeling of variable thickness plate.

It is also possible to model the soil-foundation-superstructure interaction. A structural super element is defined by its global stiffness matrix, condensed to the connection plate nodal points (Fig.A.4.4). The program adds the super element matrix to the plate stiffness matrix before solving the system of Eqs. (A.4.5).

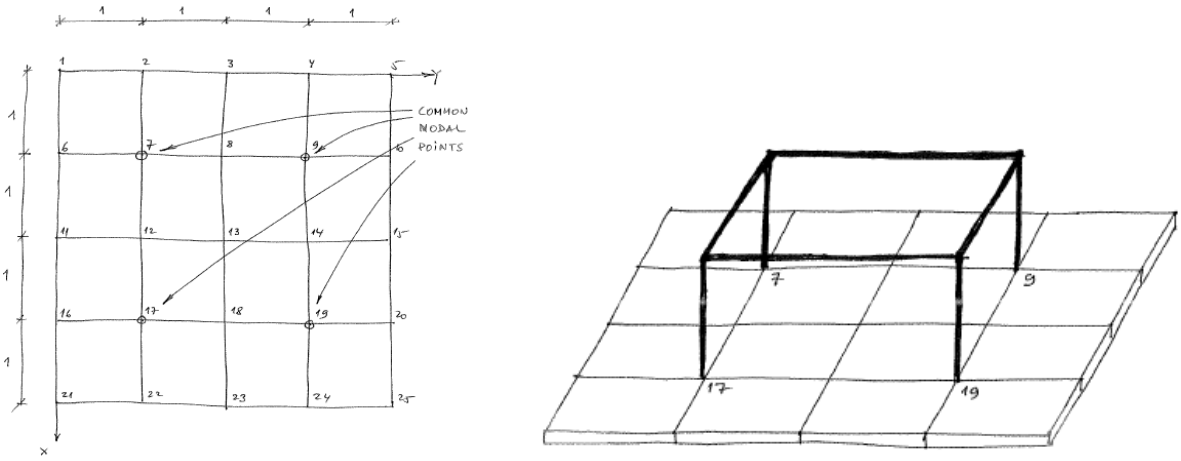

Fig.A.4.4. Modeling superstructure.

The loads are read from input file either as concentrated loads and moments at nodal points or as uniformly distributed loads over the area of one or more elements. The supporting spring reactions (contact stresses at nodal points) are modelled by using one of the following four soil models: a/elastic layered continuum, b/Winkler springs, c/non-linear supporting spring, d/1-D soil compression (settlement) model. The soil model most commonly used is the 1-D compression (settlement) model.

In this model the effective vertical stresses are first calculated by using elastic half space solutions (Poulos and Davis, 1974) and used to calculate the compression in each sublayer under each nodal point of the mesh. The sublayer compression is simply calculated as (Janbu , 1970) **:**

modulus exponent, as=1 (over consolidated clay with constant constrained modulus for stress range below p_c and with constrained modulus linear variable with effective stress for stress range above p_c) :

$$s_i = h_i \cdot \frac{\Delta\sigma'}{m_r} \qquad \text{(A.4.5)}$$

for $(p_o+\Delta\sigma') < p_c$, and:

$$s_i = h_i \cdot \left(\frac{p_c - p_o}{m_r} + \frac{1}{m} \cdot \ln\left(\frac{p_o + \Delta\sigma' - p_r}{p_c - p_r}\right)\right) \qquad \text{(A.4.6)}$$

for $(p_o + \Delta\sigma') > p_c$, where p_r is the reference stress for the soil layer.

modulus exponent, 0<as<1.0 (cohesionless / silty materials with constrained modulus variable with effective stress as $M = m \cdot p_{atm} \cdot (\sigma'/p_{atm})^{1-as}$):

$$s_i = \frac{h_i}{m \cdot as}\left[\left(\frac{p_o + \Delta\sigma'}{p_{atm}}\right)^{as} - \left(\frac{p_o}{p_{atm}}\right)^{as}\right] \qquad \text{(A.4.7)}$$

Which, for particular case of as = 0.5, gives:

$$s_i = \frac{2 \cdot h_i}{m} \cdot \left(\sqrt{\frac{p_o + \Delta\sigma'}{p_{atm}}} - \sqrt{\frac{p_o}{p_{atm}}} \right) \qquad \text{(A.4.7a)}$$

modulus exponent, as= 0 (over consolidated clays with constrained moduli linearly variable with effective stress)

$$s_i = h_i \cdot \ln\left(\frac{p_o + \Delta\sigma' - p_r}{p_o - p_r}\right) \cdot \frac{1}{m_r} \qquad \text{(A.4.8)}$$

for $(p_o + \Delta\sigma') < p_c$, and :

$$s_i = h_i \cdot \left[\frac{1}{m_r} \cdot \ln\frac{p_c - p_r}{p_o - p_r} + \frac{1}{m} \cdot \ln\frac{p_o + \Delta\sigma' - p_r}{p_c - p_r} \right] \qquad \text{(A.4.9)}$$

The total settlement of the soil is calculated by adding the compression of individual sublayers:

$$s = \sum_{i=1}^{nlayers} s_i \qquad \text{(A.4.10)}$$

A layered ground with variable depth to bedrock can be modelled by assigning different “soil profile” to each node (Fig.2.9).

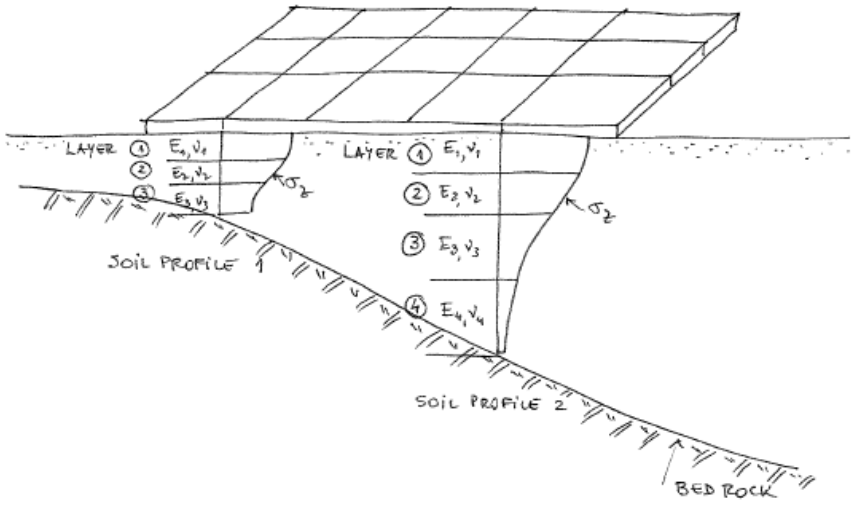

Fig.A.4.5. Modeling layered ground with variable depth to bedrock.

The solution is found by an iterative procedure as follows. The nodal plate-soil contact stresses are assumed, to begin with, equal to the average distributed load over the plate area. The normal stress at the centre of each sublayer are then calculated using the Theory of Elasticity and the settlement of the soil under the nodal point determined using one of the four soil models. An equivalent distributed spring stiffness is then calculated for each nodal point as:

$$K_s = \frac{p}{s} \qquad \text{(A.4.11)}$$

where: p is the contact stress between plate and soil in previous iteration and s is the calculated settlement.

Using the new spring stiffness a plate solution is found by solving the system (A.4.5) and a new contact stress distribution and plate deflections, w, are obtained. The iterations are repeated until the difference between old and new stress distribution and between plate deflection, w, and soil settlement, s, are within the specified tolerance.

The details of method of solution and input data are described in FPLATES User's Manual, (Athanasiu, 1994).

Appendix 5. Simplified finite element creep analysis

A procedure to calculate creep settlements in rock fills is developed and incorporated into the finite element program SSCREEP (Athanasiu, 1991). The procedure is based on the following assumptions:

a/ the creep strain increments are defined by the following stress-strain-time law:

$$\Delta\varepsilon_{vollc} = \beta_{vol} \cdot \sigma_m \cdot \log_{10}(\frac{t}{t_o}) \quad \text{(A.5.1)}$$

$$\Delta\varepsilon_{shlc} = \beta_{sh} \cdot \frac{\sigma_d}{\sigma_{df}} \cdot \log_{10}(\frac{t}{t_o}) \quad \text{(A.5.2)}$$

where $\Delta\varepsilon$ vol lc and $\Delta\varepsilon$ sh lc are volumetric and shear strain increments from time to time t during the linear phase of the creep process, respectively; β vol and β sh are creep parameters for volumetric and shear creep strains, respectively; σm, σd and σdf are mean (octahedral) effective stress, deviatoric stress and failure deviatoric stress, respectively.

$$\Delta\varepsilon_{voldc} = 2 \cdot \frac{\beta_{vol}}{c \cdot r_t} \cdot \sigma_m \cdot \tan^{-1}\left[e^{c \cdot \log_{10}\left(\frac{t}{t_m}\right)} \right] \quad \text{(A.5.3)}$$

$$\Delta\varepsilon_{shdc} = 2 \cdot \frac{\beta_{sh}}{c \cdot r_t} \cdot \frac{\sigma_d}{\sigma_{df}} \cdot \tan^{-1}\left[e^{c \cdot \log_{10}\left(\frac{t}{t_m}\right)} \right] \quad \text{(A.5.4)}$$

where c and rt are empirical constants that can be determined by the technique of best fitting the "S-shaped" diffusion creep settlement curve and tm is the time of the inflexion point of the curve.

b/ the creep displacement pattern (relative magnintude and direction) is similar to the pattern of the displacements from body forces (own weight of the soil). Using this assumption the creep strain increments components in x, z and xz directions can be computed as:

$$\Delta\varepsilon_{cx} = \frac{\Delta\varepsilon_{volc}}{2} + \frac{\Delta\varepsilon_{shc}}{2}\cos(2\theta)$$

$$\Delta\varepsilon_{cz} = \Delta\varepsilon_{volc} - \Delta\varepsilon_{cx} \quad \text{(A.5.5)}$$

$$\Delta\gamma_{cxz} = \Delta\varepsilon_{shc} \cdot \sin(2\theta)$$

where $\Delta\varepsilon_{volc}$ and $\Delta\varepsilon_{shc}$ are volumetric and shear strain increments in either diffusion or linear creep phase; θ is the orientation angle of principal (maximum) strain from horizontal (x-axis)

c/ the effect of creep strain increments on elastic soil moduli can be neglected.

The finite element procedure consists of the following steps:

1 Calculate equivalent nodal forces from body (own weight) forces of the rock fill and perform an own weight analysis to find the strains and stresses from gravity forces. The Poisson's ratio used in this analysis is calculated from the coefficient of earth pressure at rest, ko:

$$\nu = \frac{k_o}{1 + k_o} \tag{A.5.6}$$

2 For each time interval calculate the vector of creep strain increments, {Δεc}, as described in eqs. (A.5.1) to (A.5.5) using the mean and deviatoric stresses calculated in step 1. The equivalent creep stress increments and nodal force increments due to creep are then calculated as:

$$\{\Delta\sigma_c\} = [D] \cdot \{\Delta\varepsilon_c\} \tag{A.5.6}$$

$$\{\Delta F_c\} = \int [B]^T \cdot \{\Delta\sigma_c\} \cdot dV \tag{A.5.7}$$

where [D] is the elastic stiffness matrix of each element, {Δσc} is the vector of equivalent creep stress increments, {ΔFc} is the vector of equivalent nodal point forces due to creep and [B] is the strain-displacement transformation matrix.

3 For each time increment perform a "creep analysis" , i.e. solve for displacements due to equivalent creep nodal forces, {ΔFc}, calculated in step 2.

The creep parameters used with finite element procedure were first calibrated against measured creep settlements at the dynamically deep compacted rock fill for Post Terminal Building at Solheimsvannet in Bergen, Norway. The parameters were thereafter used for preliminary analyses of creep settlements of rock fill at Kollsnes On-shore Plant, Norway. Typical results from preliminary analyses are shown in Fig. A.5.2.

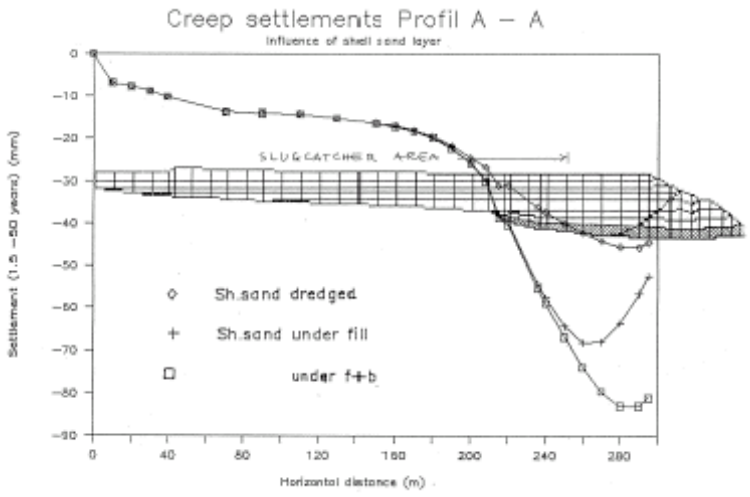

Fig. A.5.2. Result from finite element creep analyses using the program SSCREEP

Appendix 6. Discrete element method.

The program **DISEL** is based on discrete element method where the structure is divided into a number of small, rigid elements defined by their position and orientation, and contact area with the soil. The soil-structure contact is modelled by non-linear springs. The force-displacement curves for each spring are specified by a number of points along the curves.

The results consist of the following:

- displacements at the centre of the structure due to applied (specified) loads.
- resultant contact forces between each discrete element and the surrounding soil
- displacements at each discrete element centre
- contact stresses in normal, tangential (shear) and axial (shear) direction at each discrete element centre

It is possible to define groups of discrete elements as superelements and the resultant forces and moments on these superelements are written on output file together with the above mentioned results.

The method consists of the following:

The structure in contact with soil is divided into a number of small discrete elements. All discrete elements are assumed rigidly connected to the centre of structure. The contacts between soil and structural elements are modelled by contact discrete elements (springs) having a non-linear force-displacement relationship.

The soil reactions on each element are defined by three forces, one normal, Fu, and two tangential to the element, Fv and Fw. The element force vector in local co-ordinate system, u,v,w, is $\{F\}^T_l$ ={Fu Fv Fw}. The discrete element forces in the global system og co-ordinates is:

$$\{F\}_g = [T] \cdot \{F\}_l \qquad \text{(A.6.1)}$$

where $\{F\}_g^T$ = {Fx, Fy, Fz, Mx, My, Mz} and [T] is the transformation matrix. The transformation equation can also be written in displacements to obtain local displacements of the element centre from displacement vector of the structure defined in the global system:

$$\{\delta\}_l = [T]^T \cdot \{u\} \qquad \text{(A.6.2)}$$

The contact between soil and structural element is modelled by non-linear springs. The vector of local element forces can thus be expressed in terms of element local displacements as:

$$\{F\}_l = [K] \cdot \{\delta\}_l \qquad \text{(A.6.3)}$$

where [K] is the element spring stiffness matrix. Substituting $\{\delta\}_l$ from eq.(A.6.2) in eq. (A.6.3) the local element force vector is obtained in terms of global displacements:

$$\{F\}_l = [K] \cdot [T]^T \cdot \{u\} = [B] \cdot \{u\} \quad \text{(A.6.4)}$$

Where [B] is the force-displacement matrix. Using eq. (A.6.2), the global force vector can be expressed in terms of global displacements:

$$\{F\}_g = [T] \cdot [B] \cdot \{u\} \quad \text{(A.6.5)}$$

The structure equilibrium requires that the sum of all element forces equals the applied forces on the structures:

$$(\sum [T] \cdot [K] \cdot [T]^T) \cdot \{u\} = \{Q\} \quad \text{(A.6.6)}$$

Where {Q} is the vector of forces acting at the structure centre and the sum of element matrices is the stiffness matrix of the entire structure. As there is only one rigid structure, the eq. (A.6.6) represents a system of 6 linear equations, which is solved for structure displacements, {u}. The soil non-linearity is accounted for by a variable secant modulus technique in which the stiffness is gradually adjusted to match the displacements from previous iteration, until convergence is obtained. The local element displacements can then be computed from eq. (A.6.2) and the element contact forces from eq. (A.6.4).

Appendix 7. Undrained shear strength of sand. Dilatancy parameter.

A shear stress-strain relationship is proposed (Athanasiu, 1999) to describe the sand behaviour during shearing, based on the G/G_{max} vs. log γ relation:

$$\frac{q}{q_{ult}} = \frac{\gamma}{\gamma_r} \cdot \frac{G}{G_{max}} = \frac{\gamma}{\gamma_r}\left[1 - c_1 \cdot \operatorname{atan}\left(\exp\left(c_2 \cdot \log\left(\frac{\gamma}{\gamma_i}\right)\right)\right)\right] \quad (A.7.1)$$

where γ_r is the reference shear strain ($\gamma_r = \frac{q_{ult}}{2 \cdot G_{max}}$) and γ_i is the shear strain at inflection point on the curve G/G_{max} vs. γ . The constants c_1 and c_2 depend on the slope of the G/Gmax vs. γ curve at inflection point, β_o, and on the ultimate secant shear modulus ratio, Gult/Gmax. γ_r depends on ultimate deviatoric stress:

$$q_{ult} = (c \cdot cot(\varphi) + p_o') \cdot M \quad (A.7.2)$$

$$M = \frac{6 \cdot sin\varphi}{3 + (2 \cdot b - 1) \cdot sin\varphi} \quad (A.7.3)$$

and on G_{max}.

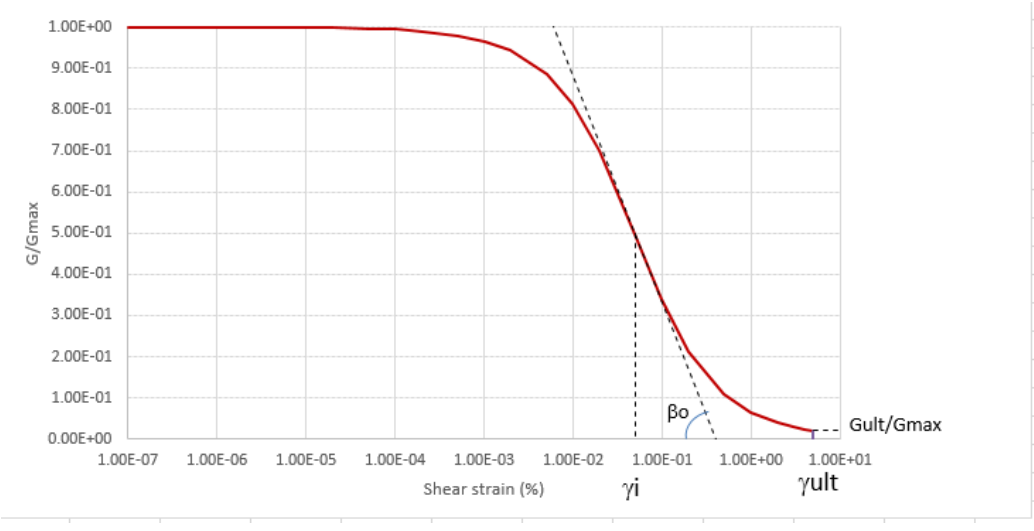

Fig.A.7.1. G/Gmax vs. γ

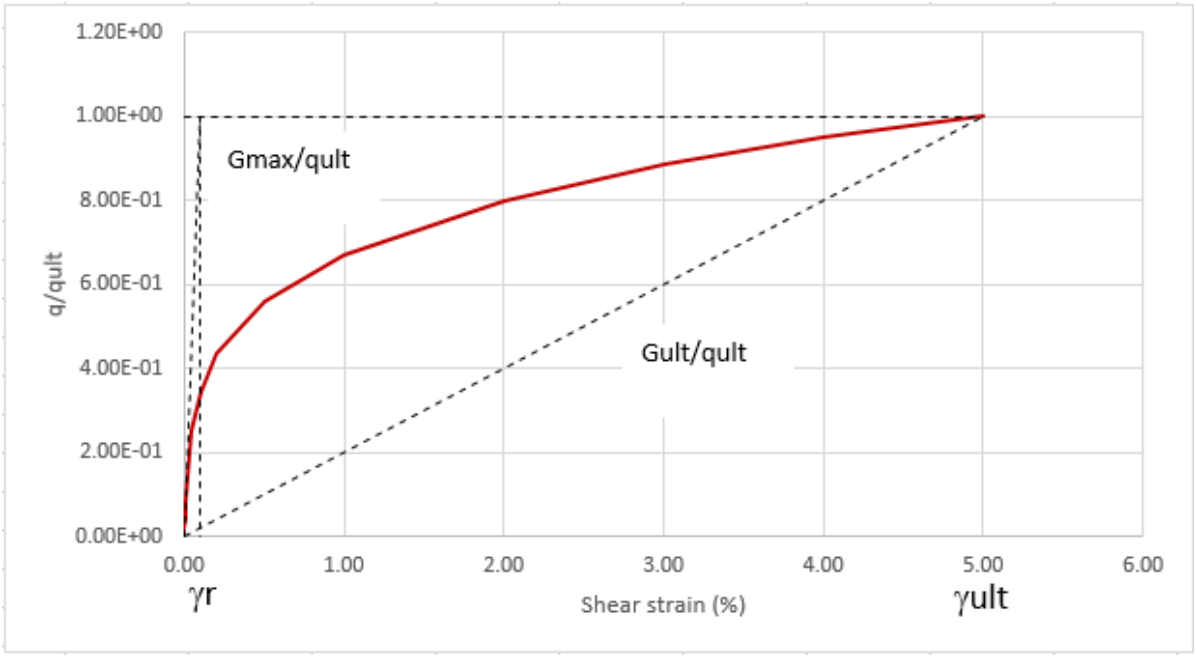

Fig.A.7.2. Deviatoric stress-strain relationship.

(A.7.1) can be solved for γ as a function of applied deviatoric stress q by a numerical iterative procedure. Once the total shear strain is determined, the plastic shear strain is found by subtracting the elastic part:

$$\gamma^p = \gamma(q) - \gamma^e = \gamma(q) - \frac{q}{2 \cdot G_{max}} \tag{A.7.4}$$

The shear hardening yield function is now defined as:

$$F_q = \gamma(q) - \frac{q}{2 \cdot G_{max}} - \gamma^p \tag{A.7.5}$$

The volumetric plastic strain increment due to dilatancy during shear is defined as:

$$\Delta\varepsilon_p^{pd} = -sin\psi_m \cdot \Delta\gamma^p \tag{A.7.6}$$

where ψ_m is the mobilized angle of friction:

$$sin\psi_m = \max\left(\frac{sin\rho - sin\varphi_{cv}}{1 - sin\rho \cdot sin\varphi_{cv}}, 0\right) \tag{A.7.7}$$

and ρ is the mobilized angle of friction:

$$sin\rho = \frac{q}{\sigma_1' + \sigma_1' + 2 \cdot c/tan\varphi} \tag{A.7.8}$$

The volumetric elastic strain increment is defined as:

$$\Delta\varepsilon_p^{ed} = \frac{\Delta q}{E_{max}}(1 + 2 \cdot \nu) \qquad (A.7.9)$$

In addition to the shear hardening yield surface, a cap yield surface as proposed by Schantz, Vermeer and Bonier (1999) is used:

$$F_p = \frac{q^2}{M^2} + p'^2 - {p'}_p^2 = 0 \qquad (A.7.10)$$

where p'_p is the pre-consolidation stress.

The elastic volumetric strain increment is defined as:

$$\Delta\varepsilon_p^{ep} = \frac{\Delta p'}{K_c} \qquad (A.7.11)$$

$$K_c = \frac{E_{oed}}{2 \cdot (1 - 2 \cdot \nu)} \qquad (A.7.12)$$

$$E_{oed} = E_{oed}^{ref} \cdot \left(\frac{c \cdot cos\varphi + \sigma'_{vo} \cdot sin\varphi}{c \cdot cos\varphi + p_{ref} \cdot sin\varphi}\right)^m \qquad (A.7.13)$$

The plastic volumetric strain increment is defined as:

$$\Delta\varepsilon_p^{pp} = \frac{\frac{K_s}{K_c} - 1}{K_c} \cdot \left(\frac{{p'}_p + c/tan\varphi}{p_{ref} + c/tan\varphi}\right)^m \cdot \Delta {p'}_p \qquad (A.7.14)$$

In undrained situation, the total volumetric strain increment must be equal to zero:

$$\Delta\varepsilon_p^{ed} + \Delta\varepsilon_p^{pd} + \Delta\varepsilon_p^{ep} + \Delta\varepsilon_p^{pp} = 0 \qquad (A.7.15)$$

The effective stress path in undrained loading can be calculated by applying small increments in deviatoric and total stresses, Δq and Δp , and determine $\Delta\varepsilon_p^{ed}$ and $\Delta\varepsilon_p^{pd}$ using (A.7.6) and (A.7.9). The remaining two unknowns, $\Delta p'$ and $\Delta {p'}_p$, are solved using (A.7.10) and (A.7.15).

Fig.A.7.3 illustrates an effective stress path for a triaxial CAU-C test. The pore water pressure development with shear strain is illustrated in Fig.A.7.4 while the development of the secant dilatancy parameter, D is shown in Fig.A.7.5.

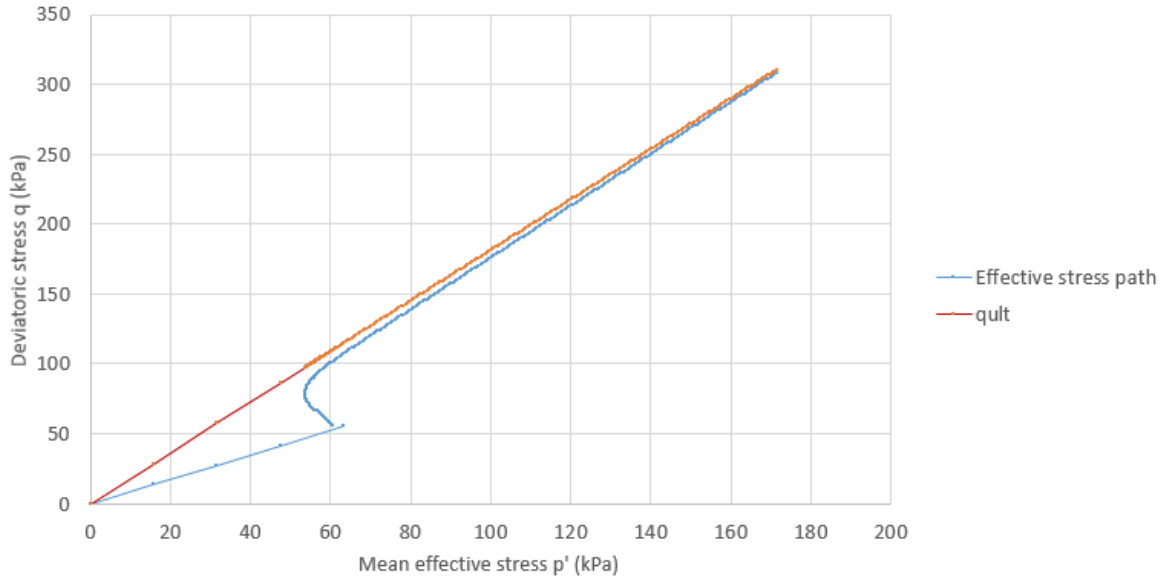

Fig.A.7.3. Effective stress path in a CAU-C test.

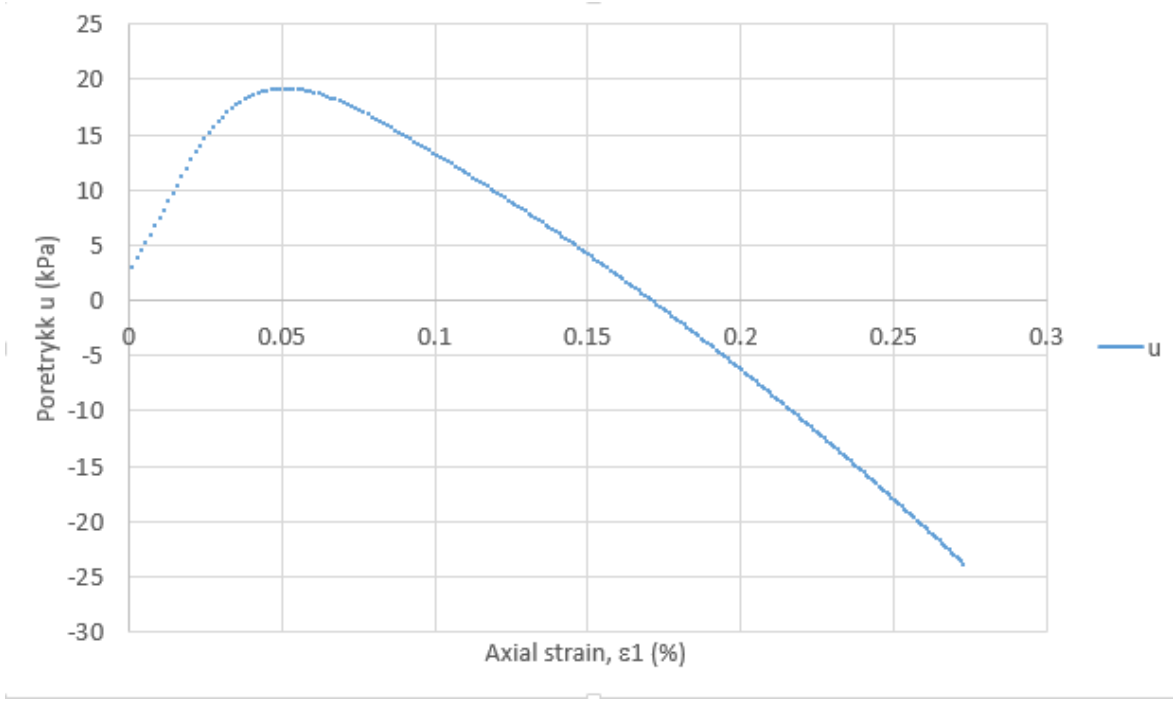

Fig.A.7.4. Pore water pressure development with shear strain in CAU-C test.

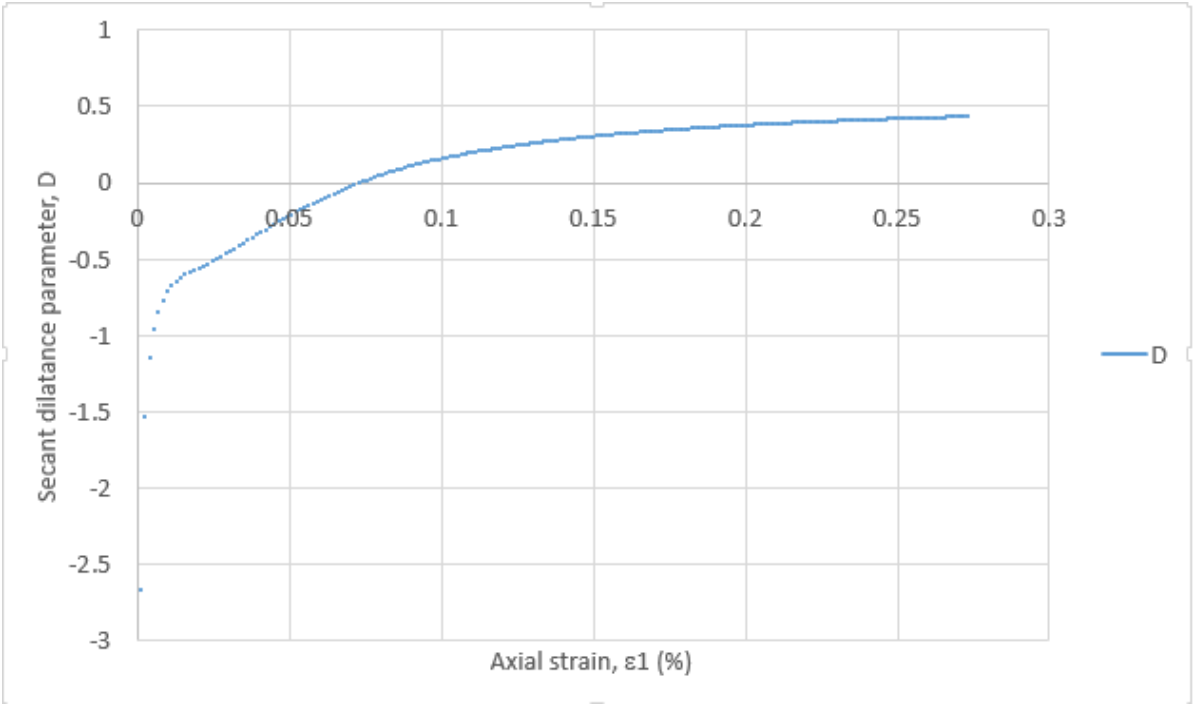

Fig.A.7.5. Secant dilatancy parameter development with shear strain in CAU-C test.

The parameter that defines the undrained shear strength of the dense sand is the ultimate secant dilatancy parameter D_f, defined as the angle between a secant line from p'_o to p'_f and vertical line from p'_o, where p'_o is the consolidation mean effective stress, prior to undrained shear, and p'_f is the ultimate mean effective stress at failure.

Laurits Bjerrums Minnefond

Statutter

§ 1 Opprettelse

Laurits Bjerrums minnefond er opprettet av Norsk geoteknisk forening, dels ved egne midler, og dels ved gaver fra private firmaer og offentlige institusjoner, samt fra enkeltpersoner.

§ 2 Formål

Fondets avkastning skal benyttes til å fremme geoteknisk forskning og stimulere det geotekniske miljø ved følgende tiltak:

(a) Laurits Bjerrums ærespris tildeles for et fremragende enkeltarbeid, eller for flere betydelige arbeider som sammen har fremmet faget geoteknikk og fundamentering.

(b) Laurits Bjerrums stipendium benyttes fortrinnsvis til å stimulere yngre, lovende geoteknikere til forskning innen faget.

(c) Laurits Bjerrums minneforedrag holdes av fremstående geoteknikere som inviteres og honoreres.

§ 3 Styre

Fondets midler forvaltes av et styre på 3 medlemmer valgt av generalforsamlingen i Norsk geoteknisk forening for en periode på 5 år, med mulighet for gjenvalg av de enkelte styremedlemmer én gang. Norsk geoteknisk forenings sekretær, kasserer og revisor fungerer som sådanne også for fondsstyret. Fondsstyret skal holde minst ett møte pr. år. Sekretæren innkaller til møtene og deltar i disse.

Fondsstyret tar avgjørelser i alle saker som vedrører bruk av fondets avkastning til ovennevnte formål Resultatet av avgjørelsen meddeles til Norsk geoteknisk forening som skal være arrangør ved minneforedragene og ved utdeling av ærespris og stipendium.

§ 4 Anvendelsesprinsipp

Anvendelsen av fondets avkastning skal så vidt mulig skje i Laurits Bjerrums ånd. Regelmessighet og rutine ved utdelingen bør vike prioritet for originalitet og oppfinnsomhet. Det eksepsjonelle skal honoreres fremfor mengde, og ved de respektive seremonier og tilstelninger skal det legges vekt på å skape særpreg og festivitas.

§ 5 Statuttendringer

Bestemmelsene i disse statutter kan etter år 2000, endres av Norsk geoteknisk forening i henhold til foreningens egne statutter. Fondsstyret skal på forhånd enstemmig ha erklært seg enig i endringsforslaget.

Statutter vedtatt av Norsk geoteknisk forenings generalforsamling 18. september 1973